Design of a

Deployable Baffle

for the Deployable Space Telescope

E.A. Korhonen

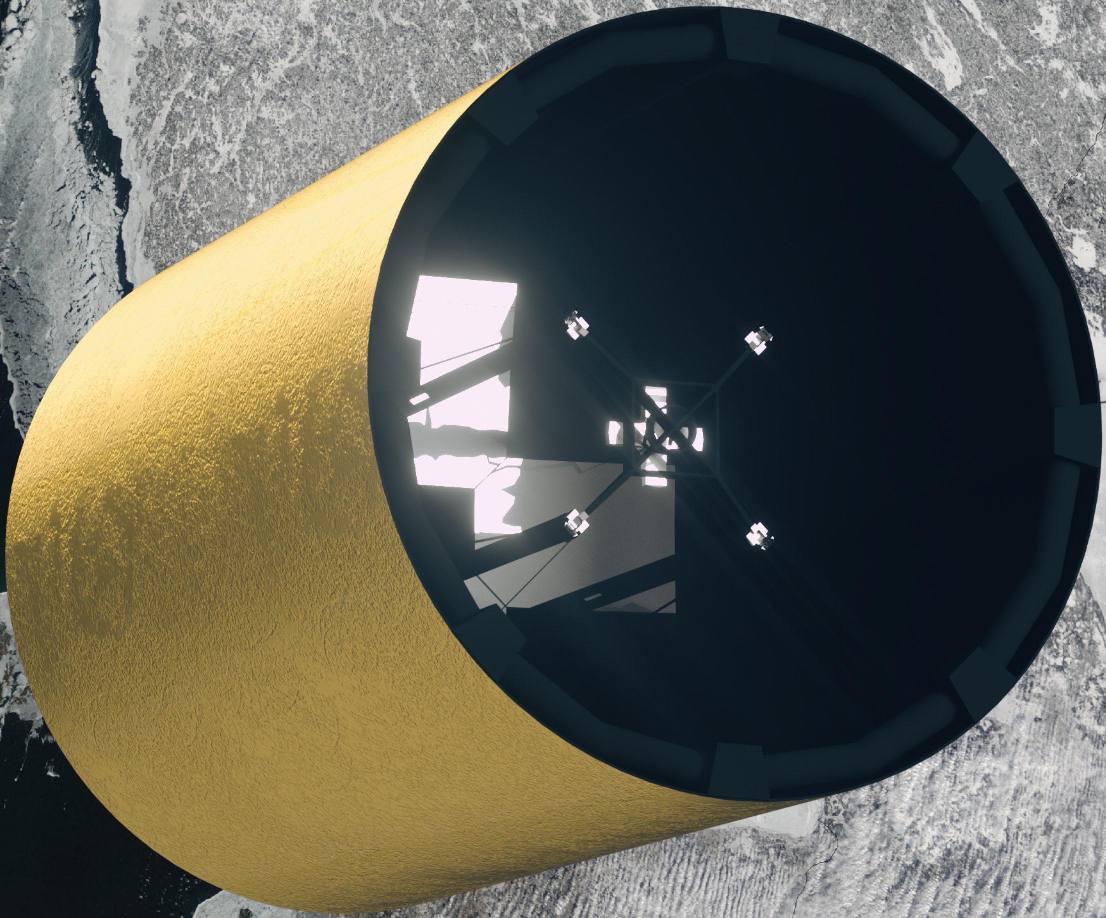

Technische Universiteit Delft

Design of a

Deployable Baffle

for the Deployable Space Telescope

by

E.A. Korhonen

to obtain the degree of Master of Science
at the Delft University of Technology,
to be defended publicly on Friday May 17, 2019 at 1:00 PM.

Student number:	4272056	
Thesis committee:	Dr. ir. J. M. Kuiper,	TU Delft, daily supervisor
	Dr. A. Cervone,	TU Delft, committee chair
	Ir. M. C. Naeije,	TU Delft

An electronic version of this thesis is available at http://repository.tudelft.nl/.
Cover image: Finland imaged by Terra satellite [72]. Render courtesy of Gavin Grant.

TU Delft

Summary

The Deployable Space Telescope (DST) project at TU Delft aims to provide the same image quality as the best current Earth observation satellites with a significantly lowered launch mass and volume. This necessitates the use of deployable optics, and leads to stringent alignment budgets to maintain the diffraction-limited performance. In previous work on the DST, thermal deformation of optical support elements has been found to exceed these limits, leading to decreased performance. Therefore, the need for a thermal shielding baffle has been identified to reduce the thermal gradients in the telescope elements during operations.

Due to the required low launch mass and volume, the baffle has to be deployable. The deployment method was selected with a trade-off. Due to the achievable low mass and stowage volume with an inflatable system, it was selected as the winning concept. The design of the geometry and materials of the baffle was then performed. The structure is formed by inflatable booms of 100 mm diameter and made of a 63 μm thick aluminium-Kapton-aluminium laminate, which can be rigidised after deployment with only the pressure of the inflation gas. The method is based on the plastic yielding of the aluminium sheets while the Kapton remains in its elastic region. The shape of the baffle was chosen to be cylindrical with an octagonal cross section based on analysis of several concepts. Based on thermal model results, the length was iterated, and the final dimensions are 3060 mm of total length and a diameter of minimum 1860 mm and maximum 2120 mm. Thermal insulation is provided by a blanket of 10 layers of multilayer insulation placed outside of the inflatable booms. For stray light control purposes, the inside of the insulation blanket and the booms are covered in a non-reflective black coating.

Thermal analysis of the whole telescope done by Tim van Wees has shown that the inclusion of the baffle reduces the maximum temperatures of all elements below 358 K from previous maxima in excess of 400 K, thus improving the survivability of the DST. The average temperatures after the inclusion of the baffle are all within 4 K compared to the 100 K range without it, meaning that the gradients between the different parts are reduced significantly. The mechanical performance of the baffle was assessed in ANSYS, and it was established that in-orbit static loads or vibrations due to reaction wheels do not endanger the DST operations or the structural integrity of the baffle. The maximum disturbance torque on the spacecraft bus due to the baffle dynamics was found to be approximately 1.4 Nm, which is seen as able to be mitigated by the attitude control subsystem.

Before launch, the whole baffle structure can be folded in a volume of 0.71 m^3 from its 10.2 m^3 enclosed volume when deployed. The mass of the baffle itself is approximately 14.7 kg, with approximately 9 kg added due to the inflation system and additional housing that needs to be added to the telescope bus. The total mass of the telescope is increased to 137 kg from an earlier estimated 126 kg, which already exceeded the 100 kg mass budget. The addition of the baffle increases the total volume of the stowed telescope to 1.8 m^3 from 0.65 m^3, which exceeds the DST volume budget of 1.5 m^3. The design should therefore be iterated to adhere to the engineering budgets.

The end result of this thesis is a feasible preliminary design of a thermal shielding baffle for the Deployable Space Telescope. In the future, more detailed thermal and mechanical modelling should be performed, but most importantly a prototype should be manufactured and tested. Furthermore, the thermal shielding should be optimised for the thermal performance needs.

Preface

This thesis is the culmination of almost six years of studies in Delft chasing a dream. I would not have got here by myself, and I'd like to thank multiple people who contributed to this thesis academically or otherwise.

The greatest gratitude goes out to Hans Kuiper for introducing me to the topic and then letting me run away with it. Massive thanks also to Victor Villalba Corbacho for brainstorming help as well as feedback on this report. Further thanks to Dennis Dolkens for advice on all things DST.

I'd also like to thank Henk Cruijssen and Guus Borst of Airbus Defence & Space on their valuable advice, which helped shape the final design.

A special thanks to the DST team and other MSc students who I've had the pleasure of sharing the master room with. We sometimes even managed to interrupt our coffee drinking with some work.

Lastly, thanks to all my family and friends who helped me have a life outside thesis. Most importantly, I could always count on the support of my family. Kiitos.

E.A. Korhonen
Delft, May 2019

List of Figures

List of Tables

List of symbols

Symbol	Quantity	Unit
C	Amplitude coefficient	[-]
d	Diameter	[m]
E	Young's modulus	[Pa]
G	Shear modulus	[Pa]
h	Engine order	[-]
i	Index	[-]
I	Area moment of inertia	[m^4]
j	Index	[-]
k	Index	[-]
L	Length	[m]
n	Index	[-]
n	Number of moles	[-]
p	Pressure	[Pa]
r	Radius	[m]
R	Radius	[m]
R	Gas constant	[$JK^{-1}mol^{-1}$]
t	Thickness	[m]
T	Temperature	[K]
V	Volume	[m^3]
V_i	Volume fraction	[-]
α	Thermal expansion coefficient	[1/K]
μ	Gravitational parameter	[m^3s^{-2}]
ν	Poisson's ratio	[-]
σ	Stress	[Pa]
σ_h	Hoop stress	[Pa]
σ_l	Longitudinal stress	[Pa]
σ_y	Yield stress	[Pa]
ω	Frequency	[Hz]
ω	Angular velocity	[s^{-1}]
Ω	Rotation speed	[Hz]

Abbreviations

Acronym	Meaning
ADCS	Attitude determination and control subsystem
ADS	Airbus Defence & Space
AHP	Analytic hierarchy process
BOL	Beginning-of-life
CAD	Computer-aided design
CGG	Cool gas generator
CSG	Centre Spatial Guyanais
CTE	Coefficient of thermal expansion
DST	Deployable Space Telescope
EO	Earth observation
EOL	End-of-life
FEM	Finite element modelling
FORTA	Fast Optical RayTrace Application
GSD	Ground sampling distance
HST	Hubble Space Telescope
IAE	Inflatable Antenna Experiment
ITAR	International Traffic in Arms Regulations
IXO	International X-Ray Observatory
LDEF	Long Duration Exposure Facility
LEO	Low Earth orbit
LEOP	Launch and Early Orbit Phase
MLI	Multilayer insulation
MTF	Modulation Transfer Function
M1	Primary mirror
M2	Secondary mirror
M3	Tertiary mirror
PMAO	Primary mirror active optics
PMSS	Primary mirror support system
PSF	Point Spread Function
RF	Radio frequency
RPM	Rounds per minute
SMC	Shape memory composite
SMSS	Secondary mirror support system
TCS	Thermal control subsystem
TRL	Technology readiness level
WBS	Work breakdown structure

Contents

1
Introduction

This chapter will introduce the Deployable Telescope (DST) project and the contribution of the thesis in its context. The aim is to provide the reader with general knowledge of the framework of the thesis, as well as the work previously done for the project. Based on this groundwork, the development of the design work can then begin.

First, the Earth observation market is briefly discussed in Section 1.1. Then, the aim of the DST is presented in Section 1.2. The need for this thesis and the research question are expressed in Sections 1.4 and 1.5, respectively.

1.1. Earth observation market

Remote sensing Earth observation (EO) data in the visible spectrum has a wide variety of uses, both military and commercial [24, 58]. Imaging the surface of the Earth with a high resolution provides accurate maps, but other information can be derived as well. Satellites are widely used to monitor, for example, weather and agricultural conditions. Disaster management also benefits from good quality Earth observation data. The global need for this data is only going to increase in the future, which creates the necessity to provide EO instruments and satellites with ever increasing coverage and resolution. The size of the EO market keeps increasing, with the data market having a value of 1.6B USD in 2014 [36]. The trend since 2005 can be seen in Figure 1.1. Of this, 63% is data used for defence purposes. The main non-defence uses are monitoring of natural resources and infrastructure development.

The development recently has been towards smaller ground sampling distances (GSD) to be achieved from orbit [24]. The best resolution commercial Earth observation imagery is currently being provided by DigitalGlobe. Their WorldView-3 and WorldView-4 satellites can provide a panchromatic spatial resolution of 31 cm, which means that very small details can be distinguished. The satellite mass required to achieve this performance, however, is high. The WorldView-4 has a mass of 2600 kg, and the other DigitalGlobe satellites are in the same class [25]. A size reference showing how large WorldView-4 is can be seen in Figure 1.2. The development and launch of these state-of-the-art Earth observation satellites is predictably expensive. The development, manufacturing and launch of WorldView-4, for example, is estimated to have cost 835 million USD [1]. The launch cost increases the total expenses significantly, as only one such large spacecraft can be launched at a time. The launchers used are also on the expensive side, for example for the WorldView satellites the Atlas V has to be used. The possibility of dividing the launch cost by developing smaller space systems is therefore lucrative.

The Deployable Space Telescope project has started at TU Delft for this purpose, and it will be discussed in the following section.

1.2. The Deployable Space Telescope aim

In this section the goal of the Deployable Space Telescope project is given along with the top level system requirements derived from it. First, a need for a deployable space telescope capable of providing high resolu-

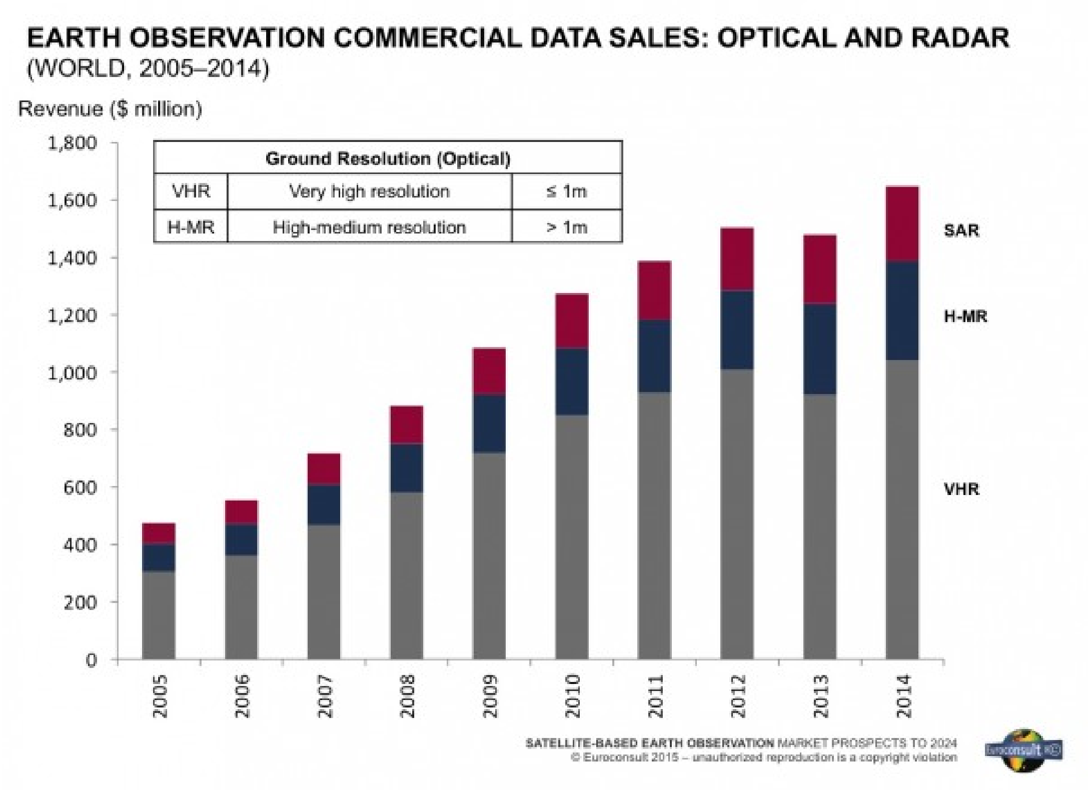

Figure 1.1: Development of Earth observation data market [36]

tion imagery can clearly be seen from the previous section. This leads to the following:

Need statement

There is a need for Earth observation telescopes that provide high-resolution images at a lower launch cost than current systems.

The Deployable Space Telescope aims to fulfil this need. This is done by developing a deployable telescope, which will have a significantly lower launch volume and mass than the current state-of-the-art systems. This is achieved by deploying the primary and secondary mirrors of the telescope in orbit to reach a high aperture size while limiting the volume taken by the telescope during launch. The mission statement that describes the goal of the project can then be expressed as below.

Mission statement

The goal of the DST project is to design a deployable telescope for Earth observation that is capable of the same ground resolution as current systems with a significantly lower stowed volume and mass.

The successful completion of this goal requires a break-down of the different aspects into distinct goals. The following requirements have been developed by D. Dolkens for the overall DST system performance [26]:

REQ-1 The ground sampling distance of the instrument shall be equal to 25 cm in the panchromatic band from an orbital altitude of 500 km

REQ-2 The swath width of the instrument shall be 1 km (threshold) / 5 km (goal)

REQ-3 The system shall have one panchromatic channel and four multispectral bands with the wavelength ranges and GSD indicated in Table 1.1.

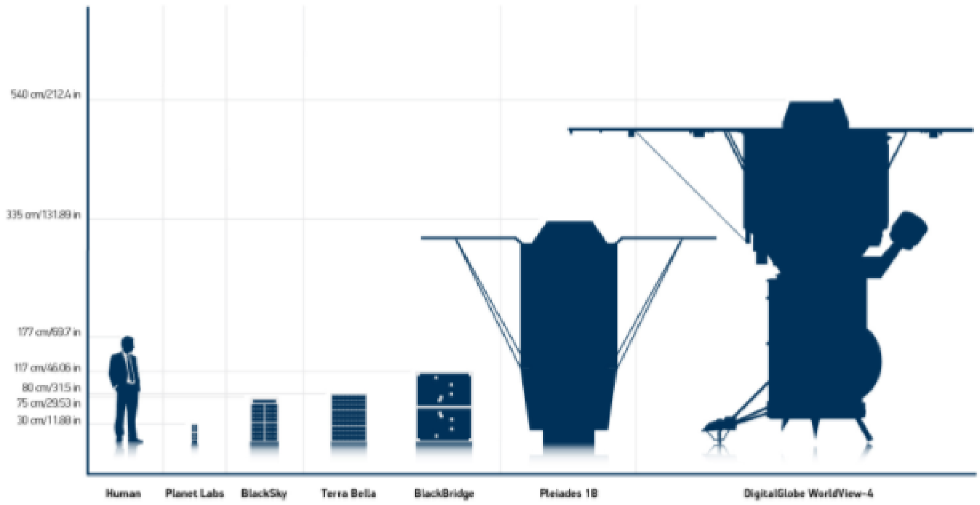

Figure 1.2: Size comparison of WorldView-4 [25]

Table 1.1: Required spectral bands of DST and their ground resolutions

Channel	GSD (@500 km)
Panchromatic (450-650 nm)	25 cm
Blue (450-510 nm)	100 cm
Green (518-586 nm)	100 cm
Yellow (590-630 nm)	100 cm
Red (632-692 nm)	100 cm

REQ-4 The Signal-to-Noise Ratio (SNR) of the instrument shall be higher than 100 for a reflectance of 0.30 and a Sun zenith angle of 60°

REQ-5 The nominal Modulation Transfer Function (MTF) at both the Nyquist frequency and half the Nyquist frequency shall be higher than 5% (threshold) / 15% (goal)

REQ-6 After calibration, the residual Strehl ratio of the system shall be higher than 0.80

REQ-7 The mass of the instrument shall be lower than 100 kg (threshold) / 50 kg (goal)

REQ-8 In the stowed configuration, the volume of the instrument shall not exceed 1.5 m^3 (threshold) / 0.75 m^3 (goal)

These top level requirements need to be met with the optical and mechanical design of the DST. For every subsystem, further requirements flow down from these top level aims of the telescope. The overview of all generated requirements is maintained in a project systems engineering file. The work done so far to meet the performance goals of the system by subsystem design will be the topic of the next section.

1.3. Status of the DST

This section aims to provide the necessary background information to introduce the context of the design work to follow in this report, as well as introduce the current status. The organisation of the DST project team is discussed in Subsection 1.3.1. The architecture of the DST is shown in Figure 1.3, which was made by S. Pepper. This diagram give an overview of all the included subsystems and elements, even those that have not been designed yet. In the following paragraphs, more detail is given on the work that has been done so far. The optical and mechanical design work done so far will be briefly discussed in Subsections 1.3.2 and 1.3.3 respectively. Due to the work in this thesis not being a direct continuation of previous design work, only a brief overview will be given for conciseness.

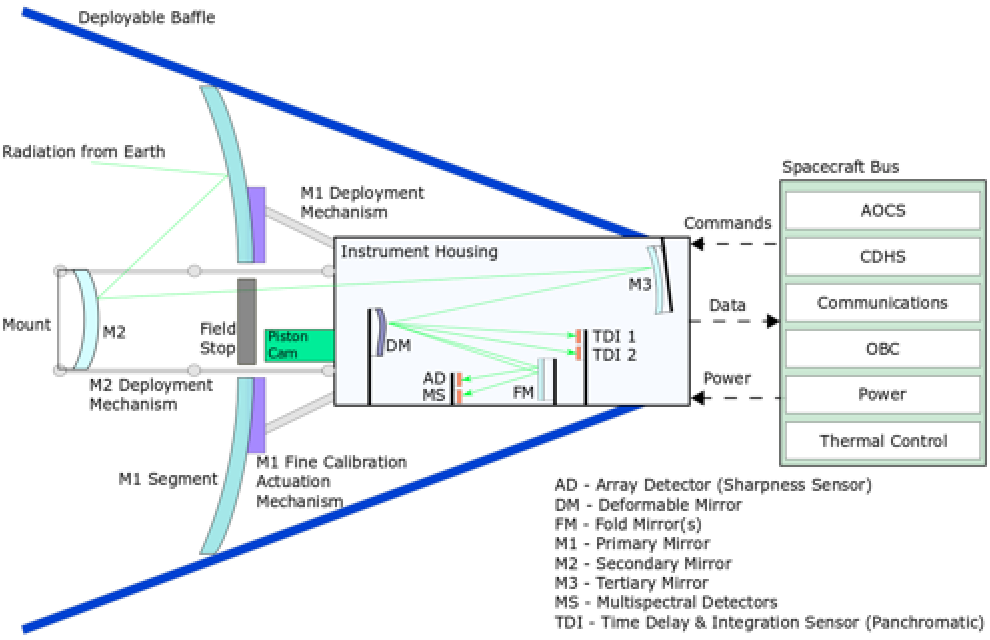

Figure 1.3: Architecture of the DST (courtesy of S. Pepper)

1.3.1. Organisation

The DST project has involved various MSc students who have graduated with a topic improving the design of the telescope. At the current time, multiple students are also working on their MSc or PhD theses on topics varying from optics to mechanical and thermal design. The structure of the team can be seen in Figure 1.4 with the former and current team members as well as the industry connections. In the following sections, the design choices made so far to meet this goal are presented to provide the context for the work done in this thesis.

1.3.2. Optical design

The telescope configuration as well as the overall optical design are the responsibility of D. Dolkens. The telescope currently has an annular-field Korsch three-mirror anastigmat design (as seen in Figure 1.5a [27]). The layout of the focal plane can be seen in Figure 1.5b. In the MSc thesis of G. van Marrewijk, an aberration correction system for the DST was developed [98]. This includes the addition of a deformable mirror at the exit pupil of the telescope as well as a stochastic gradient descent algorithm for optimisation of image sharpness. Further improvements in the optical performance were provided by D. Risselada, who developed a phase diversity algorithm in his MSc thesis [81].

For the optical design of the DST, a specialised ray tracing software called FORTA (Fast Optical RayTrace Application) has been written by Dolkens [27]. This program is written in MATLAB and will also accept mechanical inputs from ANSYS to provide ray tracing based on given deformations of the telescope. The interface between the two programs is still being developed, but promising results have been acquired for more simple optical systems [27]. FORTA is especially built to be used for segmented telescope systems such as DST, as the motion of each mirror segment can be modelled separately. It offers significant advantages in efficiency when compared to performing the same analyses with Zemax. The results that can be obtained from FORTA include the Point Spread Function (PSF) and the Modulation Transfer Function (MTF), both of which can be used as parameters for image quality when comparing the different (optical or mechanical) designs.

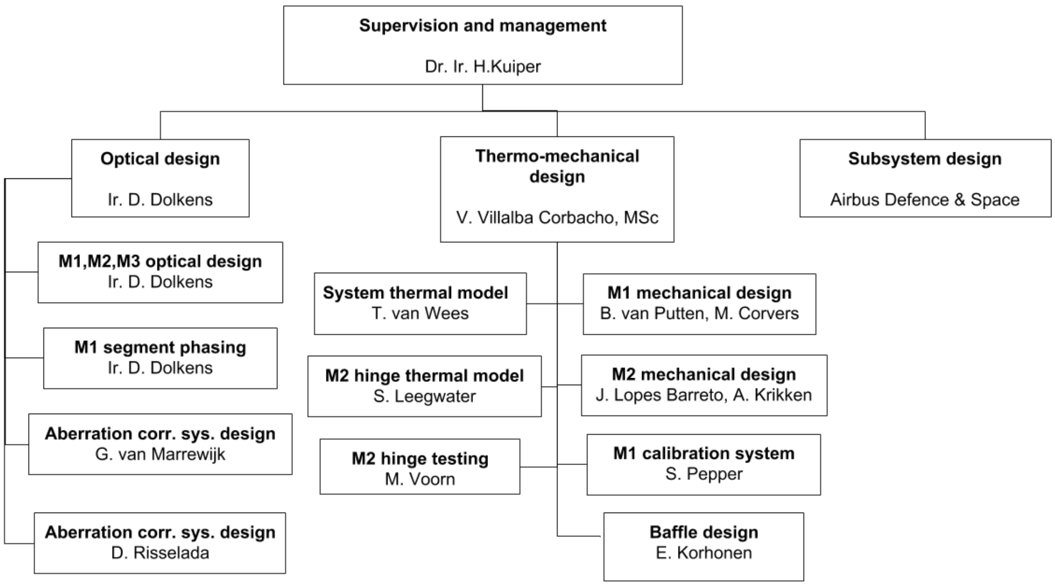

Figure 1.4: Organisational structure of the Deployable Space Telescope project

1.3.3. Mechanical design

This section gives an overview of the mechanical design of DST, which is the main driver for the need of this thesis. Only the design is explained here, and the next section gives the full reasoning of the thesis work.

The main reason for the state-of-the-art design of the DST are the deployable primary and secondary mirrors. The mechanical design of the telescope has so far focussed on the form and deployment of the mirrors. At this stage, the primary mirror (M1) consists of four independently deployable segments, and the secondary mirror (M2) is deployed by four articulated booms. Both the primary and secondary mirror deployment mechanisms have gone through two design iterations in consecutive work of MSc students. The M1 mechanism of B. van Putten [99] was redesigned by M. Corvers [23] in his work, and the current design consists of a kinematic interface that deploys the mirror segments. The calibration of the M1 segments was the topic of S. Pepper's MSc thesis, where he developed a fine actuation mechanism [76]. Articulated booms were selected by J. Lopes Barreto [11] for the M2 deployment, and the concept was refined by A. Krikken [61]. The two mirror mechanisms are now connected to each other with ribbons for increased stiffness. The most recent configuration in July 2018 can be seen in Figure 1.6, made by A. Krikken [61].

Testing of the DST mechanisms has been begun by M. Voorn, who wrote his MSc thesis on the hysteresis testing of the CORE hinges designed by Krikken [105]. The thermal modelling of these hinges is being performed by S. Leegwater, meaning that the CORE hinges will be the best known single component in the telescope. In the future, further testing of various systems is expected to occur, leading to an increased knowledge of the expected performance of the whole system. A thermal model of the whole telescope is being developed by T. van Wees.

As of the writing of this thesis, the total mass of the DST is estimated as 127 kg (including an estimate for the not yet designed baffle) and the dimensions in stowed configuration are 767 mm × 767 mm × 1100 mm, leading to a volume of 0.647 m^3. This means that there is volume left for the addition of the baffle system, but the mass budget defined in Section 1.2 has been exceeded prior to the start of the work.

1.4. Thesis need

As seen in the previous sections, the Deployable Space Telescope project has progressed from the MSc thesis of Dolkens to a more detailed design for the M1 and M2 deployment and optical correction methods, and in

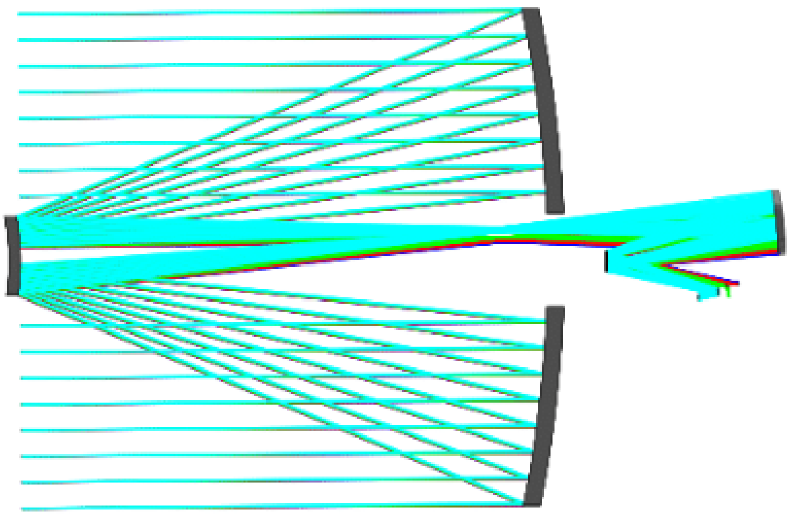

(a) Ray diagram of the Korsch telescope

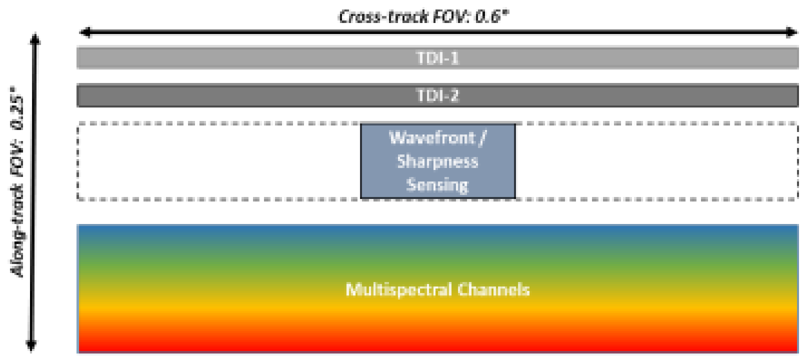

(b) Focal plane of the DST

Figure 1.5: Annular-field Korsch three-mirror anastigmat diagram (a) and the focal plane of DST (b) [27]

almost all the previous mechanical work the need for a baffle has been presented. This is due to the thermal deformations of the designed systems being beyond the tolerances required by the diffraction limited optics as a result of the low Earth orbit (LEO) thermal environment. The stabilisation of the temperatures in the telescope is a primary concern for the success of the project. It is even identified by M. Corvers that active thermal control is required for meeting these tolerances [23]. For this reason, it is important to design a baffle at this stage of the overall telescope design to constrain the thermal environment.

From the above, the justification for the deployable baffle is clear. The need statement for the baffle design can then be formulated as follows:

The Deployable Space Telescope needs a baffle to reduce the effect of thermal gradients in the optical elements

The mission statement follows from the need statement as well as the discussion in the previous section, and describes the goal of the project. It is given as follows:

The goal of this work is to design a baffle to shield the Deployable Space Telescope from sunlight

While the mission statement provides the aim of the thesis, there are also restrictions that need to be considered. These will be a part of the research question developed in the following subsection.

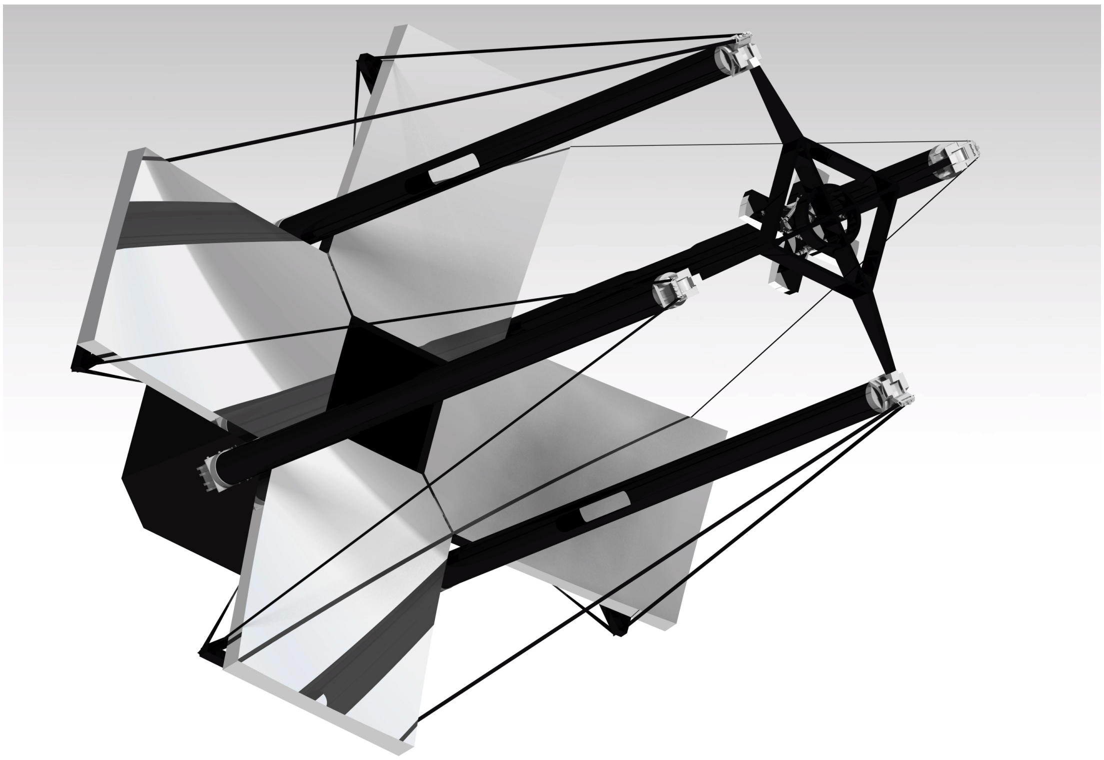

Figure 1.6: Render of the deployed mechanical design of the DST from MSc thesis of A. Krikken [61]

1.5. Research question

Separately from the mission statement, a research question will be formulated to guide the thesis work. The answer to the question will be found as a result of the research documented in this report. The research will be conducted in the framework of the Deployable Space Telescope project, which leads to the necessary inclusion of the overall systems engineering aspects of the project into this work. The design of the DST is based on the already discussed high performance at low mass and volume, which leads to multiple restrictions on the design of all elements. Based on this, the following research question is formulated:

Can a baffle be designed to provide the required thermal stability for the Deployable Space Telescope while staying within the engineering budgets?

The rest of this work aims to prove the feasibility of designing such a baffle by developing a concept that fulfils the need. The methodology used to answer this question will be presented in the following chapter.

2

Project overview

This chapter will explain the background of the problem as well as the approach that will be used to solve it during the thesis project. In Section 2.1 the problem and need for the deployable baffle are given. The functions to be fulfilled by the system are derived in Section 2.2 and the reference frame used in the thesis is explained in Section 2.3. Requirements are then derived in Section 2.4. The work packages are given in Section 2.5.

2.1. Problem description

In this section, the need for the deployable baffle will be elaborated on, to provide sufficient information for the derivation of the requirements and the plan for the thesis work. First, the currently known thermal environment of the DST will be explained. Then, some general aspects of thermal effects on spacecraft in LEO will be explored to identify needs and challenges for the design. Based on these two sections, the scope of the work in this thesis will be defined.

2.1.1. Deployable Space Telescope thermal environment

In this section, thermal environment requirements identified for the DST will be given as the design of the baffle needs to help achieve them. Only the deployed configuration will be considered, as protecting the telescope elements during the Launch and Early Orbit Phase (LEOP) would constrict the design space of the baffle significantly and is therefore left outside the scope of this thesis.

First, the sources of heat fluxes are identified briefly. In the LEO environment the DST operates in, the main contributors are the Sun and the Earth. Solar flux consists of UV, visible and IR radiation, and is highly variable over the orbit as the telescope will enter and exit eclipse frequently. Earth albedo is crucial for the functioning of the telescope, as it is technically what is being imaged. However, albedo radiation from outside the telescope's field of view is harmful for both the thermal environment and the optical imaging quality. Earth also radiates in infrared, with the flux depending on its surface temperature. This radiation is received by DST over the whole orbit, unlike the albedo which varies with the lighting conditions. In addition to these main sources of heat, internal heat dissipation from the telescope elements is also always present. However, preventing this is not possible with a shielding structure. The magnitudes of the fluxes are not relevant for this work, as only the mechanical design will be performed due to the thermal model being concurrently developed by T. van Wees. The blocking of solar flux is the main concern for the baffle, but the stray Earth albedo should also be minimised to the best capability.

At the moment of writing, the thermal environment of the DST is only approximately defined. The design will be based on operating at room temperature (298 K), which is the design point for all the subsystems. Achieving exactly this temperature is not necessary, however. The challenge of the thermal control design is achieving a stable temperature during operations and minimising thermal gradients on all telescope elements that partake in imaging, most importantly the M1 and M2 support systems. The allowable temperature variation has been defined as ± 1 K, and all mechanical elements are designed around tolerating this variation. In mechanical terms, thermal deformations are then within the allowable limits (as defined by optical

Table 2.1: Survival temperatures of certain DST elements

Part	Temperature range	Requirement ID
M2 support booms	< 473 K	M2-THE-02
PMAO universal joints	298 ± 2285 K	PMAO-THE-01
PMAO in-plane constraint flexures	298 ± 318 K	PMAO-THE-02
PMAO moving frame plate	298 ± 442 K	PMAO-THE-03

budgets) and image quality remains above the requirement. In reality, meeting this stability requirement can be very challenging depending on e.g. the orbit of the satellite. Due to the current placement of the DST in a low Earth orbit, the temperature variations are large. The thermal model of the whole telescope on a subsystem level will be made by T. van Wees, and the results will be used in this report for accurately characterising the thermal environment.

The primary concern when it comes to the temperatures encountered by the telescope is naturally whether they can be survived by all the elements. In general, the requirements for this are determined by the material choices. A few quantified values exist from prior design work on the telescope, and they are shown in Table 2.1. The requirements are taken from the internal DST project requirement document.

These temperature range requirements are quite lenient and the main concern at this stage is the M2 boom temperature, as it has the lowest maximum identified so far. The analysis of temperatures on the DST during operations will be the topic of another MSc thesis, worked on by T. van Wees. The results will be shown later on in this report, as far as they relate to the performance of the baffle.

The need for a baffle stems largely from the alignment budgets of the optical elements for maintaining the image quality. The values for the allowable mechanical deformations are given in Table 2.2. There are naturally various sources of deformation that affect meeting these budgets, but thermal effects are the relevant topic for this work. However, while the translation of mechanical deformation into temperature differences in the system could be possible with a full thermo-mechanical model, this does not currently exist and therefore allowable thermal deformations are not defined for each element. The design work of some subsystems has been based on meeting the optical budgets with a ±1 K temperature gradient. Therefore, if this temperature stability is met, the alignment budgets should be met based on the design.

Table 2.2: Stability budgets of the DST mirrors

Element	Position [μm]			Tilt [μrad]		
	X	**Y**	**Z**	**X**	**Y**	**Z**
M1	$5 \cdot 10^{-3}$	$5 \cdot 10^{-3}$	$5 \cdot 10^{-3}$	$2.5 \cdot 10^{-3}$	$1 \cdot 10^{-2}$	$1 \cdot 10^{-1}$
M2	1	1	$5 \cdot 10^{-1}$	1.5	1.5	3

The preliminary design work for the thermal control subsystem (TCS) is being done by T. van Wees. The baffle structure is a part of the TCS due to its function, so there is some design work done for the baffle in the thesis of van Wees. The suggestions obtained in that work will be taken into account in this work, insofar as they are possible to implement.

2.1.2. Thermal effects on spacecraft

Thermal control of space telescopes is known to be both complex and absolutely necessary to achieve the wanted performance. Examples include the need to cool infrared telescopes to temperatures of a few K to minimise stray radiation from the telescope elements themselves. In case of an optical telescope, as is discussed in this thesis, the telescope temperature does not affect the imaging quality in the same manner, but there are other important aspects to be considered. Thermal stability, disturbances and survival will be discussed in the following paragraphs.

Thermal effects on space telescopes have been historically been observed to be a cause of major concern for operations. The main effects of variable temperatures over the orbit are listed below[57]:

- Thermal bending
- Thermal shock
- Thermally-induced vibrations
- Thermal flutter

All of the disturbances result in torques imposed on the spacecraft as a result of thermal deformation. Thermal bending results from slowly changing temperature gradients and is quasi-static in nature [57]. The excessive misalignments of optical elements calculated in previous DST work are generally due to this kind of deflections. Therefore, the minimisation of thermal gradients in the mirror support systems is an obvious design goal for the baffle. Since the subsystems are designed around a 1 K variation in temperature, this is the required stability. However, the other disturbance modes need to be considered for the baffle itself. Out of the above disturbance modes, the dynamically unstable flutter is considered unlikely to occur except for specific cases of long gravity gradient booms, and it will therefore not be discussed further[57]. Thermal shock (also known as thermal snap) is caused by rapidly changing temperature of a structure, heating or cooling. Vibrations are a consequence of the quasi-static deflection and oscillation from superposition, and are a dynamically stable disturbance. Both of these are associated with deployed appendages, such as booms and solar arrays [57, 94]. The phenomena can therefore be induced by the baffle design itself, leading to disturbance torques that need to be mitigated by the attitude control subsystem.

A famous example of the thermally-induced vibration is the low frequency vibration observed on the Hubble Space Telescope (HST) as a result of thermal gradients in the solar array support booms upon exiting and entering eclipse. The temperature difference across the booms rapidly became 30 K, leading to a tip deflection and subsequently time-varying disturbance torques. The issue caused the operational pointing stability to decrease below the requirements of the HST, and required corrections in the flight software to account for the vibrations. Ultimately, the solar arrays were replaced during a servicing mission [43]. While the aim of this work is to design a baffle to shield the telescope itself and not take into account the (currently not designed) spacecraft bus, the probability of such effects on the DST needs to be minimised. The orbits of DST and HST are similar, meaning that the thermal environment encountered is comparable. Therefore, the effects of the baffle on the attitude determination and control subsystem (ADCS) will be evaluated to see if the attitude control budgets need to take thermal deformation of the baffle into account. The possibility of thermal snap will also be assessed.

Another important aspect of thermal shielding is ensuring the survival of all satellite elements in the extreme temperatures encountered over the lifetime. It has been found by S. Pepper and A. Krikken that the critical thermal case for survival occurs prior to deployment of the mirrors and baffle in LEOP, while operational maximum temperatures are more modest [61]. Since the baffle structure will be deployable and therefore possibly not able to be present during LEOP, this issue is not trivial and can prove fatal for some telescope elements. Extreme temperatures during operational conditions will most likely be easier to mitigate, and this is one of the aims of the baffle design. On the other hand, the baffle structure itself needs to survive the range of temperatures it is exposed to, so the design needs to take into account the fact that the baffle is the system most exposed to the extreme thermal conditions over the orbit. This will play a role in both the structural design and the material selection.

In conclusion, the main functions that the baffle has to fulfil can be written as follows:

1. Provide stable operational temperature and decrease thermal gradients
2. Protect telescope elements from extreme temperatures over the orbit
3. Avoid generating large thermal disturbance torques

2.1.3. Scope of the work

In this section, the scope of the thesis will be expanded upon. The aspects that will not be addressed are explained, and the level of detail that will be gone to is also discussed. The actual work to be done in this report will be shown separately in Section 2.5.

The end result developed will be a conceptual design of a thermal baffle for the Deployable Space Telescope. As many aspects as possible will be addressed regarding the geometry, materials, deployment process and expected performance. This however means that the level of detail will be generally quite low. This thesis will provide a feasibility study of sorts into integrating a deployable baffle on the DST and its effect on the engineering budgets as well as the thermal environment. Hopefully, the resulting design can then be verified and developed further in the future.

The design will be based on the operational conditions and not take into account extreme temperatures experienced by the other telescope elements prior to deployment. This decision is based on the relatively short amount of time available for thesis work as well as the emergence of the issue after design was already under way. The major deficiency in thermal protection over the whole mission duration is acknowledged and left for future research.

The baffle will be designed to minimise the received flux of solar radiation as the main priority. Due to the nature of the project, i.e. Earth observation, Earth albedo and infrared radiation cannot be prevented from affecting the telescope's thermal environment. In thermal models of the DST, it has been found that the effect of the Earth radiation is non-negligible, but it cannot be excluded without blocking the optical path. Accordingly, the baffle design done in this thesis will not attempt to protect the telescope from thermal effects due to Earth flux. Solar flux, on the contrary, will be minimised as well as possible.

Stray light prevention is an important aspect of most telescope baffling structures. It was found that optical design of the baffle would expand the scope of the work too much and therefore no detailed analyses will be made on the stray light behaviour. However, that does not exclude considering stray light control in the design on the general level, which will be done at all relevant stages. It will be ensured that the stray light received by the mirrors is not increased due to the inclusion of the baffle at the minimum, but will preferably be reduced. Since no measure of the stray light exists at this stage, the actual performance in this regard will be the subject of future opto-mechanical work.

2.2. Baffle functions

This section serves as an aid for the following sections. To aid in requirement development, functional flow and functional breakdown diagrams have been created. The former shows the functions the baffle has to fulfil in chronological order, and the latter expands those functions with sub-functions in a hierarchical structure. The requirements for the system can then be derived more easily, and it is ensured that all functional requirements are taken into account from early on. This also provides traceability to the requirements, as they come from functions that need to be performed in order for the mission to be successful.

The functional flow diagram can be seen in Figure 2.1. There are five main functions to be fulfilled by the baffle, shown in order of operations. In principle the last two functions, operations and space environment survival, are performed simultaneously for the whole duration of the mission, but they are shown in succession for clarity. From the functional flow, a functional breakdown can be developed. For each main function, sub-functions are generated to guide the design process in an organised way. The resulting diagram is presented in Figure 2.2. The sub-functions shown could be still further broken down into more detailed functions, but this will be left for the following section. There, the requirements derived from these baffle functions are given and explained. For each functional block, requirements will be made.

2.3. Reference frame

The reference frame used in this thesis report is shown here for clarity. It will provide the source for the terminology used when discussing dimensions and orientations throughout the report.

The origin of the reference frame is at the middle point of the bottom plate of the instrument bus, as it is initially foreseen that the baffle will be integrated at the bottom of the bus. The x- and y-axes are defined as shown in Figure 2.3, parallel to the plane of the bus bottom. The left-handed reference frame is completed by the positive z-axis pointing towards M2 (not pictured). Note that in the figure the z-axis is drawn outside the bus for clarity, while in reality it passes through the centre point of M1. In general, the exact orientation of the x- and y-axes is not as important as their plane.

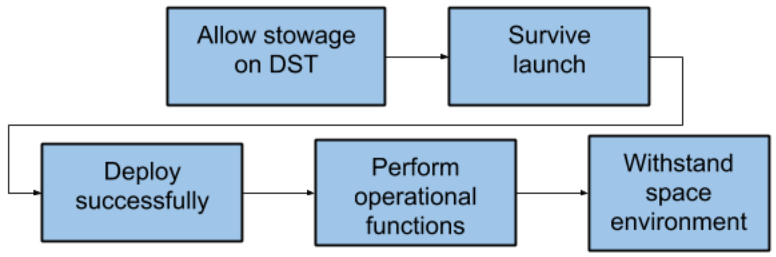

Figure 2.1: Functional flow diagram for the DST baffle

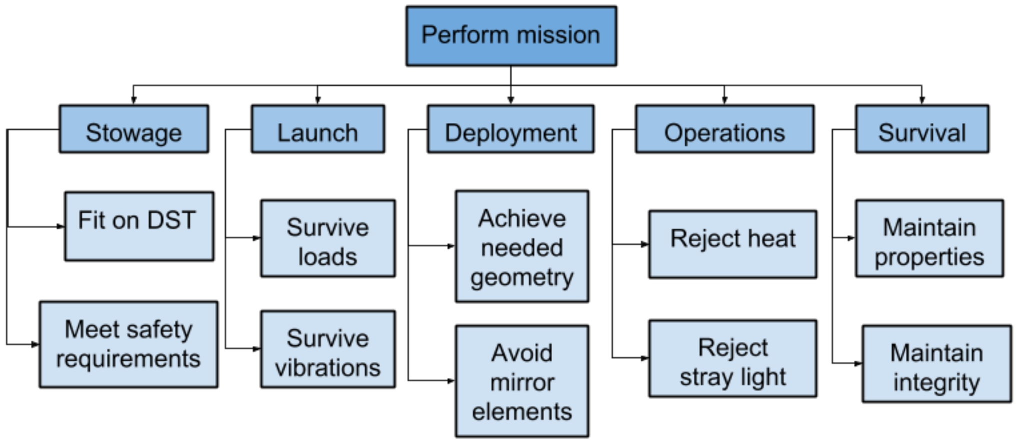

Figure 2.2: Functional block diagram for the DST baffle

When discussing elements of the baffle system, other directional terms are also used. Anything described as **longitudinal** will be parallel to the z-axis. Accordingly, length of the baffle is defined as the dimension along this axis. On the other hand, **lateral** refers to anything parallel to the xy-plane. The cross section of the baffle lies in this orientation. This is also called the radial direction when distances from the origin are discussed, for example.

In the course of the research, other coordinate systems might be used for different baffle elements, but these will be clarified in their respective sections and not included in this chapter.

2.4. Requirements generation

In this section, the justifications for the requirements of the baffle and the requirements themselves are given, together with the appropriate identifiers for each requirement.

In this thesis, the phrase "baffle system" indicates the full mechanism including the whole baffle itself, its

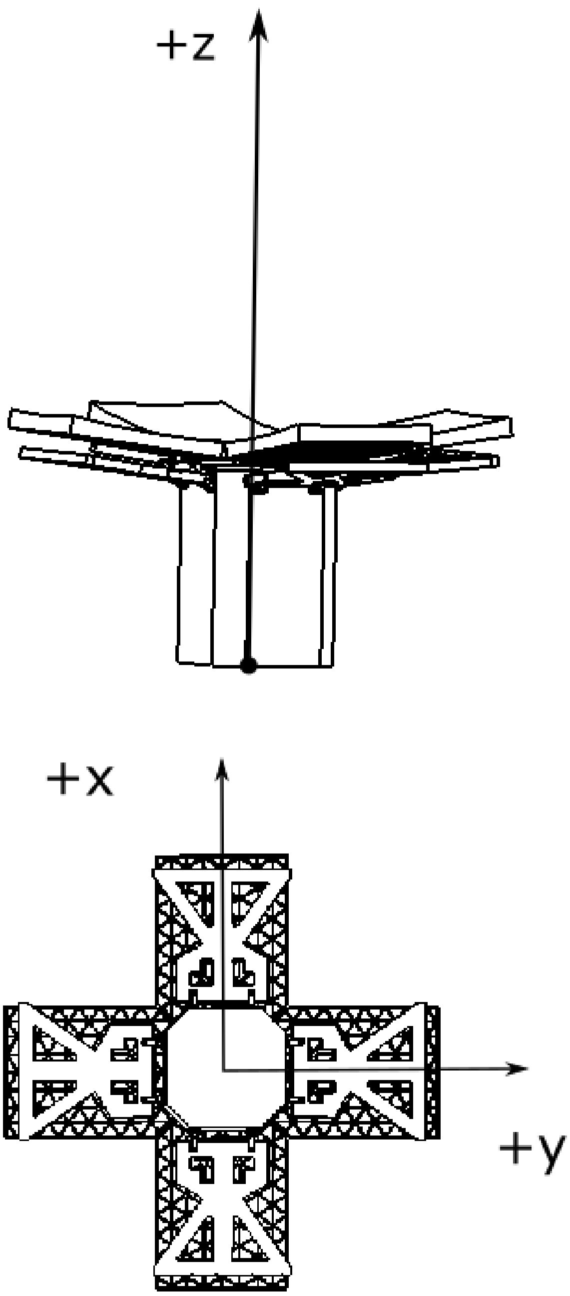

Figure 2.3: The reference frame used when discussing the baffle

interfaces with the telescope and the deployment system. In case a requirement applies to only one or a few parts of the baffle, they are named separately. The requirements given are of the form **BAF-XX-YY-ZZ**, "BAF" specifies the baffle, "XX" is the category of requirement and "YY" the running number for the category, with "ZZ" used if sub-requirements are present. The categories are MEC for mechanical requirements, THE for thermal requirements, STRU for structural requirements, SYS for general DST system requirements and OPT for optical requirements. The requirement ID system is uniform with the DST systems engineering way of classifying requirements for the whole instrument, which explains the need to specify the baffle in the identifier of each requirement.

In the following subsections, the explanations for deriving the requirements are given, divided by the phase of the mission. This is done to organise the section based on the functional diagram of the previous section,

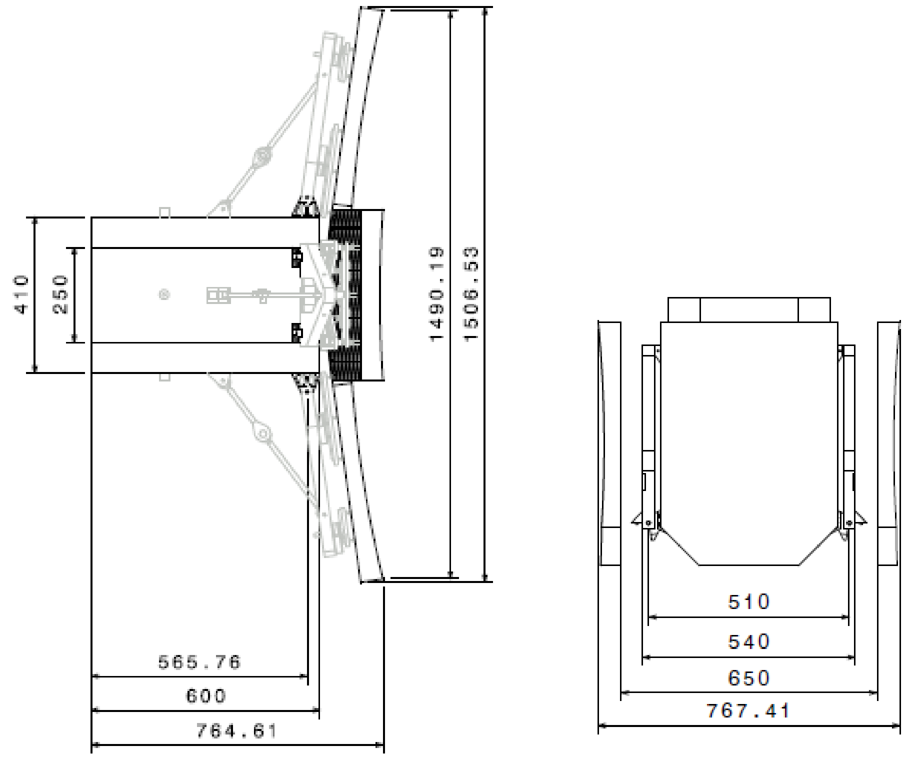

Figure 2.4: Instrument bus and M1 dimensions, all values in millimetres

which helps in covering all the mission aspects without missing any requirements.

2.4.1. Stowage and deployment requirements

This subsection focuses on the requirements on the stowage of the baffle before and during the launch, as well as the deployment after orbital insertion. The baffle is a completely new element on the DST, which means that during its development, other already designed parts of the instrument have to be carefully considered during all mission phases. Most importantly, it needs to be made sure that the baffle will not cause damage to any of the optical elements of the DST, as this would endanger the whole mission. Related to that, the obstruction of any telescope components will quite possibly decrease the imaging performance. This leads to requirements on the safeguarding of the mirrors and other elements from the baffle at all stages.

First of all, it has been defined that the baffle has to be deployable, which gives requirement **BAF-MEC-01**. It has also been determined that the baffle has to be completely attached outside the instrument bus due to its internal volume being taken by the optical systems, which leads to **BAF-MEC-02**. No quantification of the dimensions or attachment mechanisms is given since the instrument bus design is not final and these have an ample design space at this stage.

The stowed volume goal is 0.75 m^3, and by taking the dimensions from Figure 2.4, it can be calculated that the volume currently taken by the stowed instrument is approximately 0.65 m^3, also taking into account the stowed M2 mechanism. This leaves 0.1 m^3 for the baffle outside the envelope of the current stowed configuration, which can be seen to include some empty space already. The threshold stowed volume for the DST is 1.5 m^3, so there is 0.85 m^3 remaining before the highest allowable volume is met. This is the only requirement on the stowed dimensions at this point, but it gives a sufficient starting point for evaluating design concepts based on their performance with respect to stowing volume.

The mass of the whole baffle assembly has to be kept low due to the weight requirements imposed on the whole telescope. No preliminary design exists for a baseline of the mass, which means that the requirement has to be based on other sources. In literature review, the mass of the only baffle structure of comparable diameter is approximately 12 kg, accounting for the difference in total length. This is used for requirement **BAF-MEC-07**, where a 25% margin is added. This requirement might be iterated at later stages, when preliminary information on system weight is available after analysis or prototyping.

2.4.2. Operational requirements

The operational requirements of the baffle system follow from the functions that need to be performed when the telescope is operational in orbit and producing imagery. These have to do with both the thermal and stray light control needs identified in the problem statement of the thesis. Along with these functional requirements, the baffle also has to endure the operational lifetime of the DST without experiencing a significant decrease in the critical properties. This will lead to more requirements.

The thermal stability of the telescope needs to be improved drastically with the included baffle. This has been transformed into requirements on the capability of the baffle to shield the rest of the instrument from radiation in the solar spectrum. While some are unknown at the time, the expected requirements can be identified. First, the required temperature stability of ± 1 K is identified already from the nominal temperature of 298 K, and this is reflected in **BAF-THE-02**. This will require an effective emissivity of the baffle, which is yet to be defined, but is included as requirement **BAF-THE-03**.

The inner surface of the baffle has to absorb the stray light incident on it. This is defined for the wavelength range the DST operates in (450 to 700 nm), since stray light in wavelength regions that are not being measured is not considered a problem. This leas to requirement **BAF-OPT-01**. The absorption efficiency will be based on a stray light analysis at a later stage.

On top of providing the performance, the baffle has to maintain it for the operational lifetime of the telescope. In the thermal model of van Wees, a maximum temperature of 393 K for the baffle has been found, which leads to requirement **BAF-THE-01** for the survival of all the materials. In previous work, a lifetime requirement of 5 years has been presented, and this will be used for the baffle as well. The main requirement **BAF-MEC-08** is then generated. Some degradation of the optical properties is expected during this time, but they are required to stay within a certain value of the BOL values at EOL. This applies to properties such as absorptivity and emissivity and is based on an estimate of reasonable performance that can be expected from space grade coatings. The requirement is given as **BAF-MEC-08-01**. Beside the performance, the baffle has to remain structurally stable for the whole mission duration, and therefore survive e.g. micro-meteoroid impacts without losing integrity. This produces the sub-requirement **BAF-MEC-08-02**. Survival of mechanical loads is covered by requirements **BAF-STRU-02** and **BAF-STRU-03**, of which the first is currently undefined. The survival of the static micro-gravity environment is naturally crucial and will need to be verified for the preliminary design.

The baffle design will be additional to the current state of the DST, which means that it has to conform with the limitations imposed by the existing telescope geometry. It is crucial that the baffle will not interfere with the imaging operations, or damage the optical elements. The overarching requirement for this is **BAF-MEC-06**, which has five more detailed sub-requirements derived from it. These give the clearances from the mirrors during operation that need to be accounted for in the geometrical and structural design process. Firstly, the stowed baffle needs to remain out of contact with the other stowed elements, i.e. the primary and secondary mirrors. This produces requirement **BAF-MEC-06-01**. Even in non-nominal conditions, such as safe mode or when slewing, the clearances have to be maintained. Between the baffle and M1, the distance has to be >100 mm based on operational and safety considerations, as given in requirement **BAF-MEC-06-02** based on discussion within the team. The required clearance leads to the need to deploy the baffle first, in case the deployment it not completely straight, this gives give more margin between the elements. It is not foreseen that this will cause any issue with the current DST deployment process, where M2 and M1 are deployed in a synchronised manner, and it is possible that the presence of the baffle during deployment reduces risks in mirror deployment as the environment is more thermally stable. This leads to sub-requirements **BAf-MEC-06-03** and **BAF-MEC-06-04**. During imaging operations, it is crucial that the baffle structure does not enter the field of view of the telescope and thus obstruct the nominal functioning, which gives the last sub-requirement **BAF-MEC-06-05**.

General requirements on the safety and availability of components also exist. They are known from the previ-

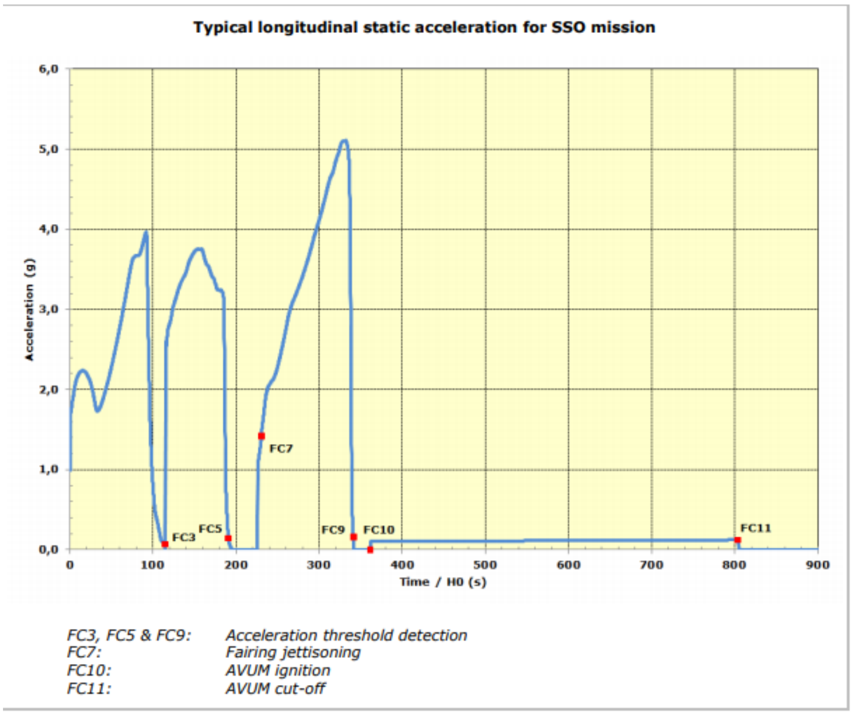

Figure 2.5: Static longitudinal loads of Vega for a typical mission to Sun-synchronous orbit [7]

ous work on the DST, as the requirements apply to the whole telescope and all its individual components. The CSG (Guyana Space Centre) safety regulations are applicable when the use of Europe's space port in Guyana is used for launch operations, which necessitates requirement **BAF-SYS-01**. The purpose of keeping the DST as a European project restricts the use of parts that fall under ITAR, which leads to requirement **BAF-SYS-02**. It is expected that these requirements do not limit the design space of the baffle in any significant way.

2.4.3. Launch requirements

The launcher used to bring the DST to LEO brings its own set of requirements for the baffle performance. A rocket launch imposes both quasi-static and shock loads to the payload, in addition to sine vibrations and fairing separation loads. All of these have to be withstood by the baffle along with all the other instrument elements. Since the baffle will be stowed for the entire duration of the launch, the requirements apply only to that configuration. Multiple launcher options available in Europe are used for generating the requirements. The launcher that will be used is not yet known for the full telescope, but the demonstration mission is planned to be launched on the European Vega launch system.

In addition to the Vega launcher, the Ariane 5 and Soyuz will be considered for launch loads. As the largest launchers in Europe, they are potential candidates for the launch of the DST. The largest loads found will be considered for the deriving of requirements. The longitudinal static acceleration is the first considered load. Tobe completely accurate, these loads are in reality quasi-static, but will be referred to as static. For Ariane 5, this is at maximum 4.55 g, whereas the Vega introduces loads up to 7 g and the Soyuz up to 4.3 g. The clearly smaller lateral static accelerations for these launchers can reach 0.25 g, 0.9 g and 0.4 g, respectively [6–8]. The longitudinal loads for a typical Vega launch into Sun-synchronous orbit are shown in Figure 2.5.

The sinusoidal vibrations are also important to consider, as resonance can occur and the eigenfrequency of the system should be designed so that this cannot happen and cause damage to the system during launch. The longitudinal and lateral sine vibration amplitudes are listed in Table 2.3 for the three launchers. It can be seen that the magnitude of the vibrations decreases at higher frequencies, meaning that the first natural frequency of the baffle should be above approximately 100 Hz, where the amplitude of vibrational loads can be seen to decrease.

Table 2.3: Sine vibration loads for Ariane 5, Vega and Soyuz

Launcher	Frequency band	Longitudinal amplitude (g)	Lateral amplitude (g)
Ariane 5 [8]	2-25	1.0	0.8
	25-50	1.0	0.6
	50-100	0.8	0.6
Vega [7]	1-5	0.4	0.4
	5-45	0.8	0.5
	45-110	1.0	0.5
	110-125	0.2	0.2
Soyuz [6]	1-5	0.4	0.4
	5-10	0.5	0.6
	10-20	0.8	0.6
	20-30	0.8	0.4
	30-40	0.5	0.4
	40-60	0.5	0.3
	60-100	0.3	0.3

The launch, including the separation of upper stages and the payload, introduces shocks to the instrument. It is important that these are also taken into account when the design loads are decided on. The shock loads can go up to 2000 g in case the Vega launch vehicle is used, for the other options the maximum shock loads are 1000 g [6–8]. However, these are not assumed to occur at the natural frequency of the baffle (in the order of 100 Hz as a first estimate), which will be significantly lower than where the highest shock loads are found. Of course, verification will be necessary once the system has been designed and its eigenfrequencies are known through analysis and/or testing.

Based on the expected shock and static loads, as well as the sine vibration behaviour, two requirements have been derived for the baffle regarding launch. These can be found in Table 2.5 under **BAF-STRU-01** and its sub-requirements.

2.4.4. Verification strategy

In this section, the verification approach used for each requirement is given. The approach used at this stage is simplified and only includes identifying the methods that can be used to verify each requirement but not elaborating on the actual procedure yet. There are four fundamental ways to verify that a given requirement is met by the final designed product:

I Inspection - Examining the design by e.g. visually or taking measurements

A Analysis - Using calculations or models to evaluate performance

D Demonstration - Utilising a system function to verify its working

T Testing - Applying specific inputs and observing system response

At least one of these verification methods will be applied to each of the requirements derived in the previous section. Sometimes multiple strategies can and should be used at different phases of the design process. By identifying the methods, it is not only demonstrated that the requirements are verifiable, but it is also found out for which requirements the compliance can be checked at the end of the report. The identified verification methods are listed in Tables 2.4 and 2.5 for each requirement.

Table 2.4: Requirements for the baffle design

ID	Requirement	Parent	Source	Verification method
BAF-MEC-01	The baffle shall be deployable.	-	Volume budget	I
BAF-MEC-02	The baffle system shall be attached to the outside of the instrument bus during stowage and operation.	-	Volume budget	I
BAF-MEC-03	The stowed baffle shall increase the volume of the DST by at most 0.1 m^3 (goal)/ 0.85 m^3 (threshold).	-	Top level requirement	A/D
BAF-MEC-04	The baffle shall have a deployment reliability of min. <TBD> %.			T
BAF-MEC-05	The baffle shall fully deploy within <TBD> seconds.			T
BAF-MEC-06	The baffle shall not obstruct any other telescope elements during any part of the mission.			I/A/D
BAF-MEC-06-01	The stowed baffle shall not be in contact with other stowed telescope elements.	BAF-MEC-04	Internal discussion	D
BAF-MEC-06-02	The deployed baffle shall have a clearance of > 100 mm from M1 in every direction.	BAF-MEC-06	Internal discussion	I
BAF-MEC-06-03	The baffle shall be deployed before the primary and secondary mirror elements.	BAF-MEC-06	Internal discussion	I
BAF-MEC-06-04	The deployed baffle shall not interfere with the deployment of the primary and secondary mirror elements.	BAF-MEC-06	Internal discussion	I
BAF-MEC-06-05	During operations, the deployed baffle shall not enter the field of view of the telescope.	BAF-MEC-06		A
BAF-MEC-07	The total mass of the baffle and its deployment mechanism shall be at most 15 kg.		Literature	I
BAF-MEC-08	The baffle shall survive the space environment for 5 years.		Project requirement	A
BAF-MEC-08-01	The deployed baffle shall survive the space environment for 5 years without a loss in the optical properties of more than TBD.	BAF-MEC-08		A
BAF-MEC-08-02	The baffle shall maintain its structural integrity for 5 years.	BAF-MEC-08	Project requirement	A

Table 2.5: Requirements for the baffle design (continued)

ID	Requirement	Parent	Source	Verification method
BAF-OPT-01	The inner surface of the baffle shall absorb at least <TBD> % of radiation in the wavelength range 450-700 nm.	Stray light		D
BAF-STRU-01	The stowed baffle system shall survive launch.			A/T
BAF-STRU-01-01	The stowed baffle system shall withstand up to 30 g of quasi-static acceleration applied simultaneously in the x- and y-axes in the launcher coordinate frame.	BAF-STRU-01	Launcher	A/T
BAF-STRU-01-02	The stowed baffle system shall withstand up to 30 g of quasi-static acceleration applied simultaneously in the x- and z-axes in the launcher coordinate frame.	BAF-STRU-01	Launcher	A/T
BAF-STRU-01-03	The stowed baffle system shall withstand up to 30 g of quasi-static acceleration applied simultaneously in the y- and z-axes in the launcher coordinate frame.	BAF-STRU-01	Launcher	A/T
BAF-STRU-01-04	The stowed baffle shall have a first eigenfrequency above 100 Hz	BAF-STRU-01	Launcher	A/T
BAF-STRU-02	The deployed baffle shall have a first eigenfrequency above <TBD> Hz.			A/T
BAF-STRU-03	The deployed baffle shall structurally survive the micro-gravity environment.			A/T
BAF-SYS-01	The stowed baffle system shall adhere to the CSG safety regulations.		Project requirement	I
BAF-SYS-02	The system shall not include ITAR restricted components.		Project requirement	I
BAF-THE-01	All baffle elements shall survive temperatures up to 393 K.		Thermal environment	I
BAF-THE-02	The baffle shall provide a temperature of 298 ± 1 K for the DST.			A
BAF-THE-03	The deployed baffle shall have an effective emissivity of at most <TBD>.		Thermal control	T

2.5. Planning

In this section, the planning of the thesis is given in the form of a breakdown of the work to be done. These will be presented to orient the reader to the rest of the report and to justify the approach used for the structuring of the design process.

The tasks to be done are identified as a succession, based on the expected logical order of design steps. The order and the justification are given below:

1. **Requirement generation**
   The design process cannot be started without first generating all the requirements that define the design space. This work package will begin with the definition of the functions that need to be performed by the system. From these, the requirements for the whole mission will be derived. The top level requirements of the DST will be adhered to at all times to make integration possible. The end result of this task is the complete set of requirements for the deployable baffle.

2. **Deployment method concept**
   The stowage and deployment of the baffle are the most critical functions for the feasibility of the design. This is why the concept for the deployment is selected first, before designing for the performance requirements. The process consists of collecting concepts and trading them off based on specific criteria, which are also developed in this work package. The end result of this work package is the concept for the deployment method, based on which the actual structure can be designed.

3. **Shape selection**
   This continues on the work after the deployment concept is known by developing the baffle further. It is thought that the shape should influence the materials used and not the other way around in this case, since it is assumed that the required geometry is a larger driver for the budgets. First, possible shapes of the baffle are identified based on the deployment method. Then a selection is made based on the adherence to engineering budgets as well as feasibility.

4. **Material selection**
   The material selection will be done based on the designed geometry and the possibilities and limitations it provides. Then, the meeting of the engineering budgets can be accounted for by a proper selection of material properties.

5. **Performance analysis**
   The performance of the baffle in mechanical aspects is assessed by means of computer modelling. This requires getting acquainted with software such as CATIA and ANSYS before starting. Then, different load cases are defined and imposed on the structure. Thermal results will be obtained from the thermal modelling work of T. van Wees and applied as far as possible. Iterations in the design are made based on the results, if applicable and feasible.

6. **Integration**
   The integration of the baffle onto the DST is designed conceptually in this thesis. The attachments to the spacecraft bus need to be determined in both stowed and deployed states, as well as the possible effect on the instrument bus design. The stowing method used for the baffle will also be determined which defines the stowed volume of the baffle and, by extension, the whole telescope.

Each of these topics will constitute a chapter in this thesis, except the generation of requirements which was already done in this chapter. The rest of this report will therefore consist of the completion of the tasks defined above.

3 Deployment concept

This chapter will lead to the selection of the deployment concept to be used for the baffle. The choice will be made based on a trade-off between different concepts that have been found in literature during previous research. The concepts that are considered will be generated in Section 3.1 and explained further with examples in Section 3.2. Trade-off criteria and their weights will be derived in Section 3.3 and the trade-off will be performed in Section 3.4. Based on the result of the trade-off, a conceptual model will then be developed in the rest of the thesis report.

3.1. Generation of concepts

In this section the concepts that will be traded off are generated by means of a concept tree. No preliminary design work is done, since the concept of deployment is considered the first priority to choose before any design choices specific to the DST are made. Concepts that are not considered further will also be identified.

3.1.1. Deployment concept tree

In this section the deployment concepts generated during the literature study and early stages of the thesis work are presented. As a result of previous literature study as well as consultations with both DST project members and external staff, various deployment mechanisms have been identified for possible use on the baffle system. Some of the generated concepts are outright infeasible within the context of the engineering budgets of the telescope, and others are very complex which makes them unattractive for the scope of the thesis. However, several mechanisms have been found which are technically possible to develop based on the maturity level and ease of implementation. For completion, the full tree of developed concepts has been included. It is divided by the mechanism of deployment, and these are subdivided based on whether it is possible to have one or multiple such deployable elements to deploy the whole baffle structure. This division is a result of the discovery of the fact that the baffle cross section does not need to be circular to attain the required stray light performance. In an earlier stage of the thesis project, the assumption was made that the baffle needs to adhere to a constant, circular cross section along the full length, which vastly limited the number of available concepts. As of the time of writing, it is as acceptable to use e.g. multiple deployable booms in a polygonal arrangement which pull up a light-shielding shroud, which then forms the functional part of the baffle.

The generated concepts are presented in Figure 3.1. The concepts are not yet ranked in any manner, as the options are only being introduced. The descriptions of the mechanisms are given in the next section.

Beside the concepts listed in the concept tree, combinations of different deployment mechanisms are also possible unique concepts. They will not be considered separately for the trade-off, since the aim of this selection is to determine only the suitable method(s) of deployment. The feasibility of all involved deployment methods is necessary for a full hybrid concept to be considered. It is, however, not ruled out that any hybrid concept will not be considered for the detailed design after suitable deployment concepts are selected. A few options for combinations of methods have been identified on a purely theoretical basis without literature references, which reduces the feasibility by a large factor straight away.

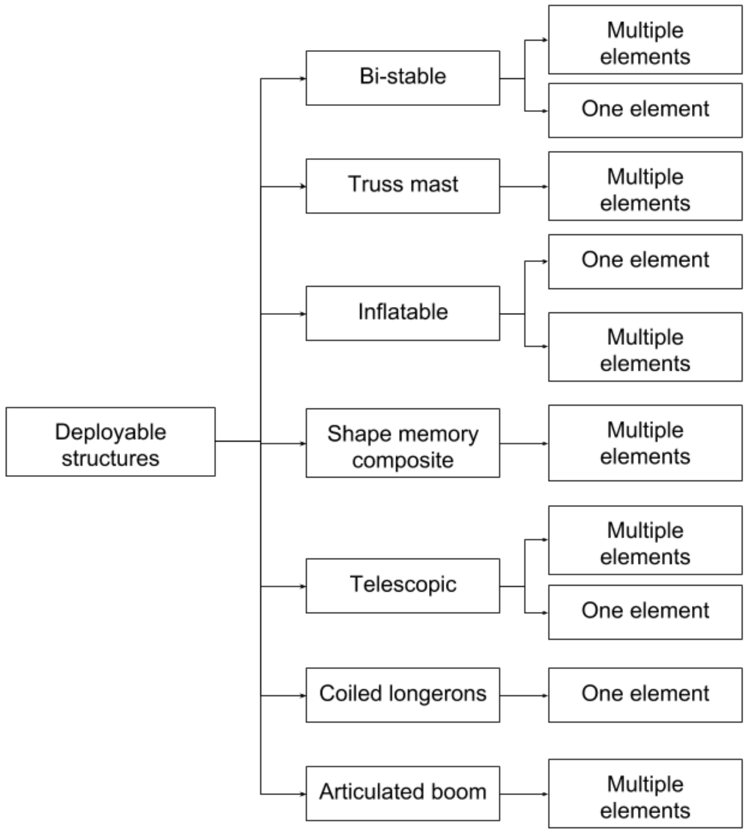

Figure 3.1: Deployment concept tree

3.1.2. Elimination of concepts

In this section, the concepts that are not considered for the upcoming trade-off are elaborated on. Brief descriptions will be given along with the justification for elimination at this stage.

Truss structures are a proven concept for space applications, including both rigid member trusses and tensegrity structures. They have been envisioned for shading purposes as well, such as a concept for International X-Ray Observatory (IXO) sunshield deployment [108]. However, there are multiple reasons why these are not applicable for the baffle master thesis project. The first reason is the expected complexity of designing a truss structure capable of providing the required 2-axis deployment with the available resources. The second reason is the identified high mass of the canister required to hold the undeployed truss, which would likely violate the given mass budget [80]. Furthermore, no deployable trusses on the same scale as the DST were found as a reference to get a more accurate estimate of the resulting volume and mass. It is therefore justified to not consider the concept for the deployment mechanism selection.

Articulated booms are deployable systems consisting of multiple sections separated by hinges. This deployment method is already used for the M2 struts, which are folded against the instrument bus during stowage. The same concept of using multiple articulated booms could be considered for the baffle, but in this case the booms would also deploy a light-shielding structure. This is another concept that has been proposed for the IXO [12]. However, while the concept is quite simple and a good performance could be achieved by including radial and longitudinal segments in one articulated boom, the concept will not be included in the trade-off. This is due to the low achievable deployment ratio of articulated booms. The deployment ratio is roughly the number of segments in the articulated boom. Due to the launch dimension constraints, the articulated booms would have to consist of at least six segments to meet the approximate deployment ratio requirements, which is not seen as feasible. This causes the rejection of the concept.

3.2. Concepts for trade-off

In this section, the remaining concepts to be traded off will be described in more detail. Their expected strengths and weaknesses as well as examples from existing literature are included. Shape memory composite structures are discussed first in Subsection 3.2.1 followed by Subsection 3.2.2 which presents the telescopic concept. Coiled boom systems are the topic of Subsection 3.2.3 and finally, inflatable structures are discussed in Subsection 3.2.4.

3.2.1. Shape memory composite booms

Shape memory composite (SMC) booms are usually made out of carbon fibre composites and exhibit high deployment ratios due to their ability to be rolled up or folded in a flattened state. They have been widely utilised conceptually for deploying membranes such as solar or drag sails, which has similarities to light shielding [80]. An example is the recent work on a self-deployable truss which can be applied in various configurations [69]. The truss is made of multiple tape springs which deploy from mandrels, also moving a membrane. The achievable deployment ratio is very high. While this technology is promising for shield structures, the baffle requires also a barrel part. All SMC booms are limited to deploying in one direction only, which would require the use of a more complex two-part deployment mechanism. A concept applying another deployment method combined with the tape spring truss has been envisioned. The shield carrying a light-shielding membrane would deploy first, followed by the deployment of the longitudinal part of the baffle by e.g. inflation to achieve the required low stowage volume. However, this concept not only requires the design of the two different mechanisms, but their reliable integration. The SMC booms as a deployment method cannot be considered without taking into account the added complexity of two-stage deployment of the baffle, which increases the complexity of using the booms.

Bistable structures are included in this concept, since the working principle fits under the same umbrella with minor variation. The main difference is the decreased storage energy, as bistable systems are defined as being in equilibrium in both stowed and deployed state. The benefit is reducing the size and complexity of the hold-down and release mechanism (HDRM), with increased complexity of the boom design on the other hand. If the SMC deployment is chosen, the selection between a bistable or conventional system can be made.

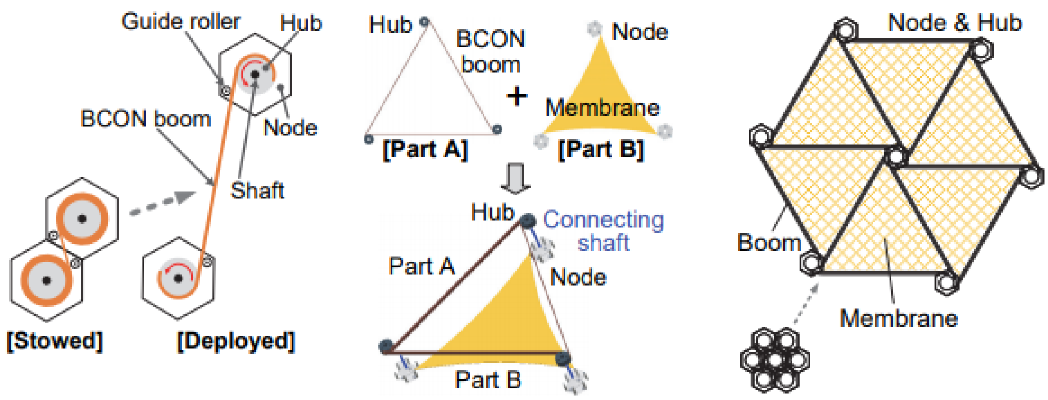

Figure 3.2: Concept of truss made of convex tapes deploying a membrane [69]

Table 3.1: Summary of the advantages and disadvantages of SMC deployment

Advantages	Disadvantages
Widely studied	Complex deployment of whole system
Good storage efficiency	Uncertainties in full design
Low mass	Possible complex HDRM
Low deployment power	

3.2.2. Telescopic booms

The first concept considered for the deployable baffle is telescopic configuration, where segments of the baffle are nested during stowage and consequently extended to reach the final geometry. The segments all have their final shape throughout storage and launch, and only the length of the system changes. There are a few recent concepts of space instruments which include a telescopic configuration for a deployable baffle, which are presented in the following paragraphs. Their characteristics will be used as a reference for the capabilities of telescopic systems in general in the trade-off that follows.

The ExoplanetSat design included a nested baffle, which consists of seven sections, with the diameter of the baffle increasing outwards [51]. The baffle includes vanes for stray light suppression, and these are located at the intersections of the segments. The stray light control is the leading design factor that also defines the number of sections and the deployment ratio. The full deployed length of the baffle is 116 mm, and its diameter is 97 mm. The mass of the baffle itself is approximately 100 g, which scaled up to DST dimensions woul lead to a mass in the order of tens of kilograms. While the deployment mechanism had not been developed by the time of the article, a spring-based mechanism was considered [51]. The baffle in deployed state can be seen in Figure 3.3.

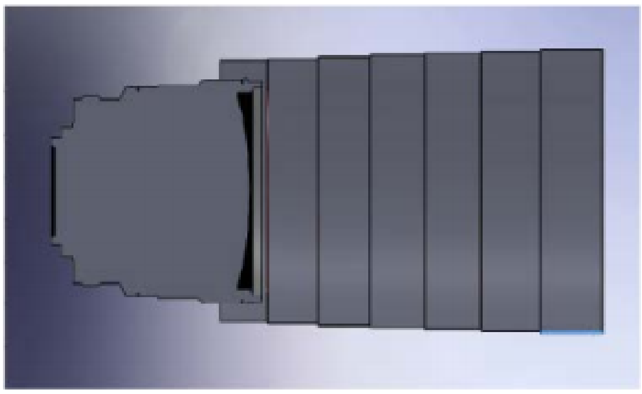

Figure 3.3: Side view of the telescopic baffle on ExoplanetSat, with the instrument lens on the left [51]

Studies have been done by Chinese researchers to also incorporate vanes on a single section of a nested baffle [29, 30]. These studies are done on baffles with three segments, and the vanes naturally can only be present in the innermost one during stowage. After analysing both options, it was found that placing the vanes in the farthest section is better for point source transmittance than in the section closest to the instrument [30]. The deployed length of the baffle is 600 mm, and the diameter is 240 mm, but no mass estimate is found. However, a deployment ratio of 2.33 can be calculated from the given stowed length of 258 mm, which is quite low. The baffle would be deployed by means of the strain energy in curved tape springs, which are combined into assemblies of 8 springs placed evenly across the baffle sections. This would lead to no extra power needed from the spacecraft bus for deployment, and a simple system overall. This baffle can be seen in stowed and deployed states in Figure 3.4.

The examples for telescopic baffles are very small in size compared to the DST, and the mass is expected to be very high for a baffle system that size. Further complications are caused by the constant diameter of the solid baffle sections during deployment, which makes it harder to stow efficiently during launch. A benefit of the method is the ability to use almost any needed coatings or additional material on the sections since they are solid and do not undergo deformation, leading to good customisability of thermal properties. Additionally, the stray light prevention properties of telescopic baffles are very good due to their controlled shape. where vanes can be added quite easily. The deployment can most likely be easily done with a strain energy based system, where no external power input is required, which is an important consideration for the system complexity. No thermal shielding was found that deploys in this manner, which raises the concern of the feasibility. It can be assumed that additional thermal control materials need to be added on the outside so that the temperature of the telescope can be stabilised, leading to additional mass and possible deployment complications. The summary of these advantages and disadvantages is seen in Table 3.2.

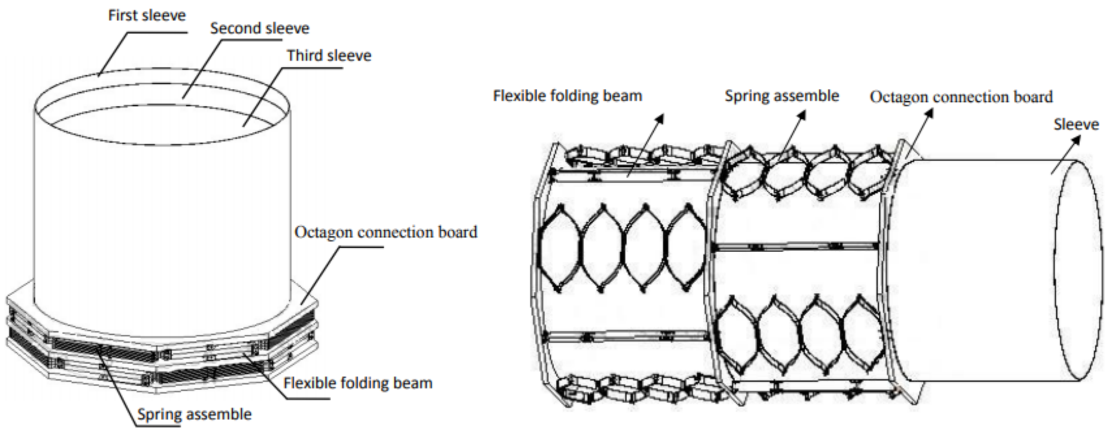

(a) Stowed state (b) Deployed state

Figure 3.4: Stowed (a) and deployed (b) conditions of the tape spring deployed baffle [29]

Table 3.2: Summary of the advantages and disadvantages of telescopic deployment

Advantages	Disadvantages
Simple	High mass
Good stray light properties	Low storage efficiency
Good thermal properties	No prior comparable systems
No external energy required	
Good deployed stiffness	

3.2.3. Coilable booms

Another method of deployment is the use of a truss structure, where the longeron elements are coiled during stowage and deploy to form a rigid system, or in some cases springs are used instead. In this kind of truss, batten rings offer further structure and tensioned cables are used to keep the system rigid. An example of the general structure can be seen in Figure 3.5. In this configuration, with slight variations, multiple space projects were found. This included both actual baffles and very similar structures.

The Collapsible Space Telescope is one of these, with the coilable truss used to deploy the secondary mirror, but also planned for use against stray light [5]. This system can be seen integrated in a 6U cubesat in Figure 3.6. Over the deployable structure, a shroud is included for stray light and thermal protection. The deploymet of this truss is driven by a motor [5]. The deployment of M2 is a common use for deployable structures on small space telescopes in general, with the Italian SMART satellite and an unnamed Chinese telescope including similar systems, although the SMART truss does not have coilable longerons but tape springs between the rings [47, 79, 109]. This eliminates the need for an external power source and is similar to the deployment mechanisms found for the telescopic baffles.

The Japanese PRISM satellite, which was launched in 2013, includes a boom which deploys a lens system [55, 59, 71]. The length of the boom is 800 mm, the aperture is 90 mm and the whole lens and boom system weighs 2 kg [59]. The stray light control on this instrument was implemented via variable inner diameter of the structural rings on the boom. There was no shroud included around the rings unlike in the other systems in this section, which means that the thermal environment is not at all controlled by the extendible structure. Since this satellite was actually launched and successful, the feasibility of the system is strongly proven. The matter is made more impactful by the fact that the satellite was a university project where students were involved in the development.

The deployment of trusses as presented here can be spontaneous and based on strain energy, or be powered by motors included in the system. The use of a system based on longerons and rings necessitates the addition of blankets on the outside of the truss, as thermal stability is the driving requirement on the DST. This could complicate the inherently simple mechanism significantly, and naturally increases the total mass.

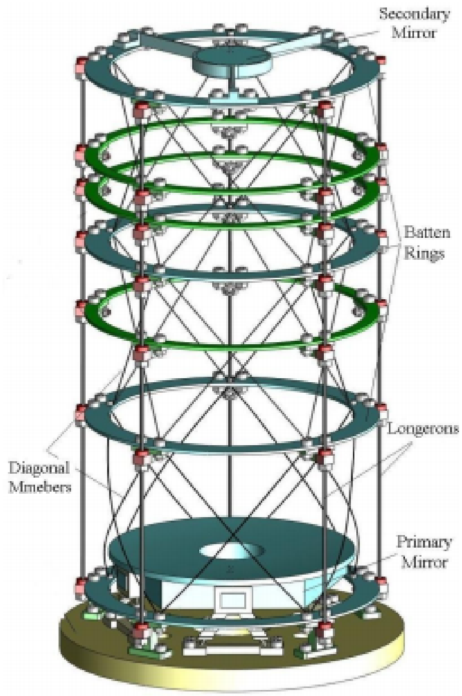

Figure 3.5: Structure of the deployable M2 structure by Zhao et al. [109]

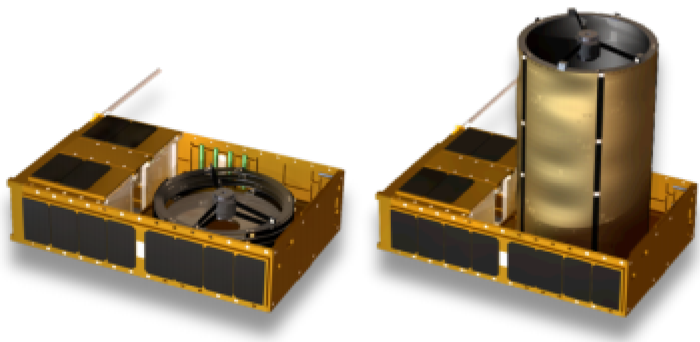

Figure 3.6: Collapsible Space Telescope in undeployed and deployed state [5]

The mass of a truss structure is however still relatively low compared to a solid system, such as the telescopic configuration. Stray light control will be based on the coatings on the inner side of a shroud, which might be slightly limited but still quite high performance could be achieved with the right materials and geometry. The storage efficiency in a longitudinal direction is very high, but the systems found in literature do not expand radially, making the required diameter of the launch vehicle equal to the deployed diameter, which is highly inefficient. As the trade-off is based on existing concepts, deficiencies such as this are assumed to be inherent to the concept. These discussion points are also listed in Table3.3.

3.2.4. Inflatable structures

Inflatable cylindrical structures have been researched for decades, although mostly as booms supporting other structures rather than complete systems in their own right. Regardless, it is an option for the deployable baffle and will be included in the trade-off due to the promise it shows, and one light shading concept has also been identified from literature to prove the feasibility. Inflation as a deployment mechanism is different from the mostly strain energy based solutions of the previous sections, but has space heritage from a longer time period, starting in the 1950s [45]. Some notable missions will be presented and the possibilities

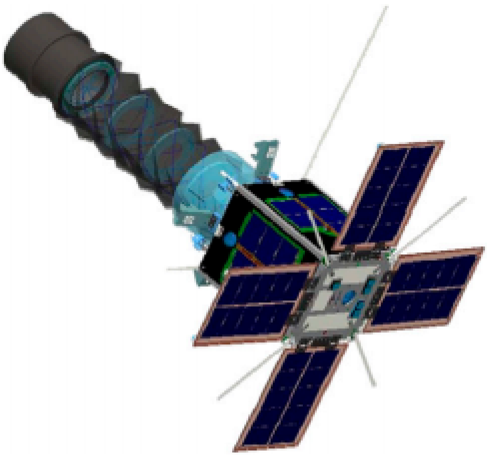

Figure 3.7: Rendering of the PRISM satellite [55]

Table 3.3: Summary of the advantages and disadvantages of coiled longeron deployment

Advantages	Disadvantages
Deployment can be without external energy	Limited stray light control
Low mass	A shroud is required for thermal and stray light purposes
Simple, proven concept	Deployment only longitudinally
Good stiffness when deployed	

they offer for the baffle design are explained. Finally, the advantages and disadvantages that are identified will be presented.

The Echo orbital balloons, and especially Echo II, are interesting projects to consider as an example. These spherical satellites were inflated in orbit and successfully functioned as reflectors used for communication. Echo II was not only inflated, but the structure was rigidised afterwards which allowed the inflation gas to be vented into space without the shape of the balloon changing [18]. This was achieved with a yielded laminate of aluminium and Mylar. A major worry with inflatable systems is the maintenance of the geometry during operations, as leaks and micro-meteoroid damage lead to loss of the inflation gas over time. Since rigidisation is proven possible, the risks of an inflatable baffle decrease regarding the feasible lifetime.

The Inflatable Antenna Experiment is another space proven concept that uses an inflatable structure. It was flown in 1996 and provided useful data on the deployment dynamics of inflatable booms in orbit. The planned deployment sequence was not achieved, and the reflector inflated earlier than planned, leading to uncontrolled deployment of the whole antenna [44]. However, the intended final configuration was achieved regardless of this issue, which provides evidence of the reliability of deployment of inflatable systems. The interference of the deploying baffle with optical elements of the DST needs to be minimised, which also makes the possible uncontrolled deployment risky. The inclusion of a control mechanism might also need to be considered to reduce this risk, based also on the recommendations of the IAE project [44]. An inflatable sun shade has been proposed at least once, for a European far-infrared telescope [13]. Multiple configurations were developed, all based on inflatable booms which deploy a blanket of multilayer insulation (MLI). A built prototype can be seen in Figure 3.8, proving the manufacturing feasibility of complex shaped inflatable structures. Concepts with circular booms are also presented in the same article, expanding the possibilities for creating inflatable thermal shielding structures [13]. It can be seen from the sketches given that a quasi-circular cross section can be achieved by including a large enough number of booms. The geometrical variation is therefore very large for inflatable boom based systems.

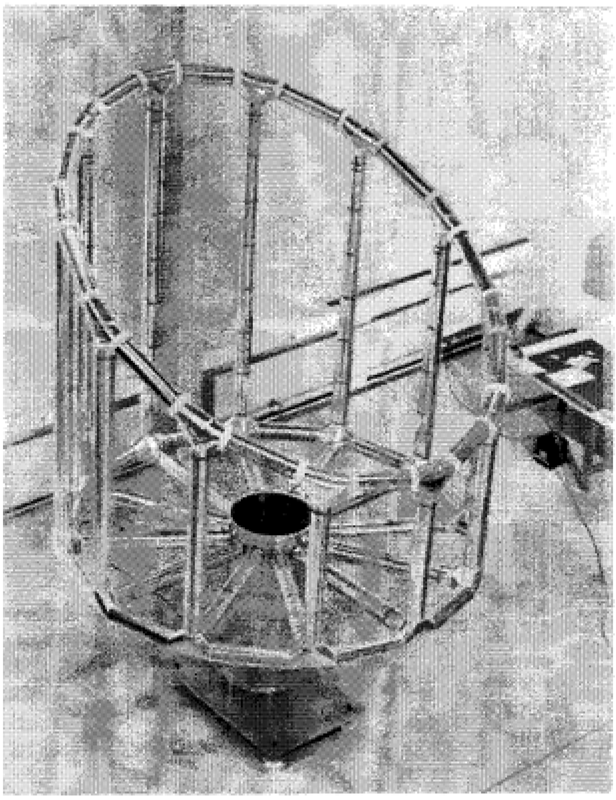

Figure 3.8: Sun shade based on inflatable booms [45]

The advantages of inflatable mechanisms include the extremely light weight and low storage volume, along with relatively simple and reliable deployment. Different geometries are also possible based on the available literature, even concepts made specifically for thermal shielding of space telescopes. Difficulties may arise from effectively stowing the baffle for controlled deployment as well as achieving the necessary rigidity during operations, since the folded structure is by necessity pliable. Rigidisable aluminium-polymer laminates are an interesting option for the structure of the baffle, were it to be inflatable. Other rigidisation mechanisms, such as thermoset or UV activated materials, are available for consideration as well [18]. This makes the lack of rigidity a solvable issue instead of an insurmountable obstacle for the inflatable concept, even though there are a lot of complications regarding the process. The properties are summarised in Table 3.4.

Table 3.4: Summary of the advantages and disadvantages of inflatable deployment

Advantages	Disadvantages
Very low mass	Low stiffness without rigidisation
Proven in space	Rigidisation complicated
Good storage efficiency	
Reliable deployment	

3.3. Trade-off criteria and weights

In this section, the trade-off criteria and their respective weights are developed. They will be then used to decide the winning deployment concept to be designed in more detail in the following phases of the thesis work. The weights will be given on a scale of 1 to 5 for each of the criteria. In this system, 1 signifies that the criterion is relatively of minimum importance in the trade-off, while 5 signifies utmost importance.

Mass of the mechanism is an important consideration, seeing that the low mass of the whole telescope is one of the main drivers of the DST design. The inclusion of weight as one of the trade-off criteria is then clearly justified. As there is no analysis done on the concepts, the absolute weights are not evaluated for this trade-off. The scores for this criterion will be given in relative terms, considering the expected materials, the size of the structures included and the required additional mechanisms to power the deployment and contain the stowed baffle. The mass needs to be kept within the budget, which leads to this criterion being of moderate importance.

The second criterion to be used is the **stowed volume** of the baffle, which also represents the deployment ratio as the required minimum dimensions are known. This is critical for both meeting the DST system requirements and imposing minimal changes on the overall bus design. The volume of the baffle should be as low as possible in stowed configuration, while still able to deploy to the full geometry reliably. All elements needed to reach the performance of the baffle are considered in the volume, including a separate shroud if required. Regardless, as with the weight, the relative volumes are used based on the components needed. Absolute volumes are not available before further analysis is performed. The volume in stowed condition is of approximately the same significance as the mass.

Complexity of the deployment mechanism has to be taken heavily into account when selecting the concept. Due to the absolute necessity to reliably deploy the baffle in orbit, this is an important aspect. The thesis additionally has a scope including the whole baffle conceptual design, which means that no extensive research and development work can be put into designing the deployment mechanism. Complexity consists of the number of elements, the number of steps in the deployment sequence and also the maturity of the technologies used. Even before the design phase, it needs to be known that the deployment is feasible in both technology readiness and repeatability. More elements naturally lead to more chances for a component failure, which might endanger the success of not only the baffle deployment but the whole mission. Systems that by necessity deploy in radial and longitudinal directions in separate motions are penalised. This criterion is critical for the development of the final concept.

Stiffness of the deployed baffle structure cannot be excluded from the trade-off. Due to the requirements to not impede the telescope elements, the deployed baffle needs to sufficiently maintain its shape and position relative to the telescope throughout the mission. While the exact dimensions and position of the baffle are not as stringent as e.g. the mirrors', large free movement is not allowed for both imaging and inertia reasons. The expected stiffness is based on purely assumptions following from literature, and an exact requirement has not been set. A grade in this category is therefore an expectation of how rigid the concept is compared to the other concepts. The requirements on rigidity are not as stringent as many other aspects, so the significance of the criterion is low.

The next criterion considered is the existing **space heritage**. This is closely related to the TRL, but has a slight distinction. Use of the the concept in space applications, regardless of the purpose, has the maximum TRL, but does not separate the exact purpose of the system. In this criterion, the concepts will be graded on whether they have been used in space, and how applicable the use is to designing a baffle. No space heritage would result in unpredictable performance, and the baffle design is preferably based on proven concepts due to the constraints of the project. The weight of this criterion is therefore quite high.

The weighting of the criteria is done by using the analytic hierarchy process (AHP). In this method, the different criteria are compared with each other to find the relative importance of each of them. The results of the process are shown in Table 3.5. The weights add up to 1 and the consistency ratio is 0.05, well within the acceptable limits.

Table 3.5: Trade-off criteria and their weights

Criterion	Weight
Mass	0.09229
Stowed volume	0.143269
Complexity	0.515466
Deployed stiffness	0.043609
Heritage	0.205366

3.4. Deployment method trade-off

In this section, the trade-off between the deployment concepts will be performed. First, the method of grading is explained. The AHP method is used to compare the concepts with each other with respect to each of the criteria defined above. The scores are then multiplied by the associated weights and added up to yield the final scores. The matrices used to calculate the scores were made using Microsoft Excel. The trade-off matrix can be seen in Table 3.6. The justification of grades given to each concept will be explained below. It can be clearly concluded that the inflatable concept can fulfil the deployment requirements to the best extent. It is therefore the winner of the trade-off and the concept will be developed further to create a design for the baffle.

The telescopic concept was considered very heavy, just on the limits of acceptable due to its solid construction. The same applies to the stowed volume, which is expected to be very high. On the other hand, the complexity of the deployment can be quite low, and the rigidity of the deployed system is very good. There have not been telescopic structures other than booms used in space, which makes the feasibility of a baffle application uncertain. Finally, the nested configuration of a cylinder does not allow for the required deployment ratio outwards from the bus, making the possible configurations very complex.

A system consisting of a coiled truss excels in multiple criteria, but is ultimately not the best suitable for the DST. It is expected to perform well in mass and especially the stowed volume due to the lightweight truss structure consisting of relatively few elements, even accounting for an additional shroud added to it. The complexity of these type of systems is shown to be low by the vast amount of examples available, and they have heritage as part of light-blocking structures, even if on a smaller scale. The expected rigidity of the deployed structure is also very good. However, no reference for a truss that deploys outwards as well as in length was found, which would make the design process too difficult if the concept was selected to be improved. This leads to the low score of the option in the complexity criterion.

The scores for the bistable and shape memory booms are similar for all aspects, which is not surprising as the almost identical properties of the concepts were already identified earlier. They are both assumed to have a low mass and stowed volume based on the examples found. The existing heritage and post-deployment stiffness were also given good scores, although the use of SMC booms is found more commonly in literature, which creates a slight difference between the two concepts. However, the downfall of these deployment methods is the uni-axial expansion. The whole baffle structure would require a two-stage deployment process, possibly combined with another mechanism. The complexity is then increased to the point where the score for that criterion is low.

The inflatable concept is the winner, as already concluded. It has a good expected mass and the volume in stowed state is assumed to be very low. Based on research, the complexity should be rather low as well, leading to a good grade. The inflatable concept has questionable performance in the deployed rigidity, since it has to necessarily be flexible when stowed. This is deemed a correctable flaw since methods exist to rigidise inflatable structures, even if further work is needed to account for this in the design. The complexity of the method is assumed to be relatively low, since inflatable systems can be deployed in various ways. There are examples of inflatable systems of different sizes and geometries, even if no baffles have been made as of yet, making the heritage also good. Lastly, and most importantly for the result of the trade-off, the deployment ratio for an inflatable system is assumed to be very high, and multiple directions of stowage are assumed possible due to the flexibility of the assumed material. This distinguishes the concept from the other two and makes it the selected option for the baffle.

Table 3.6: Results of the trade-off from AHP

Concept	Mass	Volume	Complexity	Deployed stiffness	Heritage	**Total**
Telescopic	0.051583	0.046351	0.131605	0.501589	0.096554	0.120942
Coilable	0.233013	0.283001	0.093676	0.182099	0.508960	0.222801
Inflatable	0.558936	0.535135	0.538376	0.067897	0.277694	0.465757
SMC	0.156468	0.135513	0.236343	0.248415	0.116792	0.190501

3.5. Discussion

Since the selection of the deployment method is the first and therefore most important choice made in this thesis, it is important to evaluate the result and the justification for obtaining it. This ensures that the choice is made for the right reasons before the work is continued on the grounds of the decision.

A crucial part of AHP is making sure that the method is used consistently and with great carefulness in selecting the relative grades. First, it is checked that the final grades for each criterion add up to exactly 1, meaning that errors were not made when filling out the matrices. This is seen immediately in Excel for all matrices made, and the process is verified for that aspect. Another measure of being consistent throughout the process is the calculation of consistency ratios for the grading of each criterion. This value should generally equal less than 10% for the results of the trade-off to be reliable. The consistency ratios calculated in the AHP spreadsheet can be seen in Table 3.7, and are all well below this threshold. No iteration of the process is therefore required at this stage, but the sensitivity of the trade-off to assumptions made is something to be taken into account. This has been made clear in discussions with ADS, the feedback from which has been taken into account when conducting the selection process. The process was made more transparent and based on the direct comparison of the different concepts, as described before. Therefore, the results obtained in this chapter are justified to the best possible extent and will be used as a basis for the design unless further down the road deficiencies in the process are identified.

Table 3.7: Consistency ratios of AHP criteria

Criterion	Consistency ratio [%]
Mass	5.6
Volume	5.0
Complexity	4.4
Stiffness	5.2
Heritage	5.8

4

Baffle geometry

After the deployment method has been selected, as outlined in the previous chapter, the actual shape of the baffle can be developed. This chapter presents the process for the design of the inflatable baffle concept. The geometry will consist of the definition of the number and position of the inflatable elements, as well as the additional structure required, if applicable.

The set of requirements for the geometry will be discussed in Section 4.1. Literature examples of inflatable structure geometries will be shown in Section 4.2. Concepts generated for the selection will be explained in Section 4.3 and the trade off will be concluded in Section 4.4. The properties of the baffle will be presented and discussed in Section 4.5.

4.1. Requirements

A set of geometrical constraints for the baffle structure can be derived from the DST system requirements as well as operational considerations. Some of the latter have been discovered as a result of continuous interaction with the other DST team members as well as consulted university staff.

Based on requirements BAF-MEC-01 to BAF-MEC-03, the shape of the baffle needs to allow for a deployment from the exterior of the DST bus. It is an advantage the baffle system deploys in one go as opposed to multiple steps, but this is not a hard requirement and is mainly considered for the reduction of both risks and overall complexity of the deployment system. The baffle structure should not be closer than 100 mm from M1 or M2 and their support structures to reduce hazards for the optical elements in case of uncontrolled deployment or drift during operation. This applies also to the deployment of the M1 segments, during which they will span an arc of 750 mm radius.

The optical considerations for the geometry concern sufficient tolerances between the light path and any baffle elements. The M1 needs to have an unobstructed view of the Earth at all operational times, and a sufficient margin will be applied. This is defined as >50 mm distance from any point on the M1 projected in the direction of the optical axis. To efficiently reject stray light caused by Earth albedo, the length of the baffle has to be longer than M2 distance. Due to no stricter requirement posed by the optical team at this stage, and the fact that this coincides with the M2 thermal protection requirement, it is not considered separately at this point. If it is found out at a later stage that the baffle length needs to be increased for stray light or thermal purposes, the design will be modified accordingly. Another stray light driven specification is that the baffle is not allowed to increase in diameter with increasing distance from the bus, as discussed with D. Dolkens. This rules out e.g. a conical shape, as well as various hyperboloids. In addition to these requirements, symmetrical cross-sections are preferable to irregular ones for stray light control and possibly deployment reliability.

It has been chosen to use MLI on the baffle to provide a more stable thermal environment. The decision is strongly supported by the strict thermal stability requirements, as well as the noted use of the same solution in various previous deployable sunshade concepts [13, 106, 107]. This imposes that the structure needs to be coverable in a blanket of moderate thickness (conservatively estimated as up to 1 cm), which also needs to

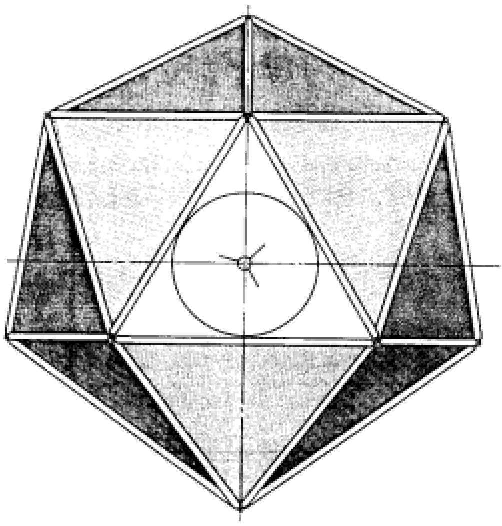

Figure 4.1: Icosahedral inflatable light shield [14]

be deployed from a small stowage volume. Due to the relatively high volume of MLI, the surface area of the baffle should be minimised to reduce its effect on the total volume, as well as mass. The MLI will form the inner surface of the baffle so that the thermal environment is controlled to the best possible ability, which has to be taken into account when developing the overall geometry. The composition and properties of the MLI itself will be designed in Chapter 5.

4.2. Inflatable structures from literature

In this section, different shapes of inflatable shape structures will be explored. Examples of various configurations found in literature will be presented to establish the feasible possibilities for the shape of the baffle structure. Especially examples of shielding structures will be discussed, as they are the most relevant for this work. This process will serve as the basis for concept creation.

The first, and most simple, shape encountered is that of the spherical, enclosed balloons such as Echo II. The concept is only mentioned for completion, as it cannot be implemented as a light shielding structure for a telescope that still needs to observe the Earth. Approximating a spherical enclosure, icosahedral inflatable truss structures for light shielding have been envisioned and tested [92]. An icosahedron is a 20-faced polyhedron. The structure is provided by a truss of inflatable members, which constitute the edges of the polyhedron, as can be seen in Figure 4.1. The faces are covered by shielding material, providing an enclosure for the optical instrument within. Observation capabilities can be enabled by not covering certain faces. The major disadvantage of this shape is the extremely large size of the structure when applied for a telescope system. This leads to both high mass and storage volume.

The majority of concepts explored by previous researchers are, in fact, truss structures. The definition used here is a backbone of connected inflatable booms combined with a separate shroud for shielding. Some of these were already introduced in the previous chapter, such as the cylindrical prism shape with supporting rings, or tori, on both ends [13]. A scale model of the full geometry, as well as a full-scale joint, have been built and successfully tested, as pictured in Figure 4.2 This general geometry can be seen to most closely resemble known space telescope baffling structures, such as the Hubble optical barrel assembly. The main difference is the flexibility of the shield itself due to the deployment, and the inevitable non-circular cross section due to using a finite number of faces. The same paper for the FIRST sunshield describes spherical shapes with the same basic concept, but only one torus located at the top. The feasibility compared to the tested cylindrical shield has been judged as approximately the same [13]. Both flat-top and obliquely cut geometries are presented. For now, as stray light or thermal analysis results are not available, only flat tops will be considered. If an oblique shape is found advantageous in the future, the design could be adapted.

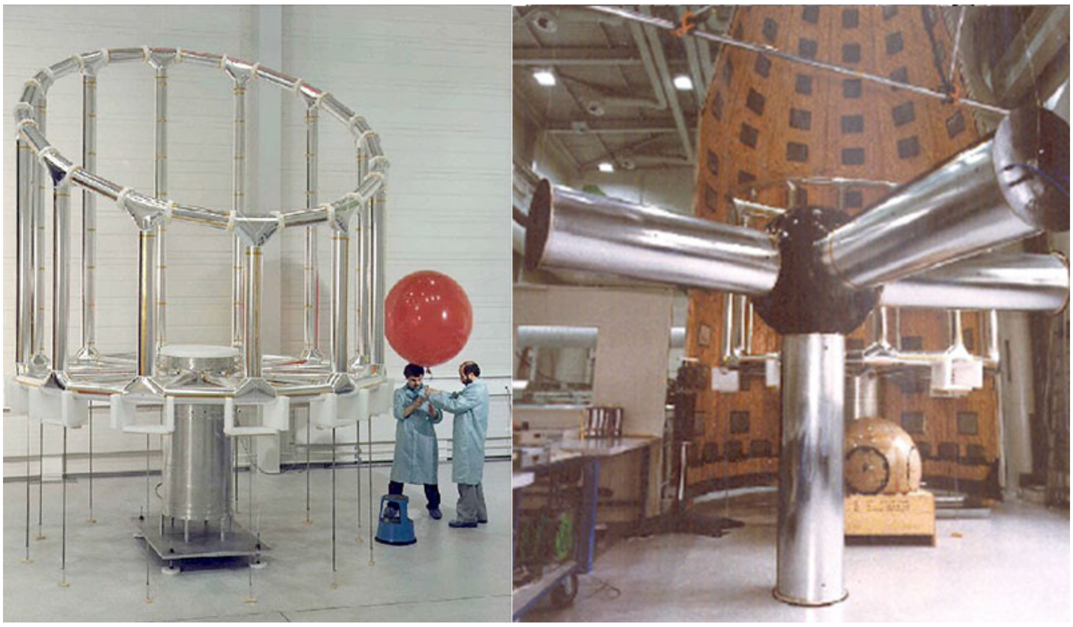

Figure 4.2: Scaled prototype (left) and full-scale joint section (right) of inflatable FIRST sunshield [50]

Possibly the most explored type of space inflatable structures have been various antennae. While the parabolic or lenticular inflatable enclosures often encountered are not relevant for current work, other elements from these systems can be considered. Tori have already been mentioned above, but numerous examples of inflatable tori can be found in antenna research, e.g. on the Inflatable Antenna Experiment, and various antenna concepts developed by Fang et al (Figure 4.3a) [38, 39, 44]. Other than closed torus shapes, curved systems of inflatable booms are not encountered beside the concept in [13].

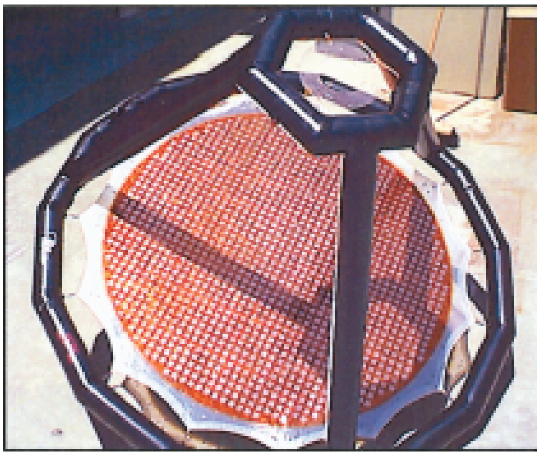

(a) One-metre inflatable antenna prototype [39]

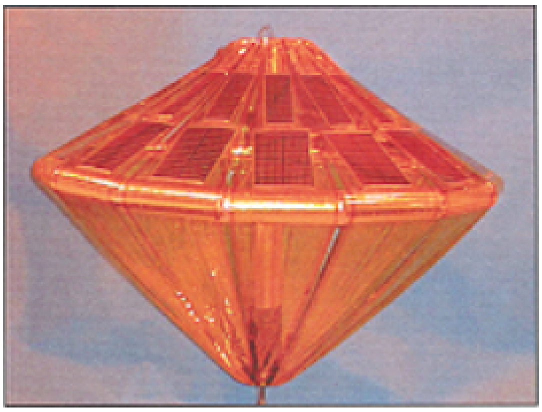

(b) Concept for an inflatable solar array of a Mars rover [17]

Figure 4.3: Examples of toroidal inflatable structures in space: X-band antenna (a) and solar array for a rover (b)

Inflatable trusses acting as booms with increased stiffness have also been prototyped. The full geometry might be from one of the above options, but the boom elements can be made more robust in combination.

4.3. Concepts

In this section, conceptual shapes for the baffle are generated and described. This will be followed by the selection of the most suitable shape in the next section based on important characteristics of the system.

At first, making a cylindrical inflatable structure consisting of two walls between which the gas is injected was considered. A cross section of this concept can be seen in Figure 4.4. This was driven by the assumption that the baffle should have a circular cross section and solid walls. Currently, it is assumed that the required stray light control properties can be achieved with polygonal as well as circular cross-sectional shapes, and symmetry is the only requirement. Flexible walls can also be considered as they are not a critical issue for stray light control. This enables multiple other design options to be considered and leads to a trade-off between the developed concepts.

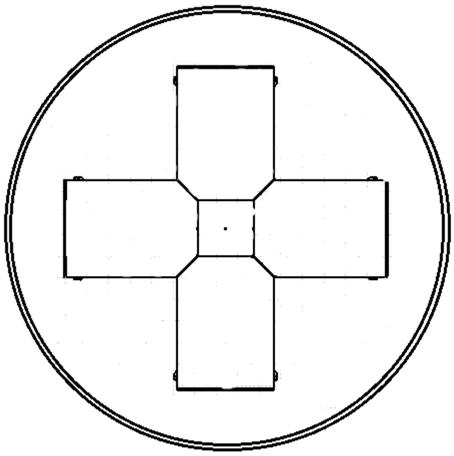

Figure 4.4: Original design of the baffle with two walls which form the inflation volume

In addition to the two-walled inflatable cylinder described above or other fully inflated configurations, it is possible to inflate multiple booms and use those as the structural elements, while the thermal and stray light protection is mainly provided by a deployable blanket of MLI or other flexible material, as found in literature earlier [13]. The advantages of this approach include a lower mass, less inflation gas needed and a greater amount of available literature for references. Inflatable booms have been widely studied and tested up to TRL 9, and are therefore a better option for confidence that the designed system will work as required. Because of this, making a baffle based on inflatable booms deploying a thermal blanket will be the only option considered in the following paragraphs. However, the shape of the system is still to be decided.

The main drivers for the shape of the baffle are the mass and storage volume. It has been established with ESATAN-TMS analysis by Villalba Corbacho that the thermal properties do not notably change with a change in the cross-sectional or three-dimensional shape, as long as the requirements given in the previous section are fulfilled by the structure. The contribution of the Earth albedo is nearly invariable for all the options and the thermal gradients present are mostly a result of its influence. The options available are circular or polygonal cylindrical shapes, or a spherical/elliptical (with the top cut off) shaped baffle. With the specified design space, a circular cylinder is in fact an extension of the polygonal cylinder, where the number of angles is large. For this reason, the circular cylinder will not be considered on its own. The polygonal cylinders considered are square, octagonal and dodecagonal (12 sides) due to their symmetry with respect to x- and y-axes. In addition, a spherical baffle with a cap cut off is considered, as well as an ellipsoidal baffle with a cap cut off as well. The ellipsoidal baffle has two equal semi-axes to maintain a circular cross section, which makes it a spheroid. The more accurate descriptions of the different concepts are given below.

The polygonal concepts all have the same main characteristics. Each corner in the cross section of the baffle is connected to the spacecraft bus with an inflatable boom. These provide the radial expansion of the structure. The booms are connected to a torus, which provides structural stiffness. Furthermore, each corner of the polygon has a longitudinal inflatable boom at a 90° angle to the radial boom, which is connected to it. At the other end, these longitudinal booms are connected to another torus element, so that the intended cross section is maintained. All booms are rectilinear, except for the tori. They will be attached to the MLI blanket that completes the system, which will be deployed when the vertical booms inflate. Concepts with 4, 8 and 12 edges are considered in this chapter. Models created in ANSYS to demonstrate the geometry can be seen in Figures 4.5a to 4.5c. The main concern with these concepts is ensuring stable deployment, since the two connected boom sections might lead to geometrical problems during inflation, e.g. obstruction of gas flow or unpredictable deployment. Minimum dimensions of the booms for each type are listed in Table 4.1 to fulfil the baffling and M1 clearance requirements. These are used for comparing the different concepts.

Table 4.1: Parameters of polygonal baffle concepts

Shape	Minimum radial boom length (m)	Minimum vertical boom length (m)
Square	1.139	2.6
Octagon	0.824	2.6
Dodecagon	0.779	2.6

The spherical and spheroidal concepts have one main difference with respect to the polygonal ones. The outer structure of the baffle will be formed of curved inflatable booms that form the external convex shape. The spherical baffle has the curvature of a sphere, and the spheroid has a more elongated shape. Conceptual models can be seen in Figures 4.5d and 4.5e. Similar to the previous concepts, the MLI blankets are attached to the booms and deployed with them. The advantage of these shapes is an assumed more reliable deployment due to the booms being formed of a single section. However, it still needs to be ensured that the direction of deployment can be predicted to reduce hazards to the rest of the telescope.

Table 4.2: Parameters of spherical and spheroidal baffle concepts

Shape	Minimum boom length (m)	Longitudinal axis (m)	Lateral axis (m)
Spherical	3.68	1.5	1.5
Spheroidal	2.38	1.5	1.2

The selection of the baffle shape will be done in the next section between the concepts discussed.

4.4. Selection of shape

Since the inclusion of MLI is required, Table 4.3 includes the area of the blankets for each of the four shapes, with the length of the baffle at 2.6 m and the margin to any side of M1 at 20 cm. The parameters are the same as described in the previous section. It can be seen that for the polygonal shapes, the required area of MLI decreases with a greater number of sides. Compared to the cylindrical shapes, the spherical baffle has a greater area due to the highly convex walls with respect to the optical axis. However, the ellipsoidal concept has the second smallest covered surface area. The amount of MLI needed correlates strongly with the total mass of the system, which makes the dodecagonal and ellipsoidal concepts the most appealing at this point. All areas are slightly overestimated, as the presence of the bus is not taken into account. This represents the worst case scenario, where the baffle is deployed from behind the bus structure and not integrated into it.

Table 4.3: Area of MLI blanket needed to cover baffles of various shapes with the following common parameters: length = 2.6 m, M1 clearance = 0.2 m

Cross-section	MLI area (m^2)
Square	23.37
Octagon	19.36
Dodecagon	18.06
Circle (sphere)	24.22
Circle (ellipsoid)	18.61

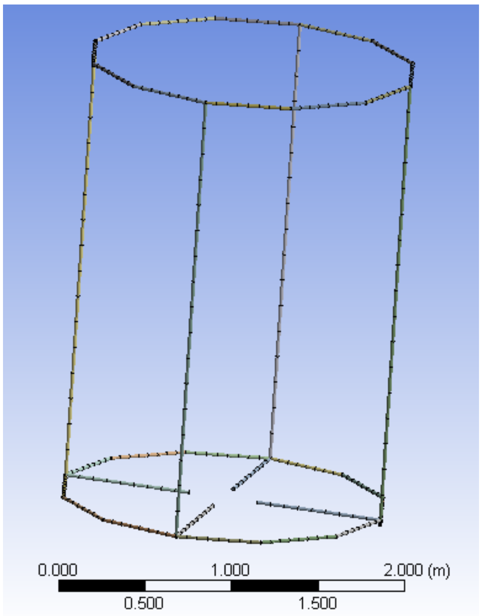

(a) Cylindrical with 4 booms

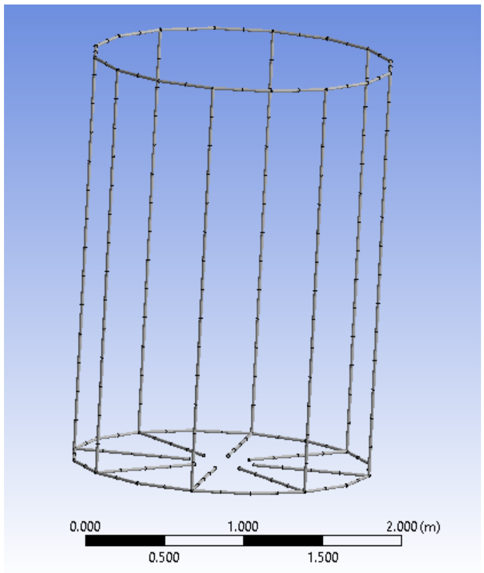

(b) Cylindrical with 8 booms

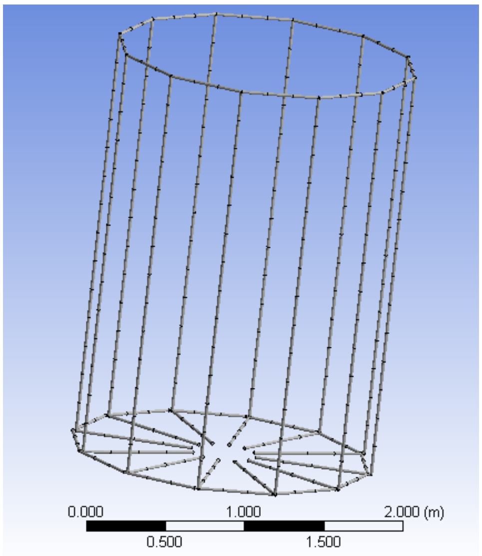

(c) Cylindrical with 12 booms

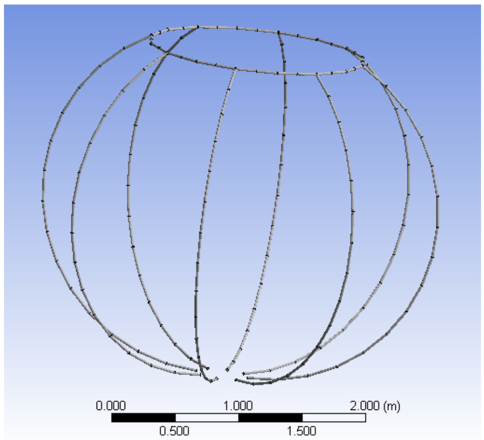

(d) Spherical

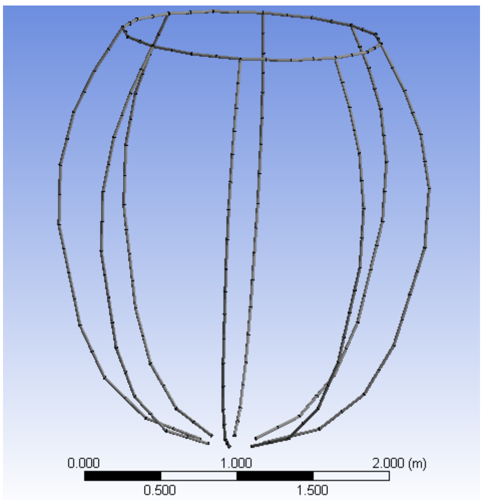

(e) Ellipsoidal

Figure 4.5: Shape concepts for the baffle geometry trade-off

Another parameter that can be compared is the total boom length, which is found by adding up the boom elements required. It will affect the inflation system design, as the amount of inflation gas required naturally depends on the volume it needs to fill, which is proportional to boom length. This assumes that the inflatable booms have identical diameters between all designs, which strictly speaking is probably not true, but suffices at this stage as the pressure requirement will be diameter dependant. The polygonal designs have as many spokes as they do edges, and the sphere and ellipsoid have 12 spokes based on reference [13] and as a worst case. The lengths of the spherical and ellipsoidal baffle booms is calculated assuming they have the arc length of the cut sphere or spheroid, but the booms are straight instead of curved. The cylindrical designs include two tori with 1.9 m diameter, and the spheroids include one torus with 1.7 m diameter. The length values also give indication of the mass of the system, although the correlation is not direct and the MLI is assumed to be the main mass contributor. The results are shown in Table 4.4. As expected, the more booms included in the design, the higher the volume. The lowest and highest values have a difference of almost factor 2, which is quite significant. The ellipsoidal shape, perhaps surprisingly, has the second least boom length, clearly out-performing the spherical baffle in this aspect as well.

Table 4.4: Total boom length of various shapes

Cross section	Total boom length [m]
Square	26.894
Octagon	39.330
Dodecagon	52.486
Circle (sphere)	49.501
Circle (ellipsoid)	33.901

The stiffness of the different geometries is assessed by creating straw-man models in ANSYS and performing a modal analysis to find the first eigenfrequency. The higher this frequency, the stiffer the geometry can be expected to be in operation. The models will consist of identical circular cross section beam elements and have structural steel assigned as the material in ANSYS. There are fixed supports placed on the locations where the baffle is expected to be connected to the instrument bus to remove rigid body motion. It is assumed that the relative properties of the concepts will not change due to these simplifications, while using accurate geometry would require extreme amounts of computational power. As a result, the actual quantity of the eigenfrequency does not indicate the properties of the actual system, and they are only used for comparison reasons. It is seen that the cylindrical prism concepts show better stiffness especially when there are 8 or 12 booms to form the cross section. As expected, the dodecagonal option is the stiffest. In case of the spheroids, it is also no surprise that the spherical shape has a lower stiffness. Based on this analysis, the cylindrical options are preferable for operational stability.

Table 4.5: First natural frequency of the shape concepts

Cross section	Frequency (Hz)
Square	1.2724
Octagon	1.5258
Dodecagon	1.5596
Circle (sphere)	1.1728
Circle (ellipsoid)	1.3782

For reliability of inflation, the number of booms should be as low as possible, regardless of whether each boom has their own separate inflation system or a common one, since leaks and obstructions remain an issue in either case. This makes the square cross section a good option, as it contains only 4 inflation points. The addition of two tori on the cylindrical concepts makes them slightly less reliable. Additionally, being able to inflate a boom in one motion (spheroidal concepts) increases the robustness of the inflation sequence. Another aspect of reliability is the known feasibility of the shape. Rectilinear booms have significantly more literature behind them compared to curved shapes. This facet is very important, as the whole baffle concept needs to be conceptually reliable at this stage, when the performance cannot yet be evaluated with hardware testing.

The spherical and spheroidal concepts fulfil the soft requirement of deployment in one motion, unlike the polygonal baffles which would most likely first need to expand radially before inflating to the full length. This makes the former concepts more suitable in terms of risk reduction, even if the number of booms is higher, as the chance of obstructions or such due to the more complex shape is lower. An additional consideration is that the spherical shape is considered more effective against stray light compared to polygonal cylinders, according to D. Dolkens. The performance of the ellipsoidal baffle is assumed to be similarly better than the polygons, but worse than the sphere.

A simple trade-off based on the characteristics discussed above is developed. The selection will be made based on a point total of the concepts in different criteria with prescribed weights. The weights will be multiplied with the grade each concept achieves, and these will be added together to obtain the final score. The criteria correspond to the previous paragraphs and they are given with their associated weights in Table 4.6. Weights are given from 1 to 5 based on the relative importance. The "mass" criterion is derived from the amount of MLI required to cover the structure, which was calculated in Table 4.3. "Reliability" combines the deployment aspects discussed, i.e. the number of booms, number of expected phases of the deployment and possible hazards from geometry. The last criterion is "stiffness" which is based on the fundamental eigenfrequency. The low weight is a result of the uncertainty in evaluating the concepts, as well as the relative closeness of the values.

Table 4.6: Criteria and weights for trade-off between shapes

Criterion	Weight
Mass	4
Reliability	5
Stiffness	3

The trade-off table can be seen in Table 4.7. The results are presented with the grades for each concept already multiplied with the criteria weights. In general the grades are given from 1 to 5 based on the order of the concepts for each category, unless two values are very similar.

Table 4.7: Trade-off between baffle shape concepts

Concept	Mass	Reliability	Stiffness	**Total**
Square	8	20	6	34
Octagon	12	15	12	**39**
Dodecagon	12	10	15	37
Sphere	4	10	3	17
Spheroid	12	10	9	31

Based on the discussion in this section, and the consequent clear results from the trade-off, the octagonal cylinder shape is chosen for the baffle. It has good performance with respect to stowage volume of MLI and total mass, and the deployment is assumed to be more reliable than most options. The dodecagonal concept excels in stiffness and MLI area, but is given a mass penalty due to the large length and volume of booms required, which will increase the mass of the baffle itself and the inflation system significantly. Since the deployment of the baffle is a critical function for the mission success, the influence of this aspect is large in the selection.

4.5. Properties

In this section, the properties of the selected baffle shape are elaborated on and a drawing will be presented. The emphasis of the section is on ensuring that all system requirements are met and that the exact geometry is known before structural analysis of the baffle is performed.

4.5.1. Geometric properties

In the previous section the full operational requirements of the baffle were not taken into account, specifically the PMSS and SMSS deployment sequence envelopes. The geometry requirements were kept for simplicity in comparing the already created shape options, even if the results are slightly inaccurate for the actual system. After comparing the concepts and finalising the actual geometry of the winner, previously unaccounted for limitations were identified. The requirements for the geometry are derived from the general baffle requirements as follows:

- The baffle needs to extend beyond the position of M2
- After the baffle is deployed, it should not interfere with M1 or M2 deployment mechanisms
- During operations, the baffle shall be at least 200 mm away from any point of M1

These qualitative requirements on the geometry can be quantified by inspecting the related systems, that is the M1 and M2 subsystems and the deployment sequences associated with them. The given 200 mm distance requirement from M1 leads to an inner radius of 950 mm from the centre of the M1 assembly. However, the deployment clearance requirements will affect this. It is quickly observed that the secondary mirror deployment provides more strict requirements, as the primary mirror will not move outside its envelope which is already taken into account as the deployed state. Based on the thesis of Krikken, the mid-point of the integral slotted mid-hinge of the booms is 658 mm from the root hinge [61]. The worst case deployment scenario is assumed to be that the bottom part of the boom is in a horizontal position, with the aforementioned length from the hinge. Adding a margin for the hinges themselves, as they protrude out of the instrument bus walls, leads to an addition of approximately 200 mm based on the CORE root hinge design of Krikken [61]. The expected minimum radius of the torus centre line is 1 metre, including a safety margin of about 5 cm from the inner edge of the torus to the SMSS during deployment.

With the above requirements in place, the parameters in Table 4.8 were decided on.

Table 4.8: Parameters of the octagonal prism used for the baffle geometry

Parameter	Value
Total length	2.6 m
Radius	1 m
Area of each face	2.1528 m^2
Area of bottom shield	3.314 m^2
Total MLI area	20.54 m^2

4.5.2. Number of booms

The total number inflatable booms used to form the baffle shape and deploy the MLI is defined in this section. This will include the radial and longitudinal booms, as well as segments for forming the torus elements.

There are eight each of the lateral and longitudinal booms, which consist of a single element each. Therefore a total of 16 booms will need to be manufactured for the baffle. There is a seam connecting each cylinder into a closed shape, the specifics of which are still to be determined. The lateral booms are shorter, and have a length of 750 mm. The longitudinal booms are 2600 mm in length at this stage of the design.

The two tori will be made out of 16 identical straight segments, which then form an approximate circle. The averaged length of each segment is then approximately 39 cm. The approach is generally used for toroidal structures in consulted literature so no concerns are seen with it. An example of the manufacturing process for a inflatable torus can be seen in Figure 4.7 where the shape of the individual gores is clearly seen. The same approach will be used in this work, although manufacturing aspects will not be discussed further at this stage. The dimensions of the torus elements are seen in Figure 4.10b.

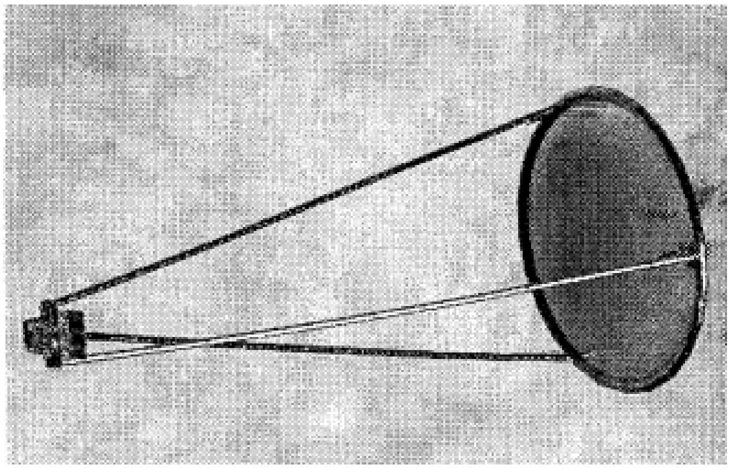

Figure 4.6: Inflatable Antenna Experiment in orbit [44]

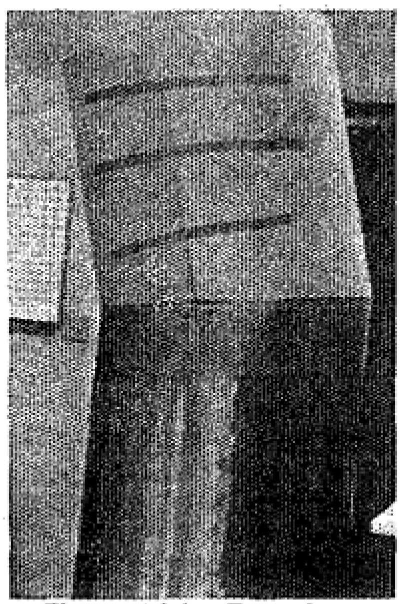

Figure 4.7: Torus segments being assembled for the IAE [101]

4.5.3. Boom diameter

The length of the booms is approximately known (exact length depending on the integration of their lower ends to the bus), but their diameter has not yet been decided. For a high flexural rigidity it is desirable to have a greater diameter, but this increases the mass and volume required for storage. The moment of inertia of a circular cross section is linearly dependent on the radius, and the flexural rigidity EI follows from it. Greater radius also enables lower pressure to reach the Von Mises yield stress of aluminium, which reduces the inflation risks.

In Figure 4.8 the common range of diameters for a given boom length is given for various types of deployable booms. It can be seen that for a boom length of about 3 metres, at least 100 mm diameter is used. It is decided for now to make the booms and torus with a constant diameter of 100 mm (as used in previous sections already) to ensure the structural robustness taking this graph into account. The torus will be joined with the longitudinal booms with sufficient seaming. The dimensions will be re-evaluated with the known performance once the structure of the booms is designed in Chapter 5. This diameter will be used for the CATIA illustration in the next section.

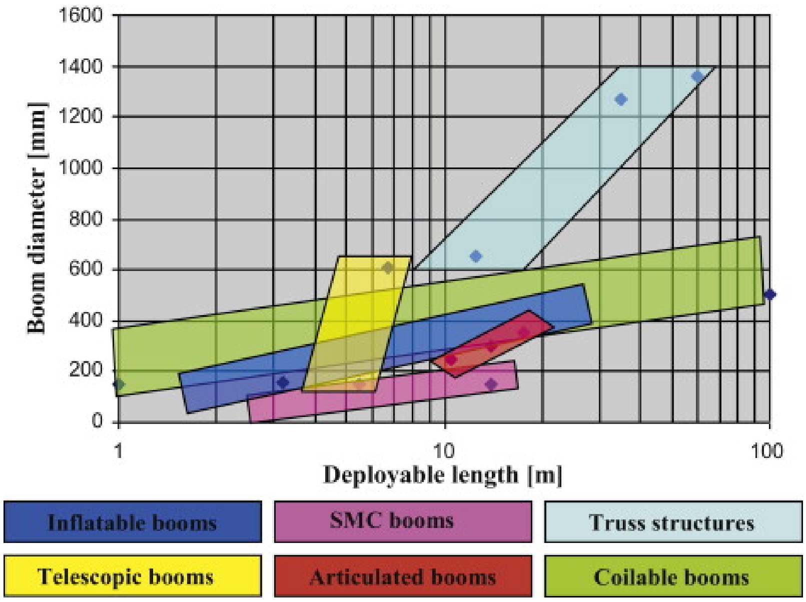

Figure 4.8: Usual diameter of deployable booms as a function of deployed length [80]

4.5.4. Complete geometry

CATIA drawings of the baffle shape and the dimensions decided earlier can be seen in Figures 4.9 and 4.10. These are subject to changes as the design is developed further, but the obtained geometry is used as a starting point for analyses. All the dimensions are obtained from the CATIA model of the structure, which results in some millimetre fraction dimensions for some parts of the geometry as seen in Figure 4.10b. The model however has been built with the dimensions discussed earlier.

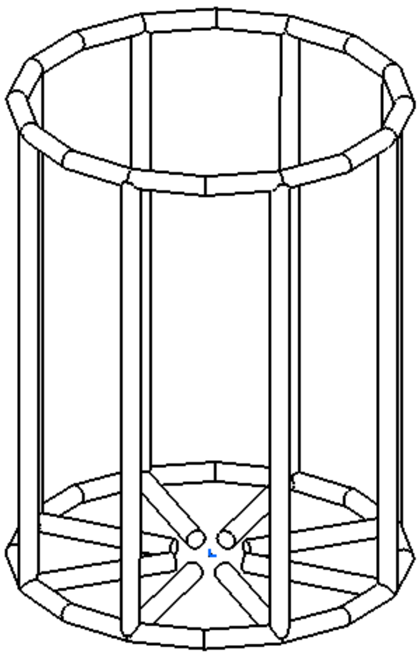

Figure 4.9: Shape of the baffle structure

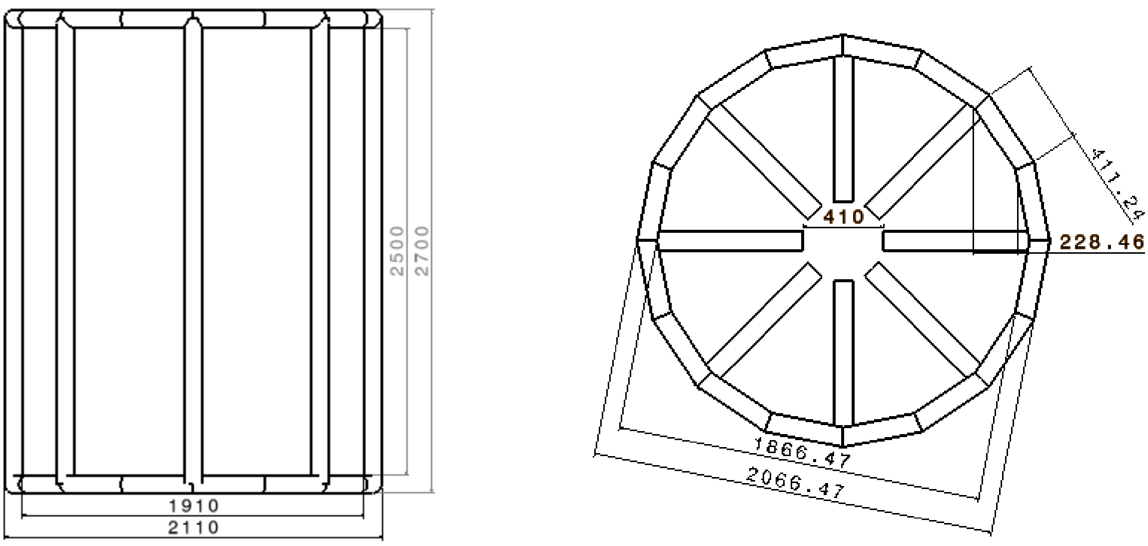

(a) Side view of the baffle geometry

(b) Bottom view of the baffle geometry

Figure 4.10: Baffle geometry, all dimensions in millimetres

5 Material selection

This chapter presents the full structural design of the baffle. The process begins with the explanation of the mechanism and general layout used, and continues with the selection of the specific materials. After determining the dimensions of the baffle elements, the mechanical properties are determined along with the thermal and optical properties.

The concept for the boom structure is discussed in Section 5.1. The materials for the booms are selected in Section 5.2 and the mechanical properties are calculated in Section 5.3. Thermal shielding is designed in Section 5.4 and the integration of the elements is discussed in Section 5.5. The results of the chapter are summarised in Section 5.6.

5.1. Structural concept

In this section, the concept for the structure of the baffle will be established. The general considerations to be taken into account are listed first in Subsection 5.1.1, after which the rigidisation aspect is discussed separately in Subsection 5.1.2.

5.1.1. Considerations

The use of multi-layer insulation (MLI) as the thermal shroud is almost necessary, and is by far the simplest option to meet the thermal stability requirements. This approach is selected to ensure the thermal stability of the telescope. Designing the MLI blanket composition is a compromise between the thermal insulation capability, the mass and volume budgets, and partially the availability of materials.

The structure has to allow for stowage, predictable inflation and a stable operational state of the booms. The stowage volume can be decreased by using thinner boom walls and an efficient folding method. The wall thickness correlates with its strength, which makes compromises inevitable. Inflation requires a path for the inflation fluid, as well as ways of controlling the pressure and avoiding leaks. Any seams and other joining points need to be carefully designed, and as few in numbers as possible to reduce the risk of unwanted leaking. Operational risks are reduced significantly if the inflation gas can be vented after deployment, while still keeping the structure of the booms in the same state. This cannot be achieved without rigidising the system in some manner, since the booms has to be flexible to allow for stowage. The system complexity needs to increase to decrease these risks, but it is worthwhile if a sufficiently easily implementable method is identified. This will be expanded on in the following subsection.

In operational state the baffle needs to resist both the radiative space environment as well as the hazards posed by impacts. The materials used for the system need to be selected with these considerations in mind. The mission lifetime is expected to be multiple years, which makes sufficient protection against the space environment important. It is especially important that the MLI blankets maintain their thermal performance over the lifetime to avoid decreasing image quality. The durability of the materials will be explored later in this chapter.

5.1.2. Rigidisation

In this work, the word "rigidisation" is used for the process to make the deployed inflatable system more structurally stiff, so that the inflation pressure does not have to be maintained during operation. The deployed baffle needs to attain a certain stiffness to endure the operational loads (from e.g. slewing) without endangering the telescope elements or its own structure. The booms have to keep the MLI elements from obstructing the field of view at all times the telescope is imaging.

Based on the prior literature review, it was found that one of the most simple and proven technologies for rigidising inflatable space systems is applying a yield load to the skin, which is formed of thin aluminium and polymer films sandwiched together. The aim is to achieve a stress just beyond the yield strength of the aluminium, while the polymer remains in the elastic region. The mechanical properties are then slightly increased and the structure remains rigid after the loading is removed [18]. The inflation gas can then be vented, and the resulting system is more rigid and resistant against impacts by e.g. debris in addition to increased stiffness. The yield load can be obtained by increasing the inflation pressure, which means that no additional elements need to be introduced to the system for rigidisation. The process is also predictable and has been used for space applications previously, with heritage starting in the 1960's with the Echo II reflective balloon as well as the Explorer IX and XIX experiments [18]. More recent concepts include the InflateSail cubesat experiment, where an inflatable rigidisable boom was used to deploy a drag sail for deorbiting satellites, and an inflatable solar array for small satellites [64, 96, 103]. A figure of the deployment and rigidisation process of the InflateSail boom can be seen in Figure 5.1.

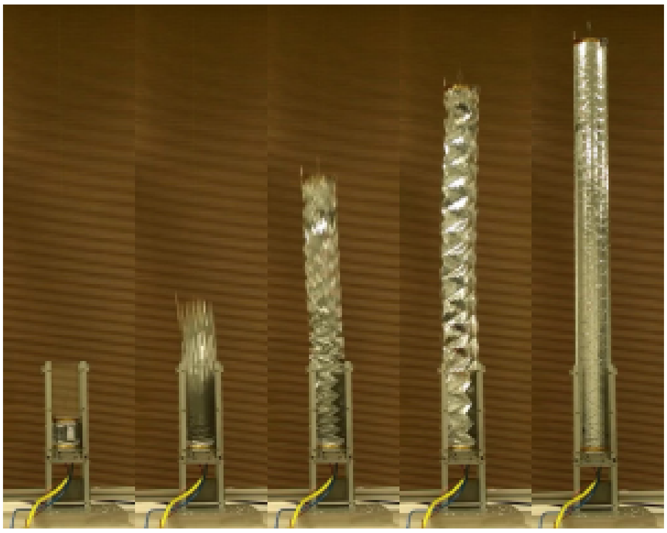

Figure 5.1: Deployment of the InflateSail inflatable boom [104]

Other rigidising methods are not considered for the baffle in this thesis. There are various other techniques to increase the stiffness of a deployed inflatable structure, but they all require additional resources and have less space heritage. The identified options are presented here for completeness along with the reasons they are not considered. Curing of a composite by using UV radiation requires an internal source for guaranteed uniform results, meaning additional complexity, mass and power consumption. Inflatable light shielding with sunlight curing has been conceptualised and prototyped, but the method is seen as too risky for this design due to the multiple manoeuvres required [13]. Temperature-based curing can be based on either thermosetting composites or utilising the glass transition temperature, both of which would require heating systems [18]. The rigidisation of an aluminium-polymer system can be achieved without over-pressurising; there has been research into spring-tape-reinforced (STR) booms for inflatable space antennas [39, 40, 65]. These achieve a higher buckling strength than the stretched laminate structures, but the inclusion of the tapes leads to a greater design complexity. The technology is considered not developed enough at this stage to use on DST, as the design process in the reference material is not quite developed enough for this project.

An example of the laminate used for the InflateSail mission can be seen in Figure 5.2, where the top and bottom sheets are aluminium and the middle one is polymer. The rigidisable structure can consist of either two films of aluminium sandwiching one of polymer, or vice versa [18]. The former option has a higher strength, and is therefore selected for the booms without further consideration, as the moderate mass increase will not outweigh the benefits of a higher strength. The aluminium outer surface is another benefit of this layout which might enable not including sleeves on the outside of the booms for a more stable temperature. In the following section, the exact parameters of the laminate layers are designed. Past rigidised inflatable structures have included an additional closed volume, into which the inflation fluid is injected to avoid leaks through the laminate walls. For example, an additional bladder to improve airtightness was included on the Inflate-Sail mast [103]. This has to be considered for the DST baffle as well, because of the danger of the aluminium films developing holes due to the folding or the inflation pressure. The structure has to have a uniform cross section for the optimal inflation, which leads to a cylindrical shape. This was already predicted earlier and therefore the nominal choice regardless. The earlier selected diameter of 100 mm will be maintained during the design process until reason to change it occurs.

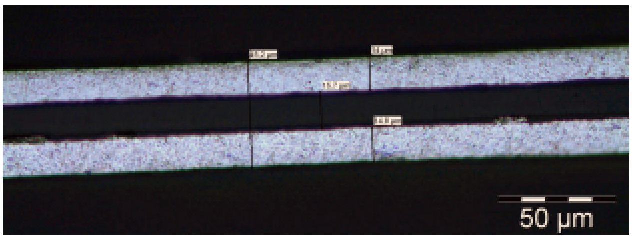

Figure 5.2: Cross sectional view of the aluminium-polymer film laminate used on InflateSail inflatable boom [85]

An important complication in the conceptual design of the rigidisable structure that cannot be ignored is the shape of the baffle. While the booms themselves form rectilinear sections, the joining areas between booms lead to discontinuities in the mechanical properties. Inflatable and mechanically rigidisable tori, however, have been in development, but the actual outcome has not been documented [46]. This implies that the process for a torus has historically not been found completely infeasible. However, the booms as well as the complexity of the complete structure pose an admittedly uncharted territory. It has been stated by previous researchers that the rigidisation of complex antenna structures is not possible with any current technology [39]. The baffle has a more difficult volume to inflate, and the numerous perpendicular booms adds another layer of difficulty. Whereas in a single straight cylinder the stresses are easily predicted, the addition of the seams between the booms can be expected to change the stresses in the skin. It has been assumed that the booms in a truss encounter the same stresses as a single boom due to the constant cross section, but this cannot be expected to hold in all situations in reality. The manufacturing and inflation are not seen as inherently problematic, but the rigidisation pressure becomes more unpredictable. The thickness of the skin also poses an issue depending on the manufacturing method. The seams have to be made stronger than the skin to reduce the risk of failure at their location. It is assumed that the inflation pressure required corresponds to a straight, perfectly uniform cylinder, while acknowledging that this cannot be guaranteed without testing.

An option for making the stress distribution in the skin more uniform involves wrapping a stiff cord around it. The performance improvements achieved with this technique have been documented by L'Garde [63]. The helical winding is not included in the boom design in this work due to the implication in literature that the effectiveness is mainly assessed experimentally, which cannot be done. This rings especially true in the case of a truss structure. It was found in previous research that the burst margin of the cylinder increased from 1.5 to 3, which is a promising result for the improvement in inflation reliability. Combined with the uncertainties in stress levels, this indicates the need to investigate the wrapping method in future work.

5.2. Laminate composition

In this subsection, the materials to be used for the aluminium-polymer laminate and their thicknesses will be decided. First, the aluminium alloy and the sheet properties are designed in Subsection 5.2.1, after which the polymer layer is considered in Subsection 5.2.2. Finally, the adhesive to attach these materials together is chosen in Subsection 5.2.3. Additions to the boom design necessary for pressurisation are discussed in Subsection 5.2.4.

5.2.1. Aluminium layers

The laminate will include two identical layers of aluminium. The choice of the specific alloy depends on the desired properties and is largely based on prior research. In literature, alloys 1100-0 and 3003-0 are identified as suitable options for inflatable aluminium-polymer laminates [18]. Of these, the former was used on the Echo II balloon, which has a similar aluminium-polymer-aluminium laminate structure as is being designed. Comparing the two alloys, the 3003-0 has a higher strength, since 1100-0 is a more pure alloy. Thermal conductivity is also slightly higher for 1100-0 since it is closer to pure aluminium, which is beneficial since the presence of thermal gradients should be minimised over the whole telescope. While specific strength is generally better when higher, in the case of the inflatable baffle a compromise has to be made. The baffle has no significant load carrying purpose, but the rigidisation process requires the aluminium sheets to be yielded due to inflation pressure. To achieve this more easily, a lower yield stress is advantageous. The minimisation of inflation pressure can be considered an important design parameter, since it affects the required storage volume of gas as well as the risks involved with the inflation, such as bursting. For this reason, as well as the heritage, aluminium 1100-0 alloy is used for the laminate.

It is known from literature that the total thickness of the aluminium sheets should not exceed 100 μm to prevent the laminate from debonding. On the Echo II balloon, the aluminium layers had a thickness of 4.57 μm each, which is only approximately 10% of this maximum [18]. However, the diameter of the balloon was above 40 metres, which makes its volume about 5000 times as large as the approximated baffle volume. This makes the reference thickness not fully applicable. Rigidisable cylinders made of variable thickness aluminium 1100-0 foil and polyester were tested in the 1980's for inflatable antenna research [46]. The lowest thickness of a single aluminium layer in this study was 25 μm and the highest 51 μm, with a constant polymer thickness of 13 μm. The diameters of the tested cylinders were of the same order of magnitude as the baffle booms, while their length was smaller. It is seen in Figure 5.4 that the elastic modulus was observed to decrease with thickness while the ultimate strength increased. Since stiffness is assumed important for the baffle structure and it is largely driven by the aluminium, the results are implemented in the design. A thickness, per layer, of 25 μm is selected here. This also has the advantage of keeping the structure more lightweight and its delamination risk low, and to minimise the inflation pressure (which directly correlates with amount of gas stored on board) needed to rigidise the structure. Additionally, the stowing is expected to be easier with a lower thickness of metal. Thicknesses below this have been used for the InflateSail but it is decided to make the structure stronger with the use of more aluminium due to the need for the baffle to be as reliable as possible [96]. Furthermore, the structure has to carry the mass of the shielding elements.

5.2.2. Polymer layer

There are two widely used options for the polymer component of the laminate based on literature. These are Mylar and Kapton, which are each common polymers for various space applications. The Echo II had a Mylar film between the aluminium sheets, whereas Kapton has been used in more recent polymer-aluminium-polymer type laminates [33, 78]. Since the polymer will be between two sheets of aluminium and therefore minimally exposed to the space environment, the main considerations for the section are thermo-mechanical. Kapton has a greater range of operational temperatures than Mylar, which is the main difference between the two polymers. Both have a low coefficient of thermal expansion (CTE), especially compared to the aluminium layer. To account for extreme temperatures, Kapton is selected as the polymer material for the laminate. This material also experiences low degradation in space, unlike Mylar which is known to degrade, even if exposure is assumed to be minimal.

In the Echo II laminate, the polymer layer was twice as thick as a single aluminium layer. However, to prevent instant buckling, it has been found that the metal layer should be thicker than the polymer for cylindrical laminate structures [46]. The availability of commercial Kapton films is also a deciding factor, since the telescope project benefits from easy acquisition of materials. DuPont provides Kapton films for a variety of purposes in multiple thicknesses from 7.5 to 125 μm [31]. Based on the laminate cylinder research referenced above, a Kapton film thickness of 12.7 μm is selected for the baffle laminate. The type considered at this stage is the HPP-ST, since its adhesion properties are better than for the HN, the other common type presented [31]. Adhesion is considered a key property due to the precise lamination process which follows from the use of thin films and foils.

5.2.3. Adhesive

Due to the inclusion of one Kapton film between two aluminium foil layers, a ready-made Kapton tape cannot be used as an adhesion solution. Therefore, a separate adhesive is selected for the laminate. The required properties are sufficient strength to avoid delamination, as well as low out-gassing in the vacuum space environment over the mission lifetime. The adhesive needs to naturally be compatible with an aluminium-Kapton interface, and provide uniform adhesion over the whole surface area. Due to the thermal insulation purpose of the baffle, it is preferable to also have a low thermal conductivity in the adhesive layers, while it is not a driving requirement. Based on ESA data on low outgassing and successful flight experiments on the Long Duration Exposure Facility (LDEF), the EC2216 (grey) adhesive by 3M is preliminarily selected [35, 37]. Additionally, it is told to have a high flexibility and be applicable for high performance aerospace applications [3]. The same adhesive has been used for bonding Kapton films for an inflatable RF antenna [39]. Other options include the Y966 adhesive tape by 3M, which is applicable due to its good properties in vacuum and high temperatures[2]. This option might be more appropriate due to manufacturing considerations.

The EC2216 adhesive is available in an already mixed state as well as separate components to be mixed right before use [3]. For the baffle laminate construction, neither seems like a superior option, so either can be used. The data sheet indicates a bond thickness of at least 3 mil (75 μm) for maximum shear strength, but this is 3 times as thick as the aluminium sheet and almost 6 times as thick as the Kapton film used. It is assumed based on previous rigidisable cylinder experiments that a 25 μm layer is appropriate for the selected metal and polymer layers [46]. The adhesive layer thickness will not be taken into account in the subsequent property analyses.

5.2.4. Pressurisation elements

The next problem is how to realise the pressurisation of the laminate beyond the aluminium yield stress. The inflation gas needs to be uniformly applied into the structure so that the walls unfold from the stowed state and eventually rigidise.

The inclusion of a separate bladder for the inflation gas becomes almost necessary for the reliability of the system. The probability of punctures in the aluminium is too high to risk for such a crucial stage of the mission. The requirements on the bladder material are less stringent than for the laminate due to the expected short operational time. However, low out-gassing properties are necessary to not disrupt the functioning of the telescope. The InflateSail bladder is made of Mylar and has a thickness of 12 microns, which is a good option also for the DST [96, 103, 104]. The folding and inflation are made more complicated by the addition of layers, but the reliability of the baffle is the main consideration for mission success.

To assemble the cylinders out of laminate sheets, a seam has to be introduced. The stiffness of the booms will be greater at the location of the seams, which will cause some incompatibilities during inflation. However, the effects of a 10 mm seam on a deployed 90 mm diameter boom have not been found to be notable [103]. The effects caused by the seams will therefore not be taken into account in the scope of this thesis work and the booms will be assumed to be homogeneous in any subsequent analysis.

5.3. Mechanical properties

In this section, the mechanical properties of the baffle structure are determined. In Subsection 5.3.1 the assumptions are listed. Subsection 5.3.2 entails the determination of the laminate properties, and the boom mass is consequently estimated in Subsection 5.3.3. The laminate properties are used to calculate the approximate yield pressure to rigidise the structure in Subsection 5.3.4. A summary of the properties will be given in Section 5.6.

5.3.1. Overview and assumptions

For calculations of the mechanical properties of the laminate, the plane of the laminate is considered the xy-plane in the coordinate system, while z-axis is along the thickness of the plate. This is shown in Figure 5.3.

Thin-walled assumptions apply because the total wall thickness is below 1% of the boom radius. The booms are considered to be circular cylinders with isotropic properties within the skin.

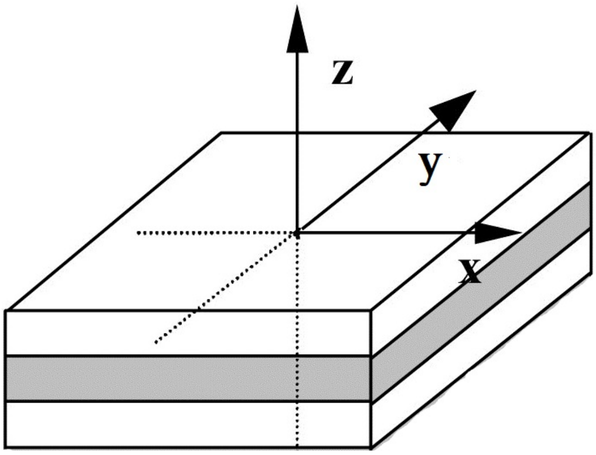

Figure 5.3: Reference frame of the laminate (figure adapted and modified from [49])

The physical and mechanical properties are assumed constant over the whole length of the baffle.

To find the skin properties, classical lamination theory is applied, where the laminate is assumed to be transversely isotropic and symmetrical by cross section. This leads to the in-plane properties being the same in longitudinal and transverse (x and y) directions.

Perfect adhesion is assumed in the calculation of mechanical properties. Each material is assumed to be in the linear elastic region for these calculations, so the results might not be perfectly representative in the rigidised state.

In pressurised state, the outer laminate wall is assumed to behave similarly to the wall of a thin-walled closed cylinder. The assumption might not be valid near the ends of the baffle, but this will be ignored in the calculations. The inner laminate is assumed to be loaded in compression, and will be assumed to have the properties of a thin-walled cylinder with external pressure acting on the walls. In other words, the interaction of the two walls and the mechanical behaviour caused by the lack of end caps for each cylinder are not taken into account.

5.3.2. Laminate properties

In this section, mechanical and thermal properties of the designed laminate will be calculated to be used in subsequent analyses. It is noted that testing the actual laminate will be necessary to obtain the realistic properties, but the values of this section serve as a first order estimate.

The classical lamination theory is used to calculate the in-plane properties of the laminate. These will be used for e.g. the subsequent numerical analyses. Classical laminate theory is used for this, with the assumptions stated above. The relations below are taken from [74]. Note that the index (3,3) of the Q matrix is labelled (6,6) due to convention.

$$Q = \begin{bmatrix} Q_{11} & Q_{12} & 0 \\ Q_{12} & Q_{22} & 0 \\ 0 & 0 & Q_{66} \end{bmatrix} \tag{5.1}$$

where

$$Q_{11} = Q_{22} = \frac{E}{1-\nu^2} \tag{5.2a}$$

$$Q_{12} = \frac{\nu E}{1-\nu^2} \tag{5.2b}$$

$$Q_{66} = G \tag{5.2c}$$

In all these equations, E is the Young's modulus of the material and ν is the Poisson's ratio. The factor G is the shear modulus of the material. The theory can be simplified due to the symmetry of the laminate, and instead of three matrices, only one needs to be defined to calculate the total properties. The A matrix is constructed as shown in Equation (5.3). Here, k is the number of the considered layer and t_k its corresponding thickness.

$$A_{ij} = \Sigma_{k=1}^{n} [Q_{ij}]_k t_k \tag{5.3}$$

The in-plane properties are calculated as shown in Equations (5.4) to (5.6). The properties in x- and y-directions are identical due to the fact the laminate is isotropic in the xy-plane, which is reflected in the equations. Here, h is the total thickness of the laminate.

$$E_x = E_y = \frac{1}{h}\left(A_{11} - A_{12}\left(\frac{A_{26}A_{16} - A_{12}A_{66}}{A_{22}A_{66} - A_{26}^2}\right) + A_{16}\left(\frac{-A_{16}}{A_{66}}\,\frac{A_{26}A_{12}A_{66} - A_{26}^2 A_{16}}{A_{22}A_{66}^2 - A_{26}^2 A_{66}}\right)\right) \tag{5.4}$$

$$G_{xy} = \frac{1}{h}\left(A_{66} - \frac{A_{26}^2}{A_{22}} + \frac{2A_{16}A_{12}A_{22}A_{26} - A_{12}^2A_{26}^2 - A_{16}^2A_{22}^2}{A_{11}A_{22}^2 - A_{12}^2A_{22}}\right) \tag{5.5}$$

$$\nu_{xy} = \nu_{yx} = \frac{A_{12} - \frac{A_{16}A_{26}}{A_{66}}}{A_{22} - \frac{A_{26}^2}{A_{66}}} \tag{5.6}$$

The properties used for the analysis are shown in Table 5.1. The aluminium 1100-0 properties are from a data sheet [66] and the Kapton properties are from DuPont [31] with the exception of the shear modulus, which is taken from [22]. It should be noted very well that the elastic modulus of aluminium foils has consistently been found to be lower than the expected standard value when tested [103]. In the analyses to follow, the value for the aluminium 1100-0 foil from Figure 5.4 will be used, which equals 8.3 GPa [46]. This will possibly provide an analysed poorer performance than will occur in reality.

Table 5.1: Properties of aluminium and Kapton layers used for laminate property calculations

Material	Thickness [μm]	E [GPa]	G [GPa]	ν [-]	α [10^{-6}/K]
Aluminium	25	8.3	26	0.33	23.6
Kapton	12.7	2.5	2	0.34	20

To quickly evaluate the in-plane properties of the laminate, an algorithm was written in MATLAB. The inputs to this code are the material properties and thickness of each material, and the outputs are the Young's modulus (E), the shear modulus (G) and Poisson's ratio (ν). These are shown in Table 5.2 for the current design of the laminate. Only one value of each is presented, as the laminate is isotropic in-plane. These values will be used to create accurate material properties when modelling the baffle in CAD software, and for any subsequent analytical calculations.

The linear coefficient of thermal expansion (CTE), represented by α can be evaluated with a simple analytical procedure. The rule of mixtures can effectively be used due to the isotropy of the laminate in-plane [49]. The equations for the coefficients in x/y- and z-directions can be seen in Equations (5.7) and (5.8), respectively. The values from Table 5.1 are filled in to obtain the laminate properties. The quantity V is the volume fraction of the laminate constituents, which here will be taken as the ratio of the material thickness to total laminate thickness without adhesive. The results can be seen in Table 5.2.

$$\alpha_x = \alpha_y = \frac{\alpha_1 E_1 V_1 + \alpha_2 E_2 V_2}{E_1 V_1 + E_2 V_2} \tag{5.7}$$

$$\alpha_z = (1+\nu_1)\alpha_1 V_1 + (1+\nu_2)\alpha_2 V_2 - \bar{\nu}\alpha_x \tag{5.8a}$$

$$\bar{\nu} = \nu_1 V_1 + \nu_2 V_2 \tag{5.8b}$$

Table 5.2: In-plane properties of the aluminium-Kapton laminate

E [GPa]	G [GPa]	ν [-]	$\alpha_{x,y}$ [10^{-6}/K]	α_z [10^{-6}/K]
7.1	21.05	0.33	23.3	22.7

5.3.3. Preliminary boom mass

A preliminary mass calculation provides evidence that the baffle structure can be extremely lightweight. The booms will contribute a small portion of the total system mass compared to the MLI, and possibly the inflation and stowage systems will also be significantly heavier. For the following estimation of boom mass, the thickness of each layer is taken from the previous section, and the number of booms specified in the previous chapter is included. The tori are assumed to be perfect circles with 1 m diameter and connections between booms are neglected. The values used and the results in kg rounded to two decimal places can be seen in Table 5.3. It can be seen that the mass of the structure is very low, which is beneficial for meeting the requirements of the system. Additional mass will be introduced by the addition of a bladder material, but this will be of the order of a few hundred grams at most, as e.g. Mylar has the approximate mass properties of Kapton, which can be seen to weigh only 230 grams. Furthermore, the seaming of the cylinders requires aluminium coated tape, which adds some weight of the same order of magnitude. Overall, these unaccounted sources of mass are expected to at most bring the boom system mass to approximately 2.5 kg, which is still compliant to the requirements.

Table 5.3: Densities of laminate materials and the preliminary weight estimate, rounded to two decimals

Material	Density (kg/m^3)	Mass (kg)
Aluminium 1100-0	2710[66]	1.69
Kapton HPP-ST	1420[31]	0.23
EC-2216	1300[3]	0.12
Total	2328.91	2.03

5.3.4. Yield pressure

The rigidisation of the aluminium laminate requires the yielding of the metal layers and the plastic deformation that follows. It is important to only introduce a stress just above the yield stress to avoid excessive strains and bursting. In this section, the pressure required to yield the laminate is calculated by using mechanical principles and literature examples. The assumptions used are a consequence of recognising that the inflated cylinders are essentially pressurised thin-walled vessels, similar to aircraft fuselages in cruise altitude.

Pressurised thin-walled cylinders have the property that the hoop stress in the skin equals twice the longitudinal stress, as seen in Equation (5.9). Here, p signifies pressure and R the radius of the cylinder. This leads to the expectation that the deformation of the booms until yielding will be mainly in radial direction instead of longitudinal. The downside of this is that the skin will be less smooth in longitudinal direction, as creases will remain on the deployed cylinder [63].

$$\sigma_l = \frac{pR}{2t} \tag{5.9a}$$

$$\sigma_h = \frac{pR}{t} \tag{5.9b}$$

For the yielding of the cylinders, the Von Mises criterion is used. The internal pressure at which the cylinder yields, p_y, can be calculated as in Equation (5.10) or Equation (5.11) [46, 103]. Both will be calculated to cross check the acquired pressure. The thicknesses and Young's moduli of aluminium and Kapton are known, as well as the boom radius. Out of the terms present, the yield stress of the aluminium layers, σ_y, is the only value that still needs to be acquired from a reference, as testing is not possible within the scope of this work. Figure 5.4 shows experimental results from development of an inflatable antenna, which are highly applicable as the alloy used is the same as here [46]. Since it was already concluded that the found low elastic moduli of aluminium foils are used in analysis, the data is useful for finding a stress level just beyond the yield stress of the material and the corresponding strain. In the same article, a stress of 28.5 MPa was selected for the determination of the yield pressure for all aluminium thicknesses, which can be reproduced from the figure [46]. Additionally, in the InflateSail research a yield stress of 50 MPa has been found for the aluminium-Mylar laminate used (total 26 μm aluminium), with a note that using Kapton instead lowers the yield strength by approximately one-third [96, 102, 103]. Based on the two references, an average yield stress of 30 MPa will be assumed for the pressure calculation, but the actual value will have to be determined by testing a prototype.

$$p_y = \sqrt{\frac{4}{3}}\frac{\sigma_y t}{R} \tag{5.10}$$

$$p_y = \frac{\sigma_y t_a}{r\sqrt{K1^2 - K1K2/2 + K2^2/4}} \tag{5.11a}$$

$$K1 = \frac{1-\nu^2-\nu C+1.25C}{1-\nu^2-\nu C+2C+0.75C^2} \tag{5.11b}$$

$$K2 = \frac{1-\nu^2-2.5\nu C+2C}{1-\nu^2-\nu C+2C+0.75C^2} \tag{5.11c}$$

$$C = \frac{E_k t_k}{E_a t_a} \tag{5.11d}$$

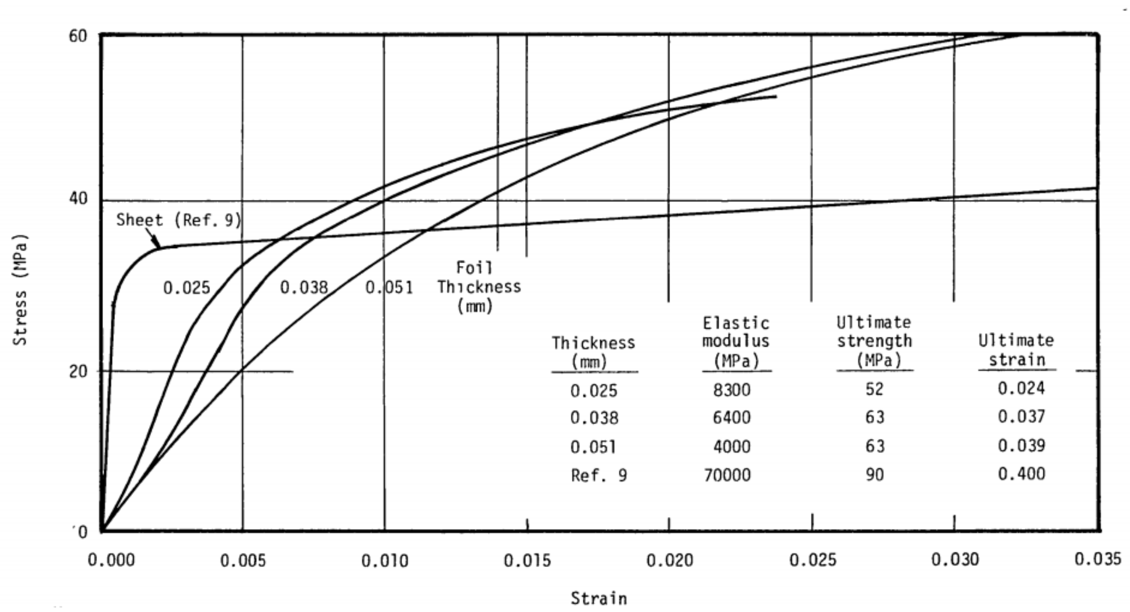

Figure 5.4: Aluminium 1100-0 foil data, from [46]

After performing the first calculation with the laminate properties and the boom geometry, a yield pressure of 34.64 kPa is found, which is in line with the pressures found in previous research referenced above. The second method provides a pressure of 36.14 kPa, which is a difference of about 4%. It is chosen to use a pressure of approximately 35 kPa for the design point of the inflation system. The method of generating this pressure will be a point of discussion in Chapter 7. The determination of the actual yield pressure requires building a prototype and testing the inflation and rigidisation sequence, which will be a recommendation for future work to resolve the uncertainties stemming from the numerous assumptions and simplifications.

5.4. Multi-layer insulation

In this section, the principle and practical aspects of multi-layer insulation (MLI) for the thermal control of the baffle is explored. The layout of the MLI will be designed and its properties will be given. The design of the MLI will be used as input for the thermal model of the DST, made by T. van Wees. The performance will therefore not be analysed in this section, but rather the results from the model will be presented in Chapter 8.

The reasons for using MLI are expressed in Subsection 5.4.1 and theory on the principle is given in Subsection 5.4.2. The materials and thicknesses of the layers, and their total number, are given in Subsections 5.4.3 and 5.4.4, respectively. The mass is then estimated in Subsection 5.4.5.

5.4.1. Method of shielding

The selection of the shielding principle, and consequently materials used, is briefly elaborated on here. The choice of the method was quite straight-forward based on the requirements on mass and stowed volume, as well as thermal performance. This section is included for completeness and to increase the fidelity of the design choices.

The requirement of deployability was quickly seen to disqualify any sort of solid barrel structures, such as can be found on e.g. the Hubble Space Telescope. The use of shrouds for thermal and stray light control is not novel, and therefore flexible membranes were seen as the obvious choice to provide the necessary shielding. The inclusion of additional rings inside the baffle for stray light control was briefly considered, but the deployment of such solid elements was deemed infeasible within the scope of this work. In the future, additional structures for stray light prevention can be looked into. For now, only shroud elements will be included in the design.

In discussion with Airbus Defence & Space, it was brought up that actual multilayer insulation might be unnecessary for the DST, as some previous thermal shielding systems in space have consisted of more simple membranes for shrouding. However, it is assumed here that the thermal stability will only be achievable with a heavily insulating structure around the telescope. If it turns out that the thermal needs can be met with a less complex shroud, the design will be iterated. In comparable thermal shielding systems found in literature and previously referenced, MLI has been used as the means of insulation.

5.4.2. Theory

Multi-layer insulation, or MLI, is a common method used on spacecraft to keep heat in or out of the subsystems and instruments. In case of DST, radiative flux to the optical and structural elements needs to be minimised to reduce the magnitude of thermal gradients and consequently deformations. Its effectiveness is based on the use of multiple layers of low-emittance materials that are insulating in their own right, and the separation of these layers to minimise conduction. The main insulators are thin films of polymer, which ideally have only radiative heat transfer between each other, aided by metallic coatings. Alongside these films, separators are included to decrease the contact area between layers. The layers on both sides of the stack generally have different properties than the inner insulation layers. A general layout with the different layers can be seen in Figure 5.5.

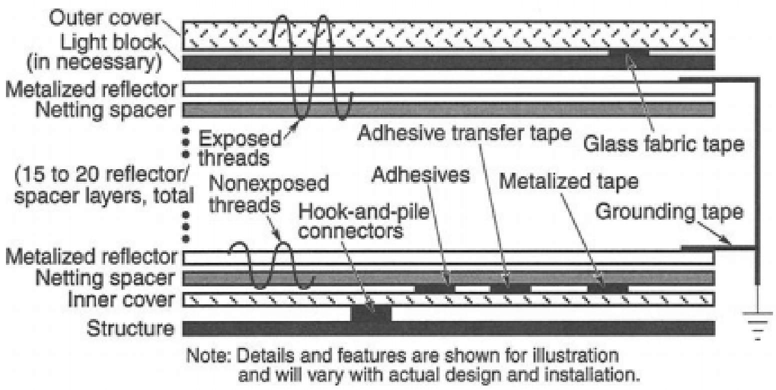

Figure 5.5: Typical layout of an MLI blanket [48]

The performance of MLI is often measured by its effective emittance, ϵ^*. This represents the fraction of heat transferred through all the layers and is naturally better for insulation when lower. The lowest reachable values are approximately 0.015 to 0.030 depending on the number of layers and the materials used, as well as the spacing between the layers [48]. The performance of a blanket cannot be accurately predicted without testing, but an attempt will be made to analyse the possible performance. In the following sections, the number of layers used for the DST thermal insulation as well as the materials used for each layer are elaborated on.

5.4.3. Layer constituents

The inner- and outermost layers in the MLI are what ultimately defines the optical properties of the baffle. The outer layer of the MLI is important for the amount of sunlight absorbed by the system. For this reason, the α/ϵ ratio of the outermost layer should be as low as possible to prevent high heat intake. A layer of silvered Teflon is the most effective solution based on literature. It is, however, important to bond the Teflon layer to e.g. Kapton for structural integrity over a longer mission duration [48]. The outer layer will have a thickness of 0.051 mm [41]. In the requirements, the absorption of stray light is defined as a necessary function of the surface seen by the mirror. The innermost layer of the blanket might not be visible to the optical system in the final design, but to eliminate stray light the inside will be made black. It is possible to load carbon on Kapton and generate a black surface to reduce glint [48]. Specialised space use black coatings can be easily found commercially. For example, the Magic Black coating by Acktar has a reflectivity of only 1% and it can be added to most surfaces [4]. An even more efficient stray light suppressor is the famous Vantablack by Surrey Space Systems, which absorbs 99.965% of incoming sunlight at 750 nm [91]. However, the high performance comes at an extremely high cost which makes the Magic Black a more suitable options due to the large area that needs to be coated. This coating will be applied to a Kapton foil with a thickness of 0.051 mm, just like the outer layer.

The insulating properties of the MLI are mainly derived from the presence of the polymer layers, which have a low conductivity and are allowed as little contact with each other as possible. The most common polymers used are Kapton and Mylar, where the former is used especially when high operational temperatures are encountered. Aluminium or gold can be deposited on one or both sides of each polymer film to increase reflectivity. Due to the unknown environment prior to deployment, Kapton is chosen for the internal layers to account for possible high temperatures. Both sides will be aluminised for higher performance. Due to the necessary folding during stowage and the possible stresses during deployment, the thickness of the layers is increased from the possible minimum. A thickness of 0.013 mm per layer is selected based on the options commonly available and taking into account the mass budget, leading to a total thickness of 0.13 mm for the raw material [48]. For venting purposes, each layer will be perforated as is the norm for systems launched to space [48].

It is common to crinkle or emboss the reflector layers in MLI to reduce contact, but due to the fact that the blankets will be folded before deployment, additional separator layers are added. The most common mesh materials used on spacecraft are Nomex and Dacron, which have very similar mechanical and physical properties [48]. Dacron is also known as the polymer PET, while Nomex is made of the presumably more expensive aramid. Dacron is used more commonly and will be included in the baffle thermal insulation. A total of 11 layers of Dacron mesh will be used between the layers of aluminised Kapton.

The closing of the MLI blankets at the edges can be done with the help of adhesive tape. Care has to be taken to maintain sufficient performance near the taped areas, as emissivity is increased closer to added seams [48]. The surface of the tape also needs to resemble the surface of the outer MLI material to avoid large temperature differences. Double-sided adhesive tape can be used to create a tape with the outer MLI layer on the outside. This is selected as the approach to be used here due to the thermal requirements. Gaps are left in the tape cover to aid venting during de-pressurisation. The blankets are sewn together much like garments, and there are different types of thread available. Since an environment with considerable atomic oxygen is foreseen, quartz thread will probably be used [48]. This level of detail is not final at the current stage of the design, but is included for reference.

An overview of the layers and their optical properties (where relevant) is found in Table 5.4. The properties are taken from [48], except the black coating properties are from [4]. The mass estimate will be done in the following section.

Table 5.4: Multilayer insulation constituents and their optical properties

Material	Number of layers	Emissivity	Absorptivity
Double-aluminised Kapton	10	0.05	0.12
Dacron net	11	-	-
Silvered Teflon	1	0.60	0.10
Black-coated Kapton	1	0.93	0.99

5.4.4. Number of layers

In this section the number of layers to be used for the MLI will be determined. The original plan for the design process was to obtain a thermal performance requirement, preferably in the form of an allowable heat throughput, but this was found infeasible in the thermal modelling process. The approximate performance of the designed thermal shielding can be verified, but the design has to be independent of the model. The usual procedure of using the emissivity is explained for background before the method that was actually used is described.

In the ideal case, the maximum allowed effective emissivity would be known for the thermal shielding. This decreases with an increasing number of layers, but in practice it is observed that the minimum achievable emissivity is obtained with approximately 25 layers of polymer [42, 48]. Figure 5.6 shows theoretical and experimental performance as a function of the number of layers for different temperatures. This plot would be used if the value of ϵ^* was known to estimate the required thickness.

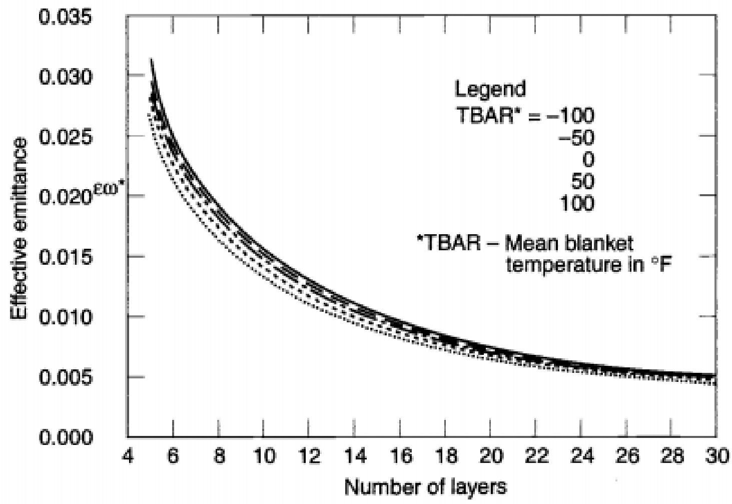

Figure 5.6: Spacelab test data of effective emittance of MLI blankets as a function of number of layers [48]

As a result of not having a pre-set thermal requirement, the MLI blanket design has to be based on other parameters. The identified options are mass, available stowage volume, and the ability to fold blankets into the stowed condition. The last option was researched, but no conclusion was found for the maximum allowed thickness or number of layers. Using simple stress calculations, the minimum bending radius for a Kapton foil was found to be in the order of 0.1 mm, providing no real limitation on the folding. Multiple thermal shielding concepts have included approximately 5 layers of shielding, most notably the inflatable shield envisioned in [14] and the James Webb Space Telescope, the five-layer sunshield of which is folded into a small launch volume. The stowed volume available has been determined to be dependant on the design of the baffle, to allow for a performance based design in the absence of strict volume budgets. However, the telescope mass is still desired to be as low as possible. Therefore, the total mass of the MLI blanket will be taken into account beside the best performing materials. Since the mass of the booms is known to be approximately 2 kg in materials only, it is necessary to keep the MLI mass below 10 kg, as the inflation system will have a mass approximated as 2 kg total for now (the design is done in Chapter 7, but will be referred to here). With the known materials, the mass of the blankets as a function of number of layers can be plotted, as is shown in

Figure 5.7. The number of layers here refers to the reflector layers, which means that there are $N+1$ spacer layers and the inner and outer foils are always included.

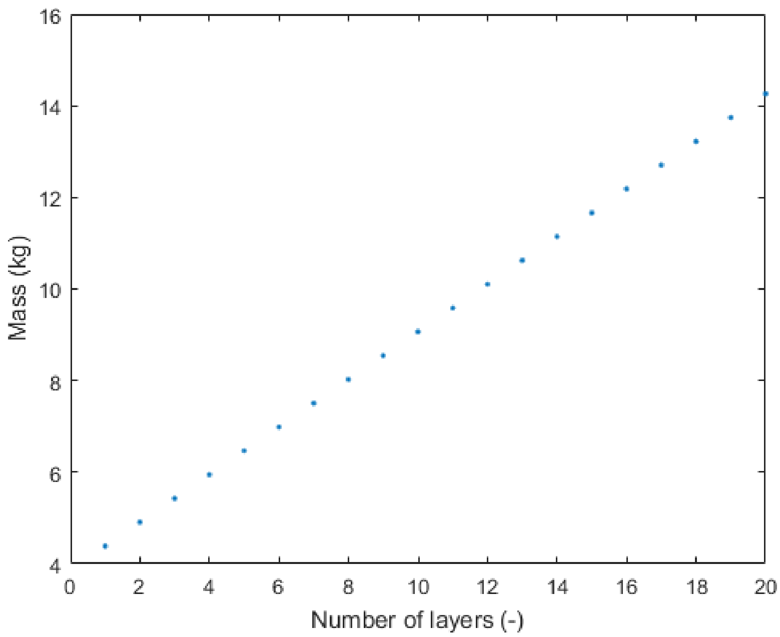

Figure 5.7: MLI mass as a function of the number of reflector layers

To stay below 10 kg, a maximum of 11 reflector layers can be used. However, this mass estimate does not take into account the seams, thread or any fasteners used for the MLI. For this reason, a margin of about 1 kg is used. This allows the use of 10 layers, which has a mass of 9.06 kg. The actual mass constituents are explained in the next subsection, for clarity. The performance of this configuration will be verified by thermal modelling, and if necessary, iterations will be made.

5.4.5. Mass estimate

Based on the decisions made in the previous sections, a preliminary mass estimate for the MLI blankets can be calculated. The estimate will be based on the properties of the bulk materials used, when the total amount of material is known. In this calculation, the shape parameters are taken from the previous chapter, so most likely the surface area of the baffle is overestimated at the bottom. This calculation will serve as a conservative estimate for the current configuration. The constituents, their amount and properties, and the total mass can be seen in Table 5.5, where the innermost black-coated Kapton layer is assumed to have twice the area density of the regular Kapton due to being twice as thick. The total material mass can be seen to be in excess of 9 kg even without taking into account the additional elements such as seaming tape and attachments to the booms. It is noted that a previous MLI blanket design consisted of more layers, but due to violating the mass requirement, the design was altered to the current version. This calculated mass is still subject to change with any design variations, but the value acquired here serves as an initial estimate.

Table 5.5: Mass calculation for the multilayer insulation material

Material	Thickness (mm)	Total area m^2	Area density (g/m^2) [41]	Mass (g)
Double-aluminised Kapton	0.013	205.4	19	3902.6
Dacron net	0.16	225.94	6.3	1423.4
Coated Teflon	0.051	20.54	110	2259.4
Black Kapton	0.051	20.54	72	1478.9
Total	1.992	-	-	9064.3

5.5. Integration and additional properties

In this section, the integration of the different baffle elements is discussed. The detailed design will be left for a later stage, but the arrangement of the booms and MLI will be conceptualised as it is critical for the whole baffle design. This will be discussed in Subsection 5.5.1. The coupling of the inflatable booms is briefly handled in Subsection 5.5.2 and the overview of the optical properties is given in Subsection 5.5.3. Finally, the expected durability in the LEO environment is discussed in Subsection 5.5.4.

5.5.1. Integration of the booms and MLI

The integration of the booms and MLI depends on the deployment, stowage as well as operational aspects. It has been established in thermal analysis by van Wees that the location of the booms could be inside, outside or in-between the MLI blankets without the thermal characteristics changing significantly. Each of these options has their advantages and disadvantages, of which an overview can be seen in Table 5.6.

Table 5.6: Comparison of different boom placements with respect to the MLI blankets (inside = telescope side)

	Advantages	Disadvantages
Inside	Simple deployment Booms protected from LEO environment	Stray light
In-between	Thermal stability of booms Booms protected from LEO environment Less stray light	Complex stowage Complex deployment
Outside	Simple deployment Less stray light	Booms exposed to space environment Stowage more complex

For stowage, it is preferred to have the MLI form the outermost structure, since it is the element that defines the stowage volume. Additional thermal protection prior to deployment is also an advantage of this approach. The main issue with the booms on the inside is the introduction of unpredictable reflections from the interfaces between the booms and the MLI, as well as added stray light reflections due to the booms. The booms naturally will need to be coated with the same black coating as the inside of the MLI to mitigate this. This is not expected to affect the mechanical properties, but care has to be taken that the coating does not crack or otherwise degrade due to folding and inflation. This option is therefore chosen, and a visualisation can be seen in Figure 5.8.

Attaching the MLI to the inflatable booms to deploy it is the next major concern in system feasibility. Due to the folding of the system being necessary, it needs to be ensured that the different elements deploy reliably from their stowed states. For thermal control performance, the blanket will be continuous around the circumference, consisting of multiple overlapping sections. The edges are preliminarily placed at the location of the booms, where the attachments are also made. The booms could be stowed separately from the MLI and only attached at the ends, which would enable using an optimised folding pattern for the booms which makes their deployment more reliable. However, this approach introduces risks with the stability of the MLI blankets during operation, as well as a higher stowage volume. The other option is connecting the booms to the MLI seams along the whole length, and stowing the whole system using the same pattern, treating the boom as embedded elements in the MLI. This will most likely lead to sub-optimal boom folding and a less straight-forward inflation process, but the final deployed shape of the baffle will be more controlled. Another advantage is that there are more options for folding the MLI blankets when they are not constrained by the boom positions. The thermal properties at the boom locations can be expected to vary from the presence of only a blanket overlap, which might require insulation on the booms as well.

To ensure reliability of deployment, the former option is chosen and the booms will not be integrated to the MLI blankets. The attachment between the MLI and the booms can be done with e.g. double-sided adhesive tape to achieve a strong bond with a relatively low thickness. The folding of the MLI blankets and booms needs to be compatible, which will be discussed in Chapter 7. It is clear that many of the system risks follow from the very tight volume budget of the stowed baffle. However, an attempt will be made to prove the

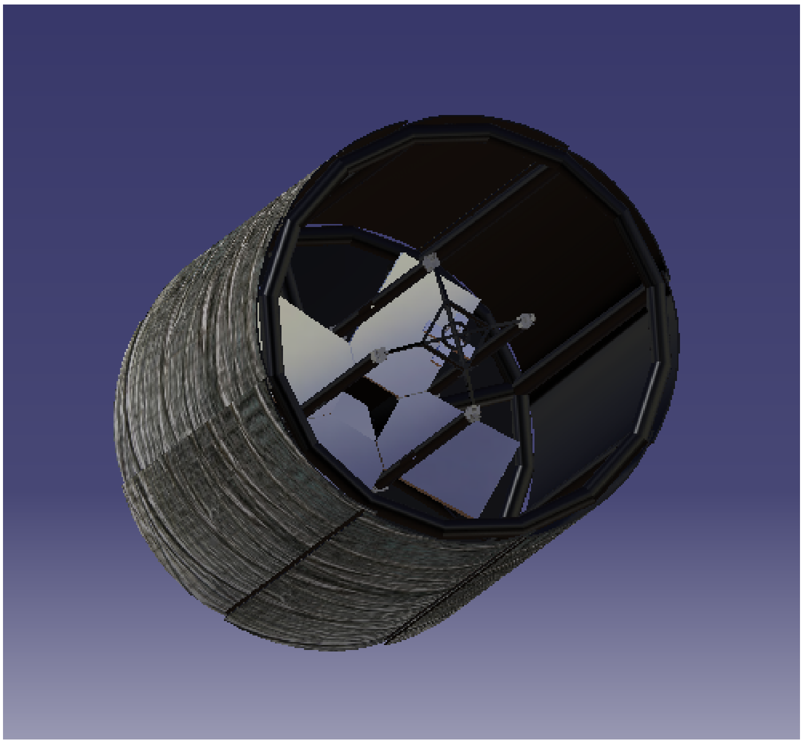

Figure 5.8: CATIA assembly of DST with the baffle (MLI texture from [9])

feasibility of the system in this aspect.

5.5.2. Joining the booms

It can be seen in the above that no interface between the booms has been designed in detail yet. Based on literature examples of inflatable truss structures, it is necessary to reinforce the locations where the almost perpendicular booms cross. At this stage, no detailed design of this will be made, but a preliminary design will be presented as a starting point for future work. Previously, a few examples were shown for inflatable structures that can be used as a reference for this section as well. One such system is the thermal shield shown in Figure 4.2 in Chapter 4.

In Figure 5.9, a design to be used for now is shown. The dimensions of the interface piece are approximate a 16 cm cube, and the mass can be expected to be of the order of 100 g in case a light material is used, such as in the inflatable tube deployment experiments in [73]. A total of 16 of these couplings are needed, with each of them interfacing three boom segments. For now, a total mass of 1.6 kg is estimated for the connecting pieces, which will have to be verified with an actual design made. For now, the feasibility of the system is not seen to be affected by these elements.

5.5.3. Optical properties

Theoretically, the effective emissivity can be calculated with Equation (5.12), where ϵ_1 and ϵ_2 are the emissivities of each side of the polymer layers (equal in case of double-aluminised Kapton) and N is the number of layers used. This equation assumes no conductive heat transfer via the layers or trapped gases, and is therefore not reliable for analysing the performance. The calculation is included as a maximum achievable performance, and an effective emissivity of 0.002 is found. Comparing to the data used to estimate the required number of layers, Figure 5.6, it is quickly seen that the calculated value does not represent the true expected performance, which will have to be estimated statistically for now, before manufacturing and testing of the MLI can be performed.

$$\epsilon^* = \frac{1}{\frac{1}{\epsilon_1} + \frac{1}{\epsilon_2} - 1} \left(\frac{1}{N+1} \right) \tag{5.12}$$

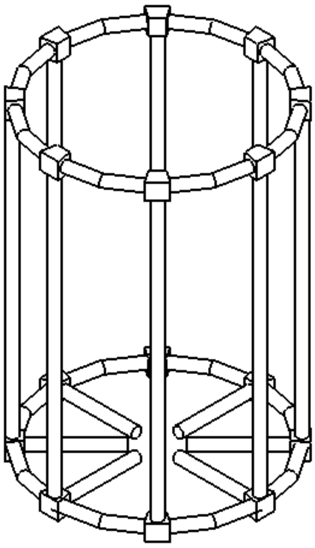

Figure 5.9: Place holder design for boom interfaces

Table 5.7: Optical properties of the baffle

Property	Value
Outer layer emissivity [48]	0.60
Outer layer absorptivity [48]	0.10
Inner layer emissivity [32]	0.84 (normal)
Inner layer absorptivity [32]	0.93
Interior layer emissivity [48]	0.05
Effective emissivity	>0.002

5.5.4. Durability

The Long Duration Exposure Facility (LDEF) allowed the analysis of LEO environment effects on various material samples over a time of over 5.7 years from the year 1984 to 1990 [10]. Since the expected DST mission duration is in the same range, the results found in LDEF experiments are highly applicable to estimate the durability of the baffle materials in the space environment they will be subjected to.

The main consideration is the ageing of the outermost layer of the MLI, which is made of silvered Teflon. These surfaces will encounter atomic oxygen as well as UV radiation over the whole mission duration. Furthermore, thermal variation during the orbit and debris impacts will deteriorate the outer surfaces. The durability concern is for both optical and structural properties of the MLI assembly. Erosion on the leading edge samples of silvered Teflon on the LDEF was observed [54]. This was mostly due to the atomic oxygen flux at lower altitudes. The trailing edge samples mostly showed signs of UV deterioration and contamination [54]. Measurements of the optical properties of a control sample and the test experiments shows a 12% increase in solar absorptivity and a less than 1% decrease in emissivity of the material [10]. It was also noted that at high atomic oxygen influence, the blanket becomes a diffuse rather than specular reflector, although it does not affect total reflectance. The simulated geostationary orbit environment testing of similar material produced more drastic degradation results, including over 100% increase in absorptance over 3 years [88]. However, the environment differed in that charged particles were introduced and the testing was done on Earth, and the material was not completely equivalent. Therefore the LDEF data is considered more reliable. The increase in absorptivity is high enough that it needs to be taken into account when estimating the thermal performance of the baffle.

The inner layer of the MLI is also considered critical for the performance, specifically for the stray light rejection. It is necessary to estimate the possible increase in reflectance over the mission duration. The selected coating, Acktar Magic Black, was not a part of the LDEF experiments so another source was consulted. In a paper to assess the space use of Acktar black coatings, they have been found to have little change in reflectance as a result of atomic oxygen flux, and it remains below 0.02 [83]. The effects of UV exposure are not discussed or tested for. It is assumed that the very small change in performance does not affect total mission performance at EOL.

The durability of the MLI against impacts by meteoroids and space debris is hard to estimate in the scope of this thesis. Based on observations on LDEF, it is certain that impacts will occur over the lifetime, and due to the large surface area of the MLI, high energy particles can also be expected to hit it. There is a possibility of a particle penetrating the MLI layers and subsequently hitting the telescope optical elements, but there is no foreseen way to prevent this from happening with the designed configuration.

Lastly, the environmental effects on the booms need to be assessed. It is assumed that the outer aluminium layer is the component affected by the space environment. The structural properties are of more importance than the optical ones, since the thermal control is fully performed by the MLI. However, there are no large changes in most aluminium alloys due to LEO atomic oxygen exposure [28]. As long as the Kapton layer is not exposed to atomic oxygen, the structure of the booms should stay relatively stable. The greater risk is posed by micro-meteoroid impacts, which can puncture the booms during the inflation/rigidisation sequence. It is difficult to estimate the number or force of impacts experienced over the mission duration. However, the thickness of the laminate is so low that very small particles will puncture it, and the probability of a puncture over the lifetime is very high, probably 100%, as can be deduced from Figure 5.10. This necessitates the deflation and rigidisation of the structure, as was already thought. The subsequent damage to the booms will then not instantly cause the collapse of the baffle shape. However, a large enough impact can practically disintegrate a boom. The probability of a large particle hitting the relatively small area with such force is assumed to be small enough to not be a concern, but further analysis would need to be conducted to be certain.

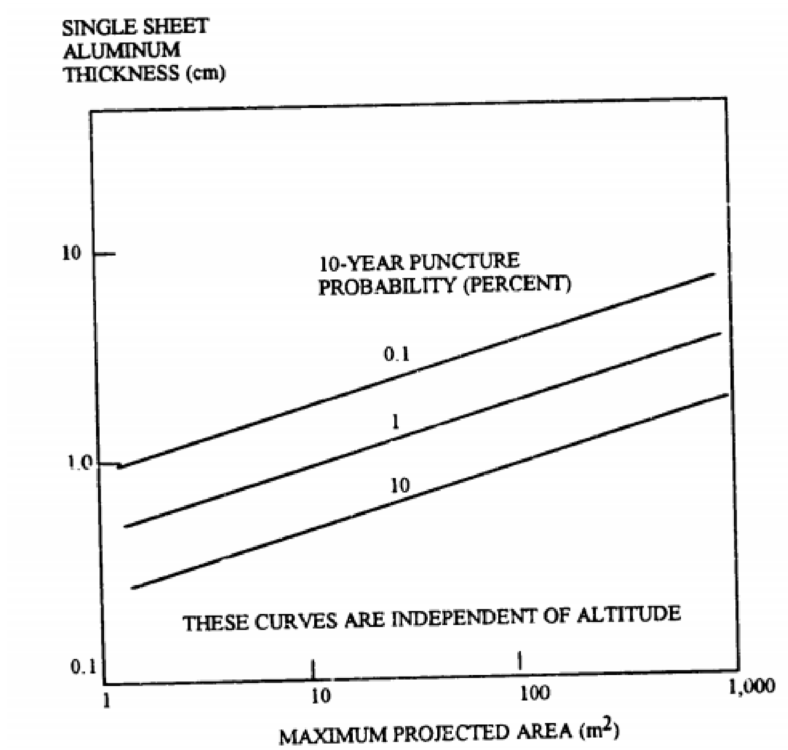

Figure 5.10: 10-year probability of a puncture as a function of aluminium sheet thickness [89]

5.6. Summary of the materials

In this section, the design choices made in this chapter are summarised in the form of tables. The methodology used to get to the selections and their properties can be found earlier in the chapter.

The booms that form the structural backbone of the baffle will be made of an aluminium-polymer laminate. The properties of this laminate for materials and their amounts are given in Table 5.8, and a visualisation of the cross section is given in Figure 5.11. The calculated properties are listed in Table 5.9.

Table 5.8: Laminate layers

Material	Number of layers	Thickness per layer [μm]
Aluminium 1100-0	2	25
Kapton HPP-ST	1	13

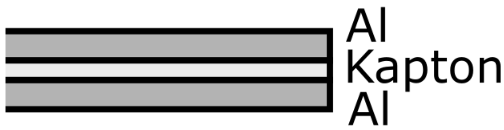

Figure 5.11: Cross section of the laminate

Table 5.9: In-plane properties of the aluminium-Kapton laminate

ρ [kg/m^3]	E [GPa]	G [GPa]	ν [-]	$\alpha_{x,y}$ [10^{-6}/K]	α_z [10^{-6}/K]
2328.91	7.1	21.05	0.33	23.3	22.7

Thermal shielding is performed by a blanket of multilayer insulation. The layers used are presented in Table 5.10.

Table 5.10: Multilayer insulation constituents and their optical properties

Material	Number of layers	Thickness per layer [μm]
Double-aluminised Kapton	10	13
Dacron net	11	160
Silvered Teflon	1	51
Black-coated Kapton	1	51
Total	23	1992

The mass of the structure resulting from the design choices made in this section is elaborated on in Table 5.11.

Table 5.11: Mass of the baffle structure

Element	Mass [kg]
Laminate boom	2.03
Multilayer insulation	9.06
Total	11.09

6
Mechanical performance

In this chapter, the mechanical performance of the baffle will be evaluated by the means of analytical and numerical analysis. For numerical work, the software ANSYS is used, and the description of the numerical model is given in Section 6.1. The modal analysis results are given in Section 6.2. Static loading and harmonic response analyses in ANSYS are explained in Sections 6.3 and 6.4, respectively. Finally, the results of the chapter are summarised in Section 6.5.

6.1. Numerical model for mechanical analyses

In this section, the modelling process and the resulting CAD model used for the numerical analyses of the baffle will be described. Assumptions and simplifications made along the way will be shown along with their reasoning and recommendations for future efforts. The considered aspects during modelling are briefly described in Subsection 6.1.1. The more simple baffle numerical model is described in Subsection 6.1.2 and the more realistic model is shown in Subsection 6.1.3.

6.1.1. Modelling considerations

The static structural, modal and harmonic response analysis work was performed in ANSYS, as it is more suitable than CATIA which is used for creating engineering models in the DST project. As a first option, creating an accurate thin-walled geometry of the whole structure in CATIA and importing it to ANSYS was explored. However, it was found that the resulting geometry could not be discretised with the available computing power, as the number of elements quickly became in the order of millions. The geometry was then decided to be modelled in ANSYS. To accurately portray the behaviour of the baffle under loading, some modelling principles had to be followed. These are briefly explained as follows:

- Student licences of ANSYS do not allow for a large number of elements. The model has to be made as simple as possible, since the scale of the structure can quickly escalate the required number of nodes for complex geometries.

- The whole geometry needs to be modelled. While the baffle has symmetry axes that allow the simplification of the model, it was deemed bad engineering practice due to not being able to analyse non-symmetric behaviour.

- The cross-sectional and material properties of the baffle should be maintained as well as possible. This means that the properties of the laminate need to be imported into ANSYS, and the mass of the structure needs to be identical to the actual design.

- Multilayer insulation has been chosen not to be structurally analysed, but its mass and placement on the inflatable skeleton need to be accounted for.

Based on these aspects, numerical models were started to be created. This will be explained more in the following paragraphs.

6.1.2. Line body model

After the initial difficulty with excessive model size, the option of maintaining some cross sectional properties, but changing the booms into solid beams was considered. The suggestion was given by a TU Delft staff member working on structural modelling. This was done by implementing Equation (6.1) to find the radius of a solid cross section while maintaining the area moment of inertia of the thin-walled, actual cross section of the booms. A simple model was then created, which can be seen in Figure 6.1. The booms are made of line bodies, with a circular solid cross section of 13.7 mm radius. The whole model consists of 248 elements. While the orientation and other dimensions of all elements are maintained reasonably well, the torsional motions can be expected to vary from the real case due to the torsional stiffness scaling with radius. The model was attempted to be verified by comparing the eigenfrequencies and static deformations of simple cantilever beam elements. However, it was soon found that while the first eigenmodes (first order bending of the beam) occurred at the same frequency to within 2%, in the next eigenmode the difference was approximately 75%, and over 200% in the third one. These results were found unsatisfactory and so the thin-walled structure was attempted to be created for better accuracy, as will be explained in the next subsection. The effect of the full baffle geometry on the accuracy of the full beam model performance has not been assessed due to the inability to discretise a sufficiently representative geometry with the actual wall thickness. It is possible that the full model is more reliable than indicated by the preliminary verification.

$$I_{thin-walled} = \pi r^3 t \tag{6.1a}$$

$$I_{solid} = \frac{\pi}{4} r^4 \tag{6.1b}$$

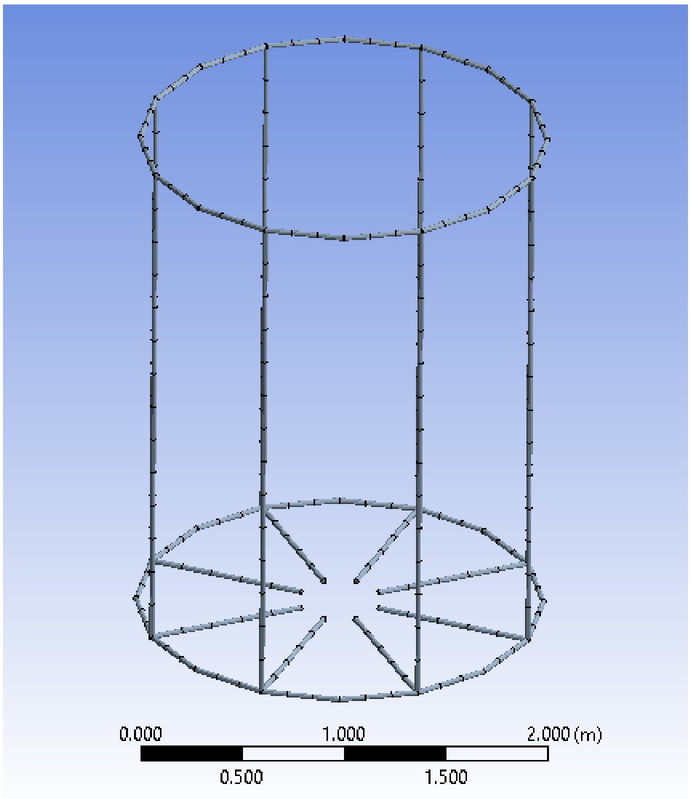

Figure 6.1: First simple approximation of the baffle geometry with solid line elements

The material properties of the laminate are implemented by assuming isotropic properties as obtained in Chapter 5. The Young's modulus and Poisson's ratio are added as a material property, and the shear modulus is derived from that by ANSYS, obtaining the same value as was calculated analytically. The elastic modulus is accurate for the rigidised structure as well as the uninflated one, as the value is not changed by strain hardening [87]. The conservative approach is used with the aluminium foil Young's modulus as discussed earlier.

The loading caused by the MLI on the booms was found to be difficult to model accurately. Incorporating flexible blankets in the structure could not be done in any realistic manner. Instead, the mass of MLI was included as a distributed mass of 10 kg divided equally over all the elements, and along their whole length. This introduces the inertial effects of the MLI on the inflatable elements, but does not provide information on the behaviour of the MLI itself. The motion of the blankets themselves is seen as unimportant compared to the dynamics of the boom themselves, but it can be expected that the results of the analysis are affected by the assumption. At a later point, a more accurate model should be created.

The interface of the baffle with the instrument bus is modelled by placing fixed supports on the edges of the baffle bottom booms where they would connect to the bus. It is a fair assumption that the ends of the booms are essentially clamped to the bus. This allows the analysis of merely the baffle structure without any interaction with the rest of the telescope. This also eliminates rigid body motion in modal analysis of the structure.

6.1.3. Surface body model

It was found that by using surface elements in ANSYS, it is possible to reduce the number of elements while maintaining the real wall thickness of 63 microns. A model was created with surface bodies for each boom, which were then connected with simple contacts. The intersections between the booms are hollow with no intersecting walls, as there is no detailed design for the boom meeting points yet. The internal volumes of the booms are however expected to be interconnected. The resulting ANSYS model can be seen in Figure 6.2. The model has 4846 elements, almost 20 times as many as the simplified beam based model. This is however still reasonable for the computational effort required for the subsequent analyses, even though acquiring harmonic analysis results takes several days and is not feasible. The model size cannot be made much larger with the available resources, so the model is taken as the best approximation available at this stage.

The material properties of the model as well as the boundary conditions are the same as in the line body model. The mass of the MLI is divided over the surfaces on all sides of the booms, which is not the realistic load case, but will be accepted for now. Due to the lack of fortifications in the boom intersections along with the mass distribution, the model cannot be called realistic, but the boom cross sections are much more representative of the actual design than in the more simplified model. It is currently not possible to model the full DST in ANSYS due to the node number limitations in the student licence. In the future, it would be beneficial to assess vibrations and load paths in the whole system.

6.2. Modal analysis

The frequency response of the baffle structure is crucial for ensuring the deployed system does not endanger operations due to e.g. attitude control vibrations. As a first step to the performance estimation, the natural frequencies are determined by frequency analysis of a CAD model in ANSYS. This section presents the methods and results of the analysis.

An analytical solution is not given here due to the complex shape of the baffle which prevents the use of natural frequency equations for beams for any representative results. The model used for the modal analysis is the same ANSYS model as described above for the static analysis. The results obtained from it will be used as a pre-loading condition on the modal analysis to represent the operational case as accurately as possible. It is important to note that the magnitude of the deformation acquired in this analysis does not yet indicate the adequacy of the design, as it is not based on any load case. The shapes seen are greatly exaggerated. The response of the system to operational loads will be the defining factor in performance, and is discussed in the next section.

The output of the analysis is the eigenfrequencies of the system as well as the corresponding modes of deformation. The most important eigenmodes will be described in this section, and the motions are shown in Figure 6.3. The first and second modes occur at approximately 0.9 Hz and are a sideways motion of the whole structure in two perpendicular planes. These modes are of principal concern for the obstruction of the mirror elements. The motion can be seen in Figure 6.3a. It is noticed that many of the other eigenmodes also repeat in two perpendicular planes at the same frequency. This applies to the 4th and 5th modes, which are an elongation of the top torus, where it becomes oval in shape, which can be seen in Figure 6.3c. Due to the

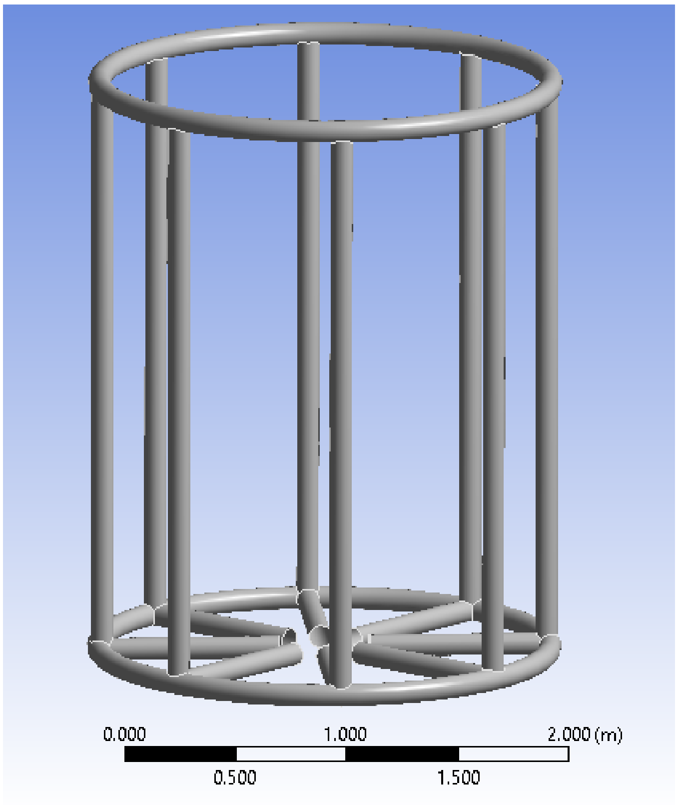

Figure 6.2: Surface body model of the baffle used for structural analysis

symmetry of the structure, the repeating frequencies are logical. The third mode is a twisting motion around the z-axis, as can be seen in Figure 6.3b, and does not repeat due to the lack of a symmetry in this orientation. The sixth mode is a longitudinal elongation, which can be seen in Figure 6.3d.

The first six eigenfrequencies are listed in Table 6.1 along with the corresponding modes and the nature of the motion. The lower modes generally correspond to larger motions of the whole body, while higher modes involve more complex motion of individual elements. The first two modes were expected to occur at virtually the same frequency, but there is a difference, albeit small. This is most likely due to asymmetry in the automatically generated mesh, and is accepted for now.

Table 6.1: The first six eigenfrequencies of the baffle and their associated motion

Mode	Frequency (Hz)	Motion
1	0.9159	Bending
2	0.9488	Bending (perpendicular axis)
3	1.6818	Torsion
4	2.6289	Elongation of the top torus
5	2.7217	Elongation of the top torus (perpendicular)
6	3.6823	Longitudinal elongation

The eigenfrequencies without the mass of the MLI were found by conducting modal analysis of only the boom structure. These results are not relevant for the operational case, but they highlight the effect of the mass on the eigenmodes. The first five eigenfrequencies are shown in Table 6.2 for this case. It is readily seen that the frequencies are consistently at least twice as high in these modes. It is observed that the modes are the same as found for the model with MLI mass, which verifies that the mass is distributed evenly in the model and does not affect the motions of the baffle.

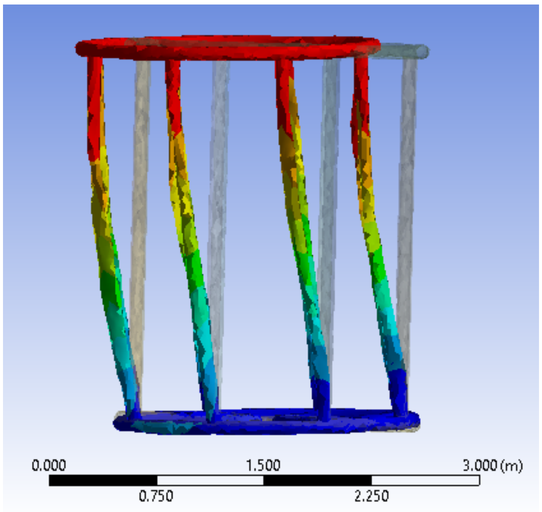

(a) Maximum deformation in the first and second eigenmodes (two perpendicular planes)

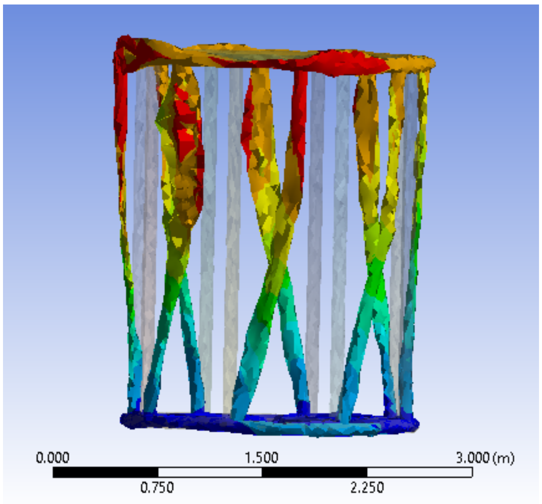

(b) Maximum deformation in the third eigenmode

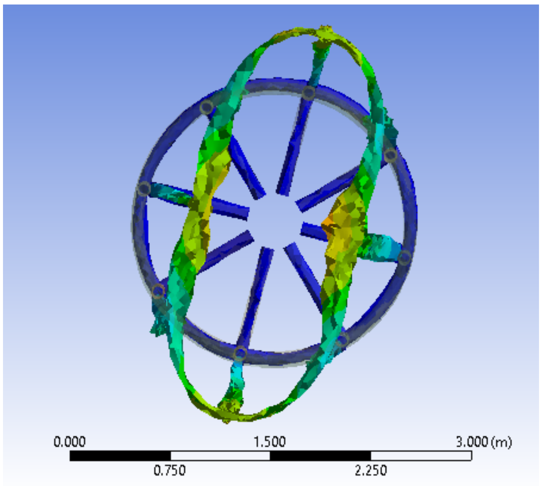

(c) Maximum deformation in the fourth and fifth eigenmodes (two perpendicular planes)

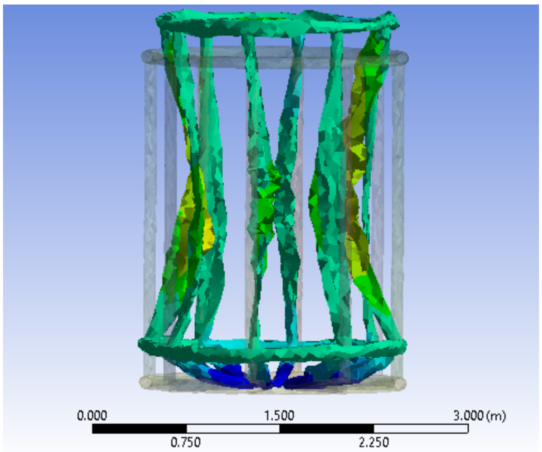

(d) Maximum deformation in the sixth eigenmode

Figure 6.3: Deformation of the baffle in the first six eigenmodes, not actual magnitude

Table 6.2: The first five eigenfrequencies of the baffle without MLI mass

Mode	Frequency (Hz)
1	2.2624
2	2.3047
3	5.2086
4	6.9109
5	8.2173

The eigenfrequencies found are low, but this was to be expected due to the large size and geometry of the baffle, along with the mass distributed around the perimeter. The eigenfrequencies are not low compared to many other space structures, such as solar array and antennae. As a next step, a more detailed model of the MLI should be made to see how the eigenmodes are affected. It is likely that the inclusion of a large amount of flexible membrane cannot be considered negligible for the dynamics of the system. However, modelling this accurately was not possible within the scope of this work, as mentioned earlier. Another aspect to consider is the inclusion of the whole telescope, as the dynamics of the full system can be expected to vary from that of the elements considered separately.

6.3. Static loading

The capability of the booms to withstand static loads during operations needs to be checked before any further analysis can commence. The sufficiency of the material selection and geometry of the booms will be evaluated, since the diameter is currently not based on any structural analysis. It is noted that in case the loading condition of the baffle does not meaningfully affect the diameter selection, the current value is kept. The main issues beside load-bearing are assumed to be related to manufacturing, and therefore literature examples of successful systems are considered a sufficient design point. Analytical calculations will be provided in Subsection 6.3.1 and numerical results will be discussed in Subsection 6.3.2.

6.3.1. Analytical results

The loads that the booms can take before failure can be estimated with some analytical equations from a NASA manual [77]. It is identified that buckling is the failure mode for thin-walled cylinders, and therefore only these loads will be used as a guideline at this stage. The results will aid in choosing the diameter of the booms to achieve sufficient structural strength. Furthermore, the effect of internal pressure on the loads the booms can take can be calculated.

The loads imposed on the booms in deployed state are due to the weight of themselves and the MLI blankets, and any experienced acceleration. The accelerations due to the reaction wheels have been determined to be in the range of e-4 to e-3 m/s^2. Gravity is acting on the structure as well, but in the orbit micro-gravity conditions are experienced, leading to an even lower, yet constant, acceleration. Therefore the effect of the reaction wheel vibration in the z-direction is taken as the worst case loading in dynamic analyses, but gravitational acceleration is the static case.

To assess if the micro-gravity can be survived by the baffle, the buckling loads can be estimated analytically and compared to the weight of the structure in orbit. The buckling load for an axially loaded thin-walled cylinder is found as follows [77]:

$$P = \frac{2\pi t_a^2 E_a \gamma}{\sqrt{3(1-\nu^2)}} \tag{6.2}$$

$$\gamma = 1 - 0.901(1 - e^{-\phi}) \tag{6.3}$$

$$\phi = \frac{1}{16}\sqrt{\frac{r}{t_a}} \tag{6.4}$$

For the equations to be valid, it is assumed that the booms are straight cylinders with a ratio of L/r less than 5. The longitudinal booms have a L/r of over 40 at the diameters considered here, so clearly the condition is not met. For a simple estimate for the load-bearing capability this will suffice, but actual testing is needed to assess actual performance. It is also assumed that the ratio r/t is less than 1500, which is true for boom diameters below 18 cm for the determined effective laminate thickness of 62.7 µm. According to Friese, the effect of the polymer layer on the buckling strength has to be included with a multiplier M on the buckling load, which depends on the laminate properties [46]. However, from the plot given, the factor M is found to be so close to 1 that it can be neglected in this case.

If the equations are used with the information found from InflateSail research, their accuracy can be checked. Tests were conducted and the rigidised boom was found to take a load of approximately 50 N before buckling [96]. Using above formulae produces a value of 15.1 N, but for an unrigidised boom. The difference is more than a factor of 3, which is not unexpected. In the research of inflatable antennas by Friese, critical buckling loads around 50 N were found for a boom with 50 µm aluminium and 13 µm polymer by testing, opposed to a calculated load of 74.5 N [46]. It was concluded that the tensile strength of the aluminium foils was assumed wrong, but further testing was recommended [46]. This might suggest an overestimation of the performance by the equations, so results should be inspected critically and used only as a first estimate. In this work, the elastic modulus will be estimated conservatively as 8300 MPa.

The critical buckling load can be plotted as a function of the cylinder radius to assess the required dimensions with the laminate properties determined earlier in this chapter. The resulting plot can be seen in Figure 6.4. It is readily seen that even at the highest used diameter, the load is above 10 N, compared to the expected loads multiple orders of magnitude lower due to micro-gravity. Hence the boom diameter does not depend on the buckling performance. The diameter of 10 cm as decided earlier is kept due to the good performance and manufacturability proven by earlier work on InflateSail and testing done in the 1980s [46, 96]. The predicted critical buckling load is then approximately 18 N.

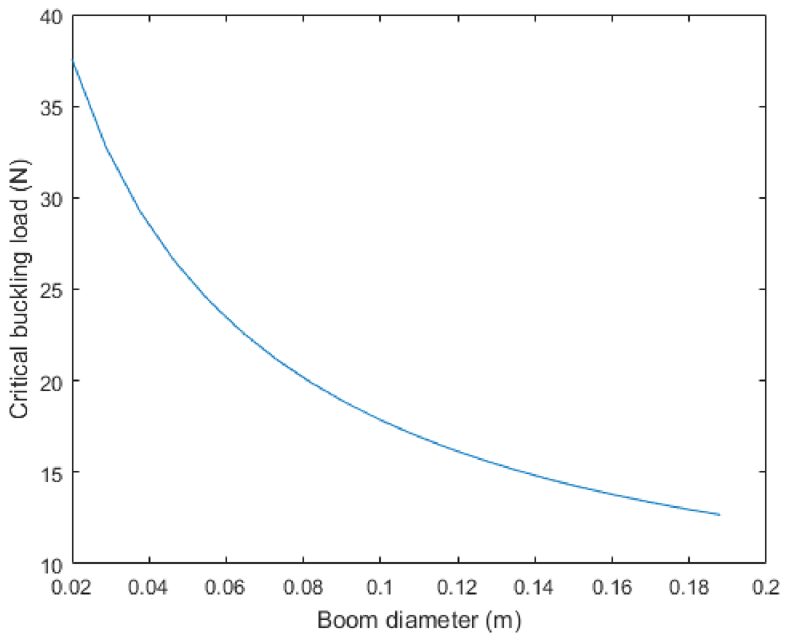

Figure 6.4: Axial buckling load of the unpressurised booms as a function of diameter

It is important to note that the calculations apply to deployed but non-inflated, non-rigidised booms and therefore provide an unrealistic scenario of loading. However, while the performance when pressurised can be estimated, the load-carrying of the boom during deployment is much harder to assess. The non-inflated buckling load is given as a worst case for the successfully inflated and rigidised structure, i.e. the strength has not increased at all.

A pressurised cylinder can withstand greater loads due to the pressure carrying loads even in the theoretical absence of wall thickness. This introduces a correction term $\Delta\gamma$ (found in [77]) and an additional term for the pressure contribution. The buckling load is then:

$$P_{press} = 2\pi t^2 E\left(\frac{\gamma}{\sqrt{3(1-\nu^2)}} + \Delta\gamma\right) + p\pi r^2 \tag{6.5}$$

The load-carrying capability of the booms during and after inflation can be assessed, although it is already seen that it is better than for the non-inflated boom in Figure 6.5. The pressurisation sequence is therefore not considered further here, but the load carrying capacity of the booms during deployment is verified here.

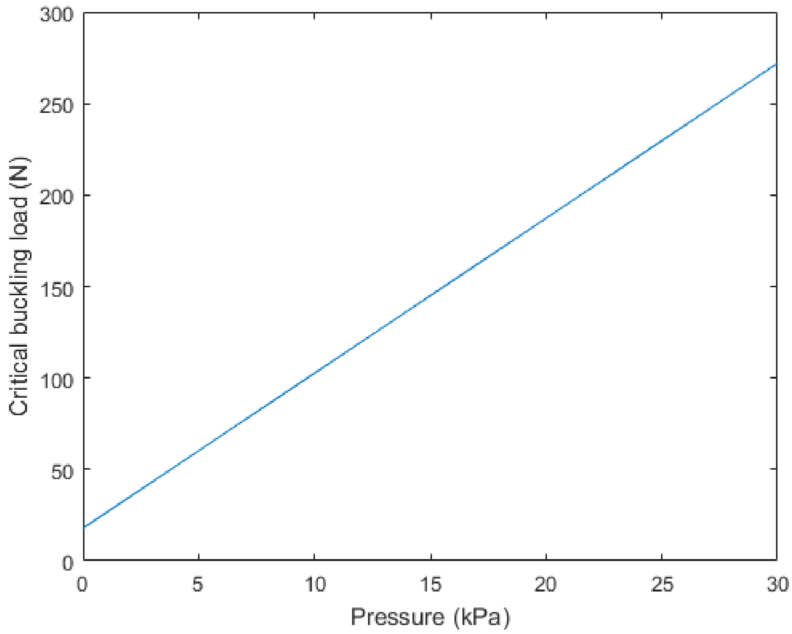

Figure 6.5: Axial buckling load of the pressurised booms as a function of pressure

6.3.2. Numerical analysis

To assess the effect of constant micro-gravitational loading on the baffle structure, the FEM software ANSYS is used. The deformation due to the micro-gravity environment can be seen in Figures 6.6 and 6.7 for gravity acting along the z- and x-axes, respectively. Due to symmetry, the y-direction is left out as it would produce the same results as x in terms of magnitude of deformation. It is readily concluded that the static gravitational environment does not pose an issue for the operational stability, as the deformation is well below micron level in all directions.

The actual load carrying capability can be estimated to find the allowable loads on the structure. Eigenvalue buckling is an analysis in the ANSYS Mechanical workbench that is based on the static structural results and provides the theoretical critical buckling loads, although these might be optimistic relative to the real behaviour due to the assumed linearity. Non-linear buckling analysis would be more conservative, but this option is not available on the ANSYS student licence. The output from the analysis is a factor of the current load that the system can take before buckling, and a number of buckling modes is given based on desired output. In this work, the first mode providing the lowest value will be checked as a first estimate. The analysis will be done for micro-gravity as well as Earth gravity, to see if testing the system is feasible outside micro-gravity conditions on ground. The results are summarised in Table 6.3.

In micro-gravity conditions, with the acceleration vector in positive x-direction, the predicted load factor on the baffle is 80287, meaning that the mass (or acceleration loading) have to increase significantly before buckling occurs due to the weight of the structure. Not surprisingly, the first failure mode is on a column boom, perpendicular to the acceleration. With the acceleration along z-direction, the factors increase significantly. The lowest factor obtained is 286460, which corresponds to a failure of one of the lateral booms as a result of

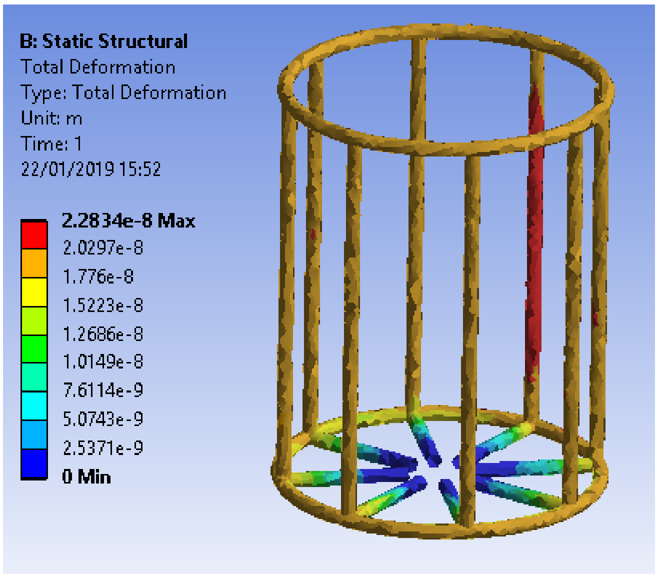

Figure 6.6: Deformation in micro-gravity conditions, acceleration along z-axis

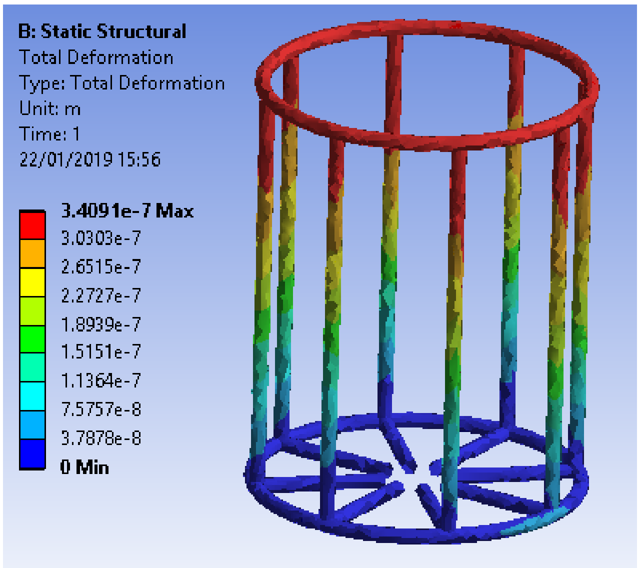

Figure 6.7: Deformation in micro-gravity conditions, acceleration along x-axis

Table 6.3: Minimum buckling load factors in micro-gravity and Earth gravity

Environment	Acceleration [m/s^2]	Lateral load factor [-]	Longitudinal load factor [-]
Micro-gravity	$9.81 \cdot 10^{-6}$	80287	286460
Earth gravity	9.81	0.00004	0.0037

bending. This failure mode was identified when the possible buckling modes in the loading orientation were thought up prior to the ANSYS analysis.

In Earth gravity, the buckling load factors decrease to below unity as can be deduced from the previous results, as the forces on the baffle become 10^6 times as great. With the gravity acting in positive z-direction, the lowest factor is about 0.005, where the failure occurs on the bottom torus. This effectively means that the baffle can only carry 0.5% of its own weight on Earth without buckling, if hung "upside down". With gravitational acceleration in the reverse direction, the resilience to buckling can be seen to get worse. The lowest multiplier is 0.0037, which corresponds to one of the long booms buckling near the middle. The difference is assumed to be due to the fixed supports on the bottom along with the lateral booms.

With gravity acting in the lateral direction, the obtained buckling loads vary depending on the orientation of the acceleration vector, presumably due to asymmetry of the mesh. The lowest found value for the load factor is 0.00004, but the values vary by up to 2 orders of magnitude. The reason for this cannot be distinguished, but it is not considered important for this work. It is expected that the baffle will not be placed perpendicular to the gravity field on Earth.

The results of this section indicate that the baffle will survive the operational phase when it comes to gravitational loading, but on Earth the structure cannot bear its own mass. If testing of the whole baffle with MLI is done, a gravity compensation method needs to be implemented to avoid buckling. This will make testing more complex, but is necessary as testing the baffle to find the actual properties is one of the main recommendations following from this work.

6.4. Frequency response

In this section, the response of the baffle system to harmonic excitation will be analysed. Deformations due to vibrations during operation are one of the determining factors in whether the system meets the requirements of not obstructing or endangering telescope elements over the mission duration, as well as whether large stresses will be introduced to the structure. The analysis type used for the harmonic response in ANSYS is mode superposition, which is useful for finding the response to disturbances especially near the eigenfrequencies of the system. The eigenmodes found in modal analysis will be superimposed to find the response over the whole frequency range. First, the load case will be defined, and then the analysis itself will be discussed, and finally the results will be evaluated.

6.4.1. Loading definition

The main source of vibrations on the DST is assumed to be the attitude control subsystem, which is however yet to be characterised. Specifically reaction wheels will be considered as the only significant source of unwanted accelerations. This approach has also previously been used by van Putten and Krikken in their work [61, 99]. Here, the same reaction wheel assembly is considered as the vibration source as in Krikken's thesis, namely the Bradford W45E [15]. Some properties of this wheel are given in Table 6.4. For this reaction wheel, the excitation spectrum can be found and approximately recreated to estimate the induced accelerations over the relevant frequencies. The spectrum can be seen in Figure 6.8. Based on the eigenfrequencies of the system found above, the most important parts of the spectrum can be selected for analysis. Only the accelerations caused by disturbance forces are considered, and the moments are neglected. The accelerations will be applied as a base excitation with the fixed supports as the boundary condition at the location of integration to the instrument bus.

Table 6.4: Properties of the Bradford W45E reaction wheel [15]

Property	Value	Unit
Momentum storage	45	Nms
Maximum speed	4000	RPM
Maximum torque	0.248	Nm
Assembly mass	7.45	kg

The frequencies of the disturbances depend on both the rotation speed of the wheel (Ω) and the order of

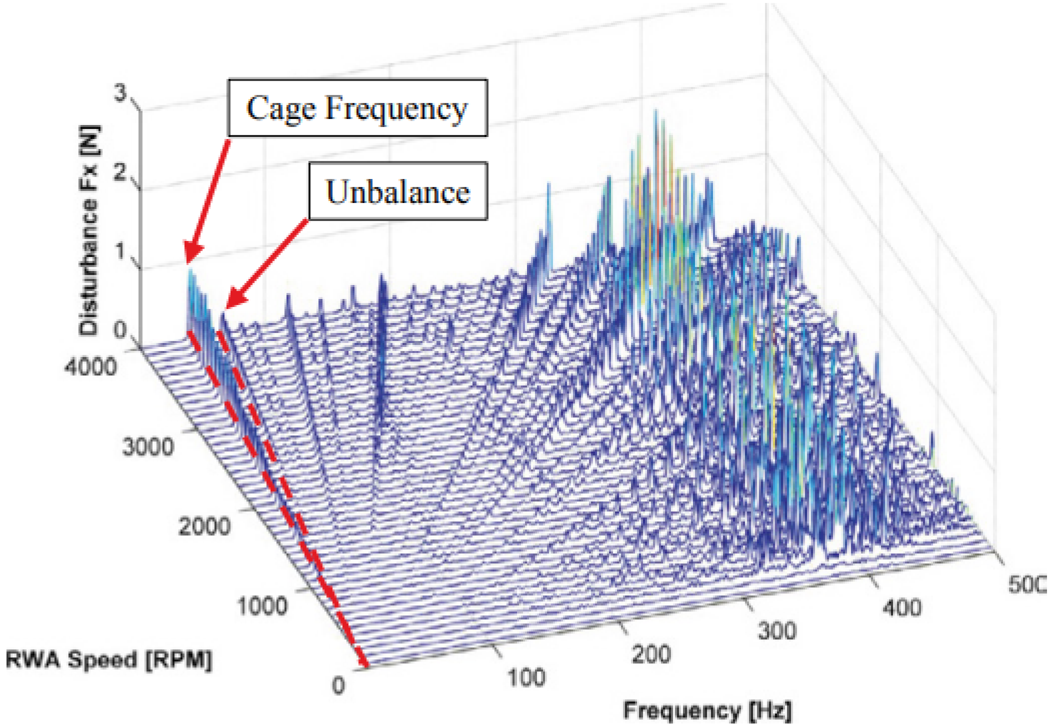

Figure 6.8: Vibration spectrum of the Bradford W45E reaction wheel [62]

the disturbance (h), which depends on the source. In the PhD thesis by Le, the sources of the disturbance forces of different orders are described. The order is essentially the number of occurrences of the disturbance during one wheel rotation. The frequencies where the accelerations are experienced for a wheel speed Ω can be determined by the equation below, where the full vector of engine orders is used [62].

$$\overline{\omega} = \overline{h}\Omega \tag{6.6}$$

Here it suffices for now to consider the greatest forces seen in the spectrum. The orders observed in the wheel are given in the thesis, and from the waterfall plot the amplitude of the force at a certain rotation speed can be estimated. The empirical approach from the thesis by Le is used to estimate forces. The amplitude (A) is related to the rotation speed by the following, where C_i is the amplitude coefficient at a given engine order [62].

$$A = C_i\Omega^2 \tag{6.7}$$

Approximating the coefficients can be done from the given waterfall plots, and then the amplitudes at different frequencies can be found based on the known engine order. The list of orders and coefficients used is given in Table 6.5. The total vibration spectrum is found by superposition of the disturbances of different orders [62]. The same loading will be used for all axes, since only radial disturbances are given and the vibrations in z-direction cannot be found [62]. This approach does not take into account resonances of the wheel, seen around 400 Hz, and therefore the highest peaks of the plot are missed. The main resonance effects will be added to the spectrum by estimating the amplitude from the plots. The quadratic relation approximation is seen to overestimate the disturbance forces at low wheel rotation speeds compared to the waterfall plots, which makes the load case more conservative than the actual situation.

The loads are applied to the FE model as accelerations, which necessitates dividing the forces by spacecraft mass, following Newton's second law of motion. The mass is assumed to be 150 kg as per the DST system requirements. Accelerations encountered at various wheel speeds are used to create multiple cases. The speeds are based on the amplitudes of the responses encountered, as well as the frequencies affected. The eigenfrequencies of the system are attempted to be covered as well as possible in the analysis to find the worst case harmonic responses. To accurately find the harmonic response up to 500 Hz, there were 200 eigenfrequencies extracted up to 1231.6 Hz, but the main ones to be considered are the first modes with side-to-side motion of the structure. Due to these modes, the critical acceleration direction is in the x- and y-directions, which are expected to produce the highest deformations of the baffle at the first eigenfrequency, possibly causing obstruction. The expected deformations in z-direction are not as critical for the operational performance.

Table 6.5: Coefficients used to find the vibration spectrum of the Bradford RW45E reaction wheel

Order	Amplitude at 4000 RPM	Amplitude coefficient
0.61	0.125	0.000028
1	0.75	0.000169
2.88	0.17	0.000038
3.89	0.25	0.000056
4.73	0.17	0.000038
6.11	0.25	0.000056
6.77	0.83	0.000187
7.63	0.25	0.000056
8.77	0.17	0.000038
10.63	0.125	0.000028
12.97	0.17	0.000038
14.60	0.125	0.000028

6.4.2. Numerical model

The results of the harmonic response analysis will be presented in this section. On top of applying the actual reaction wheel disturbance spectrum as described in the previous subsection, the maximum acceleration found over the whole spectrum will be applied at all frequencies to demonstrate that the structure is robust against disturbance accelerations. The emphasis will be on the motion in xy-plane, as that is the plane of M1 where obstruction needs to be avoided.

The ANSYS harmonic response analysis takes a table of frequencies and corresponding disturbance accelerations as input and outputs the response of the system across a spectrum of frequencies. The selected calculation type is mode superposition, which clusters the response around the eigenfrequencies of the system calculated earlier. The full harmonic response analysis is computationally more demanding and considered unnecessary, as it is likely that the response is critical around the eigenfrequencies of the system.

It was rapidly found that using the full shell model of the baffle in ANSYS led to unacceptably high computational times with the existing resources. The frequency response could not be calculated with a 60 hour attempt, after which it was decided to use the simplified model of Subsection 6.1.2 and Figure 6.2. There are multiple issues with this approach that need to be addressed and taken into account. Firstly, the eigenfrequencies are different from the ones listed above. The eigenmotions occur at consistently higher frequencies, with the first eigenmode at 1.48 Hz. The first five modes can be seen in Table 6.6. This will inevitably lead to different response spectra, where the peaks in the response amplitude occur at higher frequencies.

Table 6.6: The first five eigenfrequencies of the simplified baffle

Mode	Frequency (Hz)	Motion
1	1.4775	Bending
2	1.484	Bending (perpendicular axis)
3	2.6461	Torsion
4	5.9358	Longitudinal motion
5	7.2334	Elongation of the top torus (two directions)

A comparison of frequency responses in a small range of frequencies is done to assess the reliability of the results. A constant acceleration of 0.006 m/s^2 was applied to both models in the x-direction, and the magnitudes of the response can be compared. The responses around the first eigenfrequencies can be seen in Figure 6.9. The peaks occur at different frequencies due to the difference in the fundamental frequencies, as expected. It can be seen that the response of the more realistic model is approximately 4 times as large as that of the simplified model, meaning that the results obtained with the latter can only be taken as a first estimate, and to gauge when and where the maximum response occurs. Then, if possible, the thin walled model will be used to estimate the actual response.

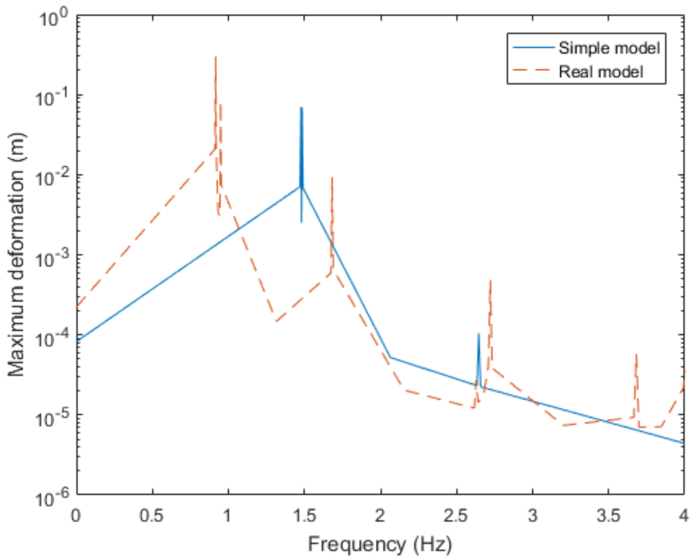

Figure 6.9: Frequency responses of the real and simplified baffle models to a constant harmonic excitation of 0.006 m/s^2

The damping properties of the structure are not known, and will most likely require experimental testing to be found. For this analysis, a constant damping ratio will be used to obtain first order results. The used value will be taken as a conservative estimate based on references. A constant 1% value is considered realistic based on a few experimental papers on inflatable structures [52, 90]. The suitability of this value will need to be assessed later, but for initial analysis, it will be assumed that the results are representative.

6.4.3. Frequency response to wheel vibration spectrum

The vibration spectrum of the reaction wheel is used as input for the harmonic analysis at different wheel speeds, taking into account the highest disturbances as well as the inclusion of the most important eigenfrequencies. The highest accelerations overall are found at the highest reaction wheel speed, 4000 RPM. The frequency response to the wheel spectrum applied in x-direction at this speed is shown in Figure 6.10 for all axes. The graphs present the deformation of the top torus edge, since the maximum movement is observed at this location for the x/y-direction, which is the main consideration. As expected, the greatest deformations overall are in this direction, as seen in Figure 6.11a where only the range 0 to 10 Hz is shown for clarity. It can be seen that the first eigenfrequency is where the maximum occurs, and the magnitude is of the order 4 mm, which does not pose a threat to telescope operations. In the other directions, the resulting deformations are orders of magnitude smaller and of no concern. It is noted that if the same vibration spectrum is applied in y-direction, the frequency response plots will be identical, except the x- and y-graphs will be switched. For this reason, the plots will not be repeated.

In Figure 6.12 the response of the system to acceleration in z-direction can be seen. The most important eigenfrequency for this longitudinal axis is the third one at approximately 5.9 Hz, where a peak can be seen in the graph representing z-motion, Figure 6.12b. This is in line with the expected behaviour, as this is the main eigenmode resulting in movement primarily in z-direction. The amplitude of the motion can be seen to be only approximately 0.2 mm, which will not be of any concern for the performance when it comes to obstruction. As above, along the other directions the response is orders of magnitude smaller.

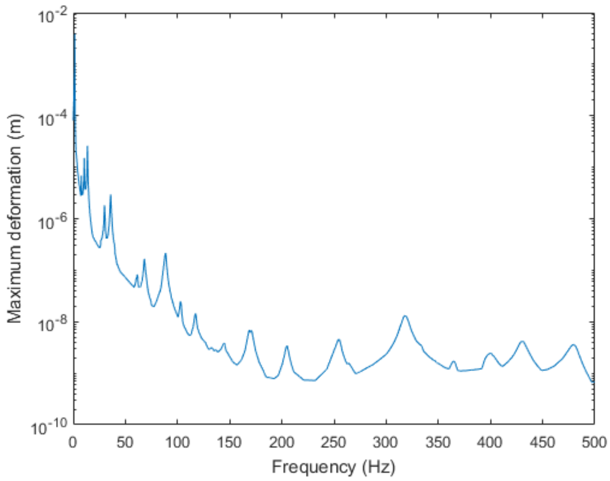

(a) Deformation in x-direction of the baffle as a result of harmonic excitation in x-direction at 4000 RPM

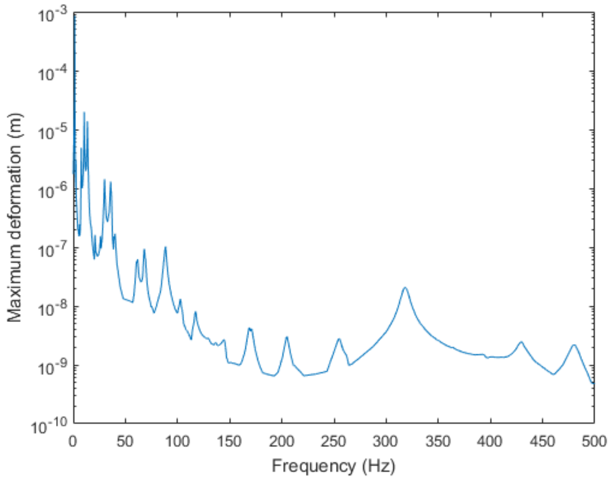

(b) Deformation in y-direction of the baffle as a result of harmonic excitation in x-direction at 4000 RPM

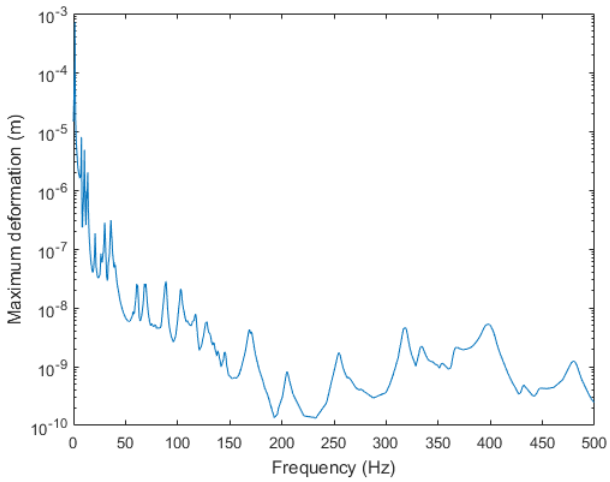

(c) Deformation in z-direction of the baffle as a result of harmonic excitation in x-direction at 4000 RPM

Figure 6.10: Deformation of the baffle after harmonic excitation in x-direction at 4000 RPM wheel speed

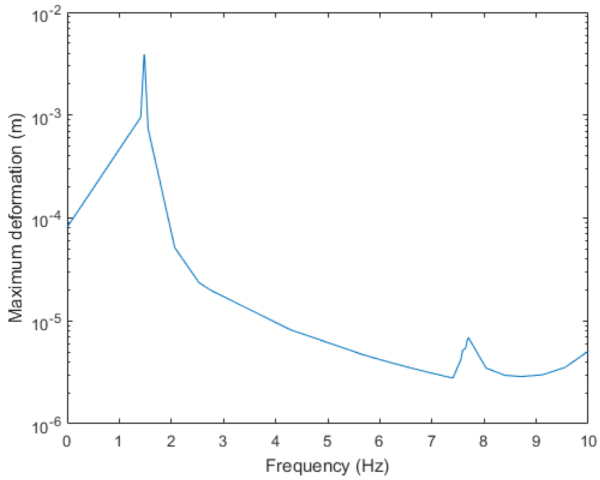

(a) Deformation in x-direction of the baffle as a result of harmonic excitation in x-direction at 4000 RPM

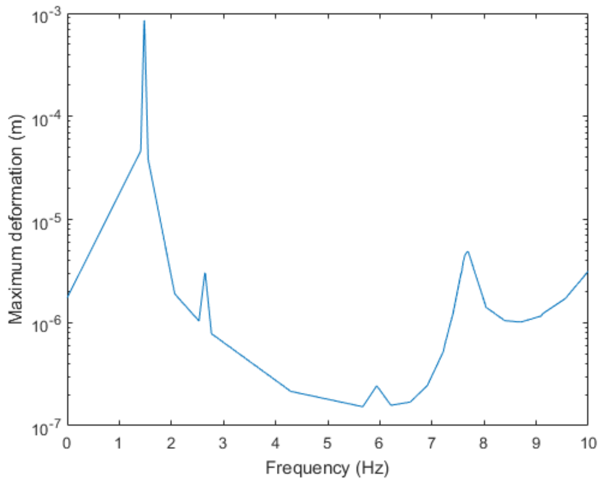

(b) Deformation in y-direction of the baffle as a result of harmonic excitation in x-direction at 4000 RPM

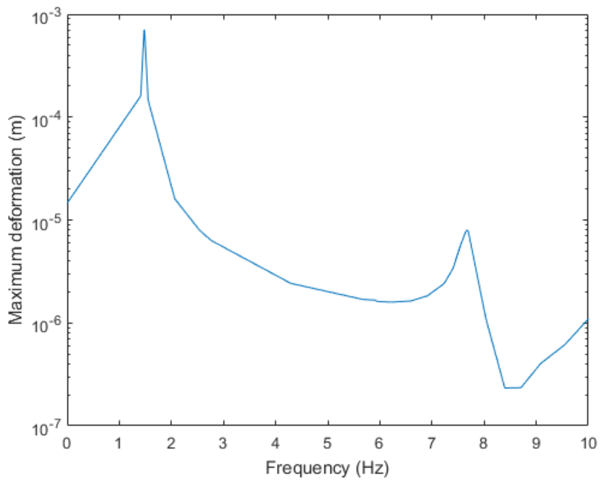

(c) Deformation in z-direction of the baffle as a result of harmonic excitation in x-direction at 4000 RPM

Figure 6.11: Deformation of the baffle after harmonic excitation in x-direction at 4000 RPM wheel speed (up to 10 Hz)

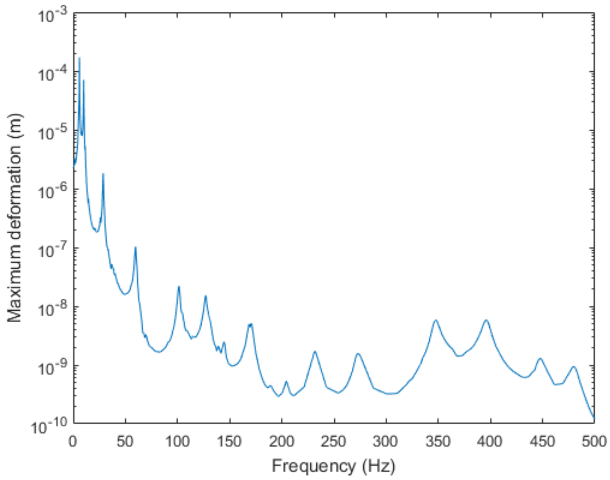

(a) Deformation in x- and y-direction of the baffle as a result of harmonic excitation in z-direction at 4000 RPM

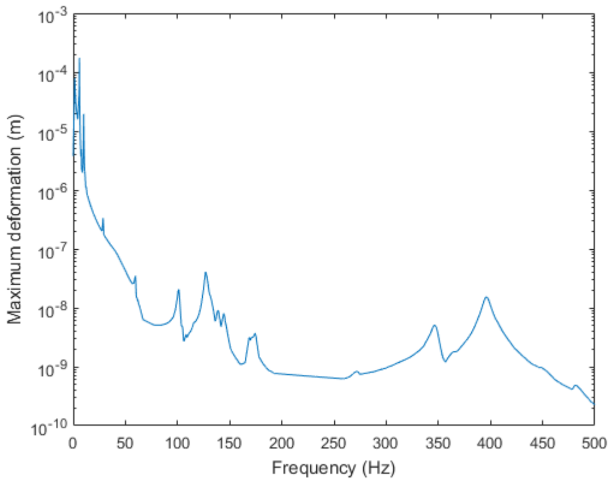

(b) Deformation in z-direction of the baffle as a result of harmonic excitation in z-direction at 4000 RPM

Figure 6.12: Deformation of the baffle after harmonic excitation in z-direction at 4000 RPM wheel speed

To check performance when vibrations are induced at low frequencies closer to the first eigenfrequencies of the system, the harmonic response to the vibration spectrum at 500 RPM is also obtained. The magnitude of the forces is much smaller at low wheel speeds, so the response is expected to be smaller than for the 4000 RPM case. In Figure 6.13 the x-deformation of the baffle (maximum observed response) is shown. It is quickly noticed that the magnitude of the deformations is 2 orders of magnitude smaller than at 4000 RPM, and the same can be seen in the omitted graphs of other response spectra. The vibration from the reaction wheels at low frequencies therefore does not cause a response comparable to the greater vibration magnitudes at frequencies well above the fundamental bending eigenfrequencies.

The deformations observed are not immediately worrying for the observational performance of the telescope, but it is important to evaluate the effects of the deformation on the rest of the spacecraft. This will be addressed in Section 8.2. The results are found encouraging that the inclusion of the baffle will not result in instability of the whole telescope, and that obstruction of the optical elements will not occur.

6.4.4. Worst case vibration

While it is still infeasible to analyse the frequency response of the thin-walled model in the full frequency range, due to the occurrence of the major deformations around the first eigenfrequency allows for a limited harmonic response sweep. The aim is to see the realistic response to the reaction wheel vibrations in the

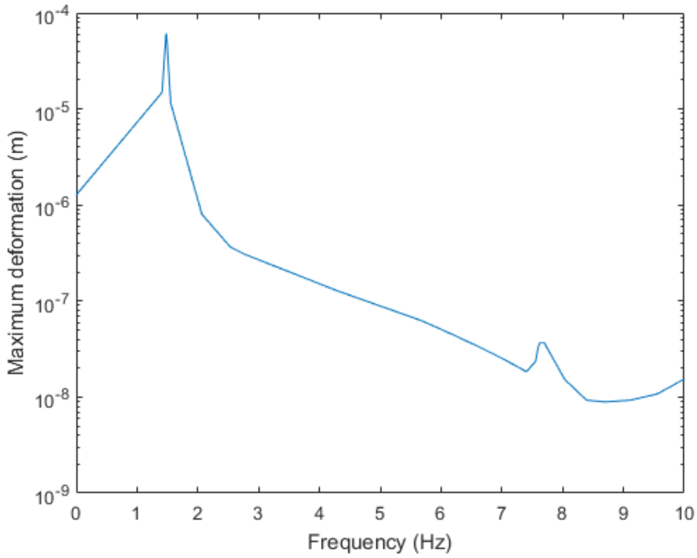

Figure 6.13: Maximum deformation in x-direction with vibration spectrum at 500 RPM applied in x-direction

worst case scenario, and assess the stresses in the structure. The full modal result as calculated earlier will be used for the superposition.

The response spectrum up to 3 Hz can be seen in Figure 6.14, where the maximum amplitude can be seen to be approximately 9 mm. While this is twice as high as the result obtained earlier with the more simple model, it is still not a cause for concern for the operational stability of the baffle. It was verified with the simple model that doing the harmonic response analysis only over the small range of frequencies does not cause accidental omission of response modes, so this result can be seen as reliable.

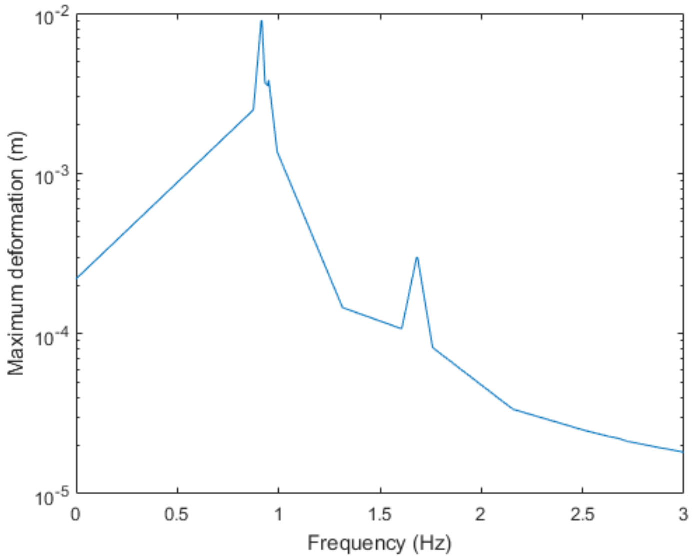

Figure 6.14: Frequency response in x-direction of the realistic baffle model to wheel vibrations in x-direction at 4000 RPM

To limit the amplitude of the response, if required, the reaction wheel speeds can be kept low, if at all possible. This requires designing the ADCS subsystem in a way that accommodates the baffle design. The influence of the baffle on the attitude control budget will be assessed preliminarily in Section 8.2 as the effect of a flexible deployable element on the spacecraft dynamics can prove difficult for e.g. pointing accuracy.

The stress on the structure can be evaluated from this result, too. The Von Mises stress over the structure can be seen in Figure 6.15, where the maximum can be observed to be less than 1 MPa. This occurs at 0.95086 Hz according to ANSYS, and therefore corresponds to the second eigenfrequency, which could be expected based on the loading direction. Most of the structure is under a much lower stress, and this will therefore not be expected to cause any issues for the integrity of the structure. Therefore, the harmonic response analysis generally proves the feasibility of the baffle structure in handling operational loads from the spacecraft bus, and aids in future development as a proof-of-concept.

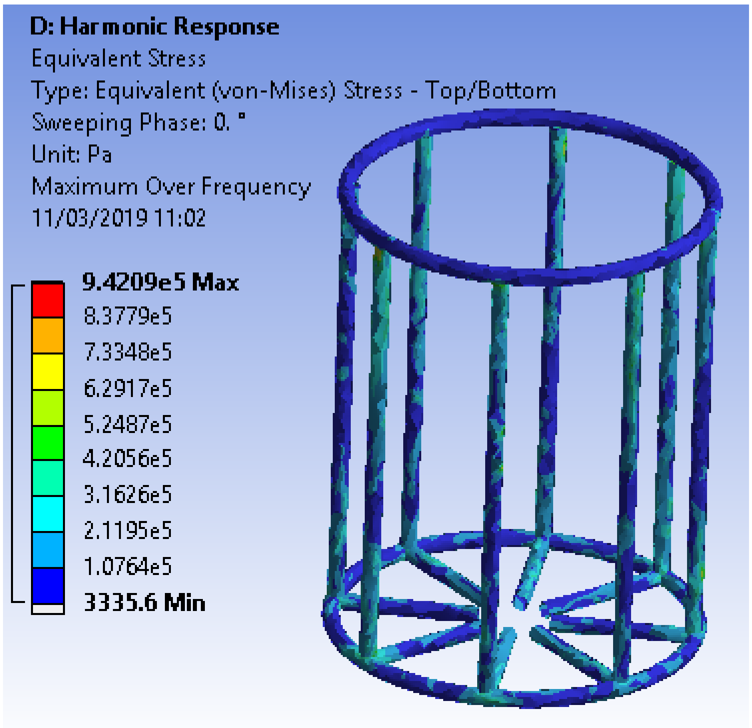

Figure 6.15: Maximum equivalent Von Mises stress on the baffle due to harmonic loading (up to 3 Hz)

6.5. Chapter summary

In this section the findings of the chapter will be summarised. This is done to provide a quick overview of the results and their implications. The performance and properties of the structure were found by using ANSYS, where the baffle was modelled ina simplified manner.

Static gravitational loading was found to be a negligible load in the orbit environment, where the expected buckling load is a factor of minimum 80287 greater than the experienced micro-gravity. However, in Earth gravity, the structure will buckle under a fraction of its own weight, which means that the baffle cannot be tested on Earth without gravity compensating measures.

Modal analysis of the structure provided eigenfrequencies and eigenmodes that are used for the subsequent analyses. The first two eigenmodes were found to be the most critical for the operational condition, as they consist of a bending motion of the whole baffle structure. These occur at approximately 0.92 and 0.95 Hz, which means that excitations at these frequencies should be avoided to the best extent. The reason for the difference in frequencies of these identical but perpendicular motions is not known, as the structure should be symmetric.

Harmonic excitation analysis was conducted based on the modal results and the vibration spectrum of an appropriate reaction wheel. The model had to be made more simple due to the computational effort required to evaluate the full spectrum from 0 to 500 Hz. After identifying that the maximum deformation was obtained at the highest wheel speed and at the fundamental frequency of the baffle, the more realistic ANSYS model could be used to evaluate the deformation at only low frequencies. It was found that the maximum deformation of the structure is approximately 9 mm, which leads to a maximum stress of 0.9 MPa in the structure at a frequency of 0.95 Hz.

As a whole, the results of this chapter show that the design of the baffle can withstand the loads expected in orbit without compromising the performance of the DST. The systems engineering result is that the attitude control subsystem will not have to be designed based on the disturbances of the baffle, but more work is required especially concerning the dynamics of the system when it comes to thermal gradients over the orbit.

7

Deployment and stowage design

In this chapter the deployment sequence of the baffle will be designed. This includes the layout of the inflation system and the way it functions, as well as the method of stowing the baffle that allows for smooth and reliable deployment. First, in Section 7.1 the gas used to create the required internal pressure is selected. Then, the storage, release and venting are addressed in Section 7.2. Integration of the baffle to the DST will be briefly discussed in Section 7.3. The stowing of the booms and MLI will be discussed in Section 7.4.

7.1. Inflation gas

The selection of inflation gas needs to be done before the rest of the inflation system is considered. Different gases have variable masses, chemical properties and storage needs. In this section, the different options are evaluated and the final inflation gas is selected. After this, the details of the required system can be established.

It is preferable to use chemically passive inflation fluids to maintain the structural integrity of the system. Only such compounds are therefore considered, as it is unlikely that a reactive inflation gas (such as ammonia) would be significantly better in all other aspects. Water vapour and carbon dioxide were considered in antenna research in the 1980's, where CO_2 was used for the rigidisable part due to the higher required pressure. With water, the risk of freezing is present before succesful inflation is achieved [46]. Due to the largely unknown thermal environment at and before the time of inflation, water is ruled out as an option for the baffle. Active thermal control of the inflation subsystem is possible, but considered a disadvantage due to the added mass and required power. Newer inflatable systems, such as InflateSail and the IAE, use nitrogen [103]. The use of hydrazine is also presented as an option; unlike the above fluids which stay in the same molecular form, it decomposes into nitrogen and hydrogen which are used for the inflation [46].

It is selected to use nitrogen (N_2) as the inflation gas for a few reasons. First, it has been used in various previous systems, as was found in literature. Second, the storage and release of nitrogen is assumed to be fairly simple, since e.g. cool gas generators (CGG) can be used and no chemical reactions are present [103]. Lastly, the venting of the gas into space will not cause damage to any DST elements that might encounter it, although this will be avoided to the best ability. The inherently low risks make nitrogen the most attractive option for the baffle inflation.

7.2. Inflation design

In this section, the inflation system will be designed. This includes the components for storing the nitrogen, its release and all other parts needed for the successful deployment.

7.2.1. Sizing of gas storage

The starting point for the sizing is the required pressure as calculated in Chapter 5, approximately 35 kPa. Due to uncertainties in the volume and strength of the structure (as discussed in length) and the possibility of leaks during inflation, the pressure producing capability will be calculated with a factor of 1.5. As a result of the deliberate over-sizing, the system must be equipped with regulators to avoid bursting due to application of too much gas.

The ideal gas law will be used for the calculation of the amount of nitrogen required. The assumptions for the relatively small size of the molecules compared to the gas volume and the dominance of kinetic interactions between the molecules can realistically be used for the application. The temperature is assumed to equal room temperature, approximately 298 K, during inflation. The approximate volume to be inflated totals 0.325 m^3 based on the dimensions of the inflatable booms. The relation between the properties is seen in the well-known Equation (7.1). The gas constant R equals 8.314 $JK^{-1}mol^{-1}$. After filling in the known values, it is easily found that 4.591 mol of nitrogen is required. The molar mass of molecular nitrogen is 28 g/mol, leading to a total of 128.553 g of inflation gas, or 192.830 g with the margin of 50%. The storage of this amount of gas in a pressure vessel of e.g. 0.000125 m^3 (a cube with 5 cm sides) would require a pressure of 136.5 MPa. It is clear that introducing such a high pressure vessel in the DST leads to a drastically increased risk of a failure in the inflation system as well as a high mass. Therefore, other options for the nitrogen storage are explored.

$$PV = nRT \tag{7.1}$$

Since the nitrogen cannot be stored in its gaseous form aboard the spacecraft, the only reasonable option is to use a gas generator to produce the gaseous N_2 just prior to inflation. A promising option to produce the nitrogen gas is the use of solid propellant cool gas generators (CGG). In fact, there has been extensive development of these systems in the Netherlands by TNO and Bradford, and currently by CGG Safety & Systems [16, 21, 84, 93, 97]. Small nitrogen CGG's have been tested in space on the Delfi-n3Xt cubesat, while the PROBA-2 mission by ESA includes four larger ones, of which three have been tested [16, 93]. These two successful space applications of the generators make the technology TRL 9 and therefore highly suitable for use on the DST. The CGG are based on the release of N_2 from a solid propellant by decomposition, which removes the need of a high pressure tank and enables long storage times, even up to 10 years without loss in function. The gas output is at ambient temperature, which makes the heat shielding of inflation components unnecessary and improves the system safety. Furthermore, the purity of the released gas is above 99% for nitrogen systems [97]. The initiation of the propellant decomposition can be achieved without pyrotechnics by using a resistance wire [21, 103]. The gas production capability is measured in normal litres, which is a measure for the mass of gas that takes 1 litre of volume at a temperature of 273 K and 1 atm of pressure. The inflation gas need of the baffle equals 154.5 normal litres, which can be found using the ideal gas law.

The PROBA-2 gas generators are sized similarly to the current need, which gives a good indication of the mass and volume taken by the inflation system if proven components are used. Each of these CGG's produces 40 normal litres of nitrogen, which means that four of them would be required for deploying the baffle with the calculated contingency. With a mass of 400 g each, the total mass of the system can be estimated as approximately 1.9 kg with the added tubing and vents [21]. The PROBA-2 CGG's can be seen in Figure 7.1. However, the size of the system will decrease with the use of a custom system. The gas production density for nitrogen generators is 260 normal litres per kg of mass, meaning that a sufficient CGG for the DST would weigh less than 600 g [21, 97]. The required volume is also low, approximately half a litre for the required capability, which eases the integration onto the instrument bus [97]. It is also possible to use multiple generators that are ignited in succession, which could decrease the risk of bursting the baffle structure due to too much gas input, as the CGG's produce their full gas capability in a very small amount of time. The use of 4 CGG's with a capability of 39 normal litres each would enable not using up to a whole CGG in case rigidisation is achieved when predicted, while also providing time to evaluate the pressure in the inflatable structure between firing the CGG's. The integration of these smaller, approximately 150 g generators in the spacecraft bus also requires less robust structure, e.g. a clamp band can be used [103].

7.2.2. Inflation system elements

Prior to deployment, the stowed structure needs to be restrained in place to ensure surviving launch and avoiding premature deployment of elements. The design of the bus integration and release mechanism will be done in the future. For now, it suffices to say that the inflation will be started by the release of the stowed system from the bus.

Figure 7.1: Cool gas generators of the PROBA-2 experiment [16]

The ignition of the CGG's needs to be reliable and non-hazardous, seeing that safety of the system is defined in the requirements. It is wished to not use pyrotechnics for this purpose, but it is possible to start the decomposition by using a glow plug, as was used on both Delfi-n3Xt and the Deploytech mission [21]. The ignition will then only require temporary power from the bus, in the case of Delfi-n3Xt this was approximately 10 W for a duration of 10 seconds at most[53]. The availability of the power is not seen to be a problem, especially since the telescope is not operational at the time of deployment so the electronics of the optical system consume no power at the time. The ignition train on Delfi-n3Xt was not redundant, and it failed between the ignition of the second and third CGG experiments. For this reason, two parallel ignition systems will be implemented on the DST for all generators.

Due to the need for high reliability, a bladder is added to the boom design to avoid leaks, as was briefly discussed in Chapter 5. The material for this is Mylar, since exposure to the LEO environment or high temperatures is not foreseen. All booms and the tori will have an inner lining of Mylar of sufficient thickness to avoid tears, approximately 12 microns as discussed in Chapter 5. The tori will have their own separate bladders, which are interfaced with the boom bladders. These bladders will be considered as the inflatable structure from this point on, and the actual laminate section of the booms only serves the part of the outer layering until yielding is achieved. The added mass of this will be of at most the order of 200 g due to the low density of Mylar, similar to Kapton, the total mass of which was calculated as 230 g in Chapter 5.

Tubing will be needed to connect the inflatable booms and the CGG's. The seal between the tubing and the bladder will be sufficiently reinforced to eliminate the chance of bursting or leaking, as a failure in the pressurisation system at this location would be hazardous for the rest of the instrument bus. A filter will be added to remove impurities from the gas, which might impede the inflation, as on Delfi-n3Xt [70]. This will be located downstream from the CGG's, before the gas flow gets divided between the booms. This should be the best location for smooth deployment. Pressure transducers are added to the system to monitor the pressure during the whole deployment. These will be placed in all the booms if possible, and historically the IAE had pressure sensors in each inflatable strut which proves the feasibility.

Besides the tubing and bladders, vents and valves need to be added to control the inflation and subsequent venting after successful deployment. The first valves considered are the ones that release the nitrogen into the tubes. It is necessary that the rate of flow is similar into all sections of the baffle to ensure stable deployment. After rigidisation, the nitrogen in the structure is vented to space. For this purpose, a vent is added to the inflation system architecture to safely dispose of the gas into space, avoiding the telescope elements. This valve will also be open during launch so that any trapped gases in the baffle can be vented, which will make the deployment more predictable. To prevent propulsive effects and to make the venting more efficient and reliable, multiple vents can be added symmetrically around the bus if needed.

A simplified diagram of the inflation system can be seen in Figure 7.2. The elements mentioned earlier in this section are included in their schematic positions. The diagram does not represent the actual physical locations or geometries of the elements.

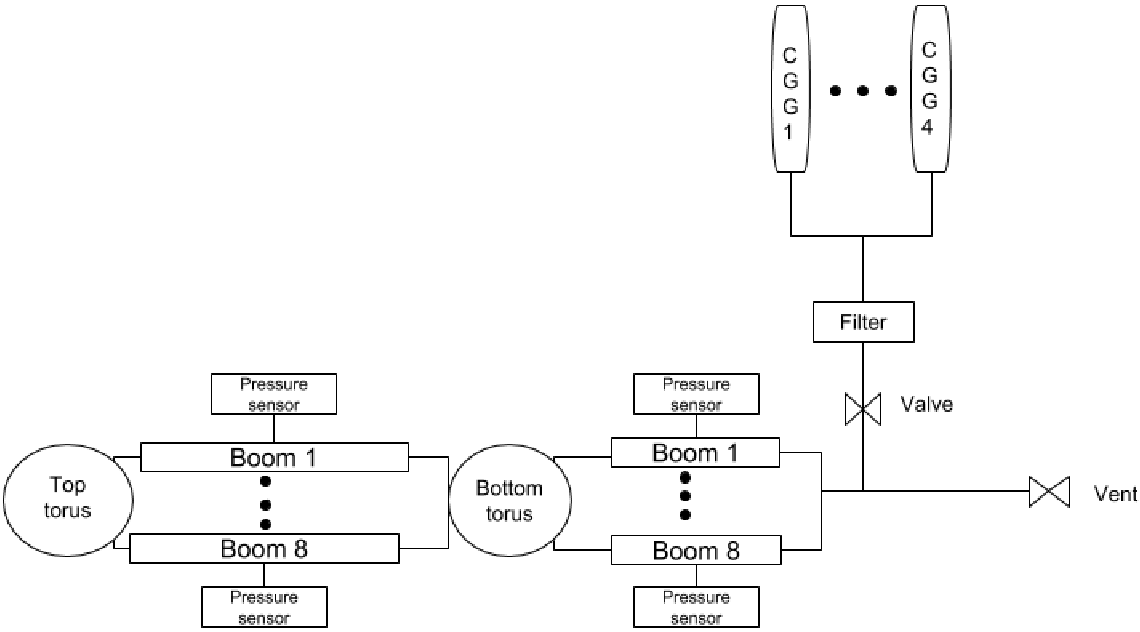

Figure 7.2: Diagram of the inflation system

7.2.3. Inflation sequence

During the inflation process, the deployment of the whole structure is mandated mostly by the stowage geometry since the gas is inflated only from the ends of the 8 radial booms. This makes the sequence of events to be performed relatively simple. In Figure 7.3 an outline of the order of events is presented. The detailed flow of events as well as the time taken for/between each step will be the subject of future work. At this stage, only the preliminary concept of the deployment will be given with the foreseen issues identified to aid the detailed design.

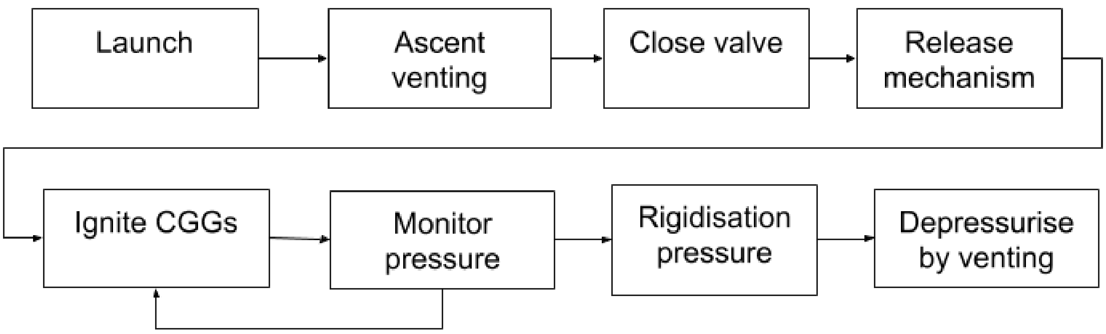

Figure 7.3: Flowchart of the deployment sequence

For a stable deployment, it would be preferable to inflate the bottom torus first, so that the MLI and the longitudinal booms spread out around the bus and therefore have room to deploy in the intended manner. The inflation of the torus before the other elements was also the plan for the Inflatable Antenna Experiment, but the deployment ended up being quite unstable due to unexpected trapped air [45]. Such behaviour is highly undesirable from the baffle deployment, so the inflation sequence needs to be planned carefully. However, it is currently assumed that the gas feed will start at the interface between the radial booms and the housing, leading to their inflation first. Testing is needed to see whether the torus will then fully deploy before the longitudinal booms are inflated. Further, the top torus should also fully deploy before the longitudinal deployment, but this would probably require tubing to be extended into the torus volume. The simplified illustration in Figure 7.4 shows the deployment in two directions in succession.

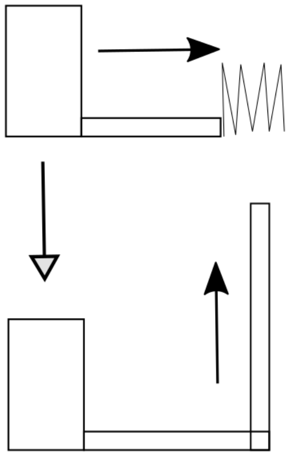

Figure 7.4: Illustration of the deployment sequence

During the inflation and stabilisation of the baffle, disturbing forces and moments are expected to occur, which will have to be counteracted by the attitude control system on DST. At this stage, the magnitude of these disturbances cannot be estimated, and the task will be left for future work. It is however expected that the effect of the deployment on the spacecraft cannot be neglected. It is therefore recommended that the analysis of the deployment loads is done as soon as possible.

Venting of the nitrogen will occur shortly after rigidisation. It was found in the testing process for InflateSail that viscoelastic shearing of the seams becomes a significant risk if the inflatable cylinder is kept pressurised for long durations. It was therefore decided to limit the time under pressure to 15 seconds [102]. This guideline will be followed for the baffle as well, but due to the more complex geometry, testing is required to find out the actual duration of the deployment sequence. Care has to be taken to vent the gas symmetrically, therefore reducing propulsive effects on the spacecraft and reducing ADCS workload when large disturbance torques are expected as a result of the deployment.

7.3. Integration to telescope

In this section, a preliminary design for the housing required for the baffle deployment system will be presented. The design is only based on geometric aspects at this stage, and is used to illustrate the elements needed for the baffle. Therefore there is not much detail provided for the system in this report.

To integrate the inflation system elements to the DST without taking up space in the instrument bus, an additional section will be added to the existing bus design. The inflatable and MLI elements will not be contained in this storage volume. The main purpose of the container is to house the cool gas generators and their firing system, and provide a reliable interface between them and the booms. Since the radial booms are in the shape of an octagon, the housing will have the same shape to be as efficient as possible while providing the right geometry. Initially, the housing is given an edge length of 170 mm to fit on the 410 mm instrument housing. The height is 160 mm, to provide an interface for the 100 mm diameter booms to connect to the housing reliably. Besides the gas generators, all electronics required for them and monitoring the deployment will be placed in the housing. A CAD model of the housing with just representative gas generator models is shown in Figure 7.5 to give an idea of the volume taken by the generators.

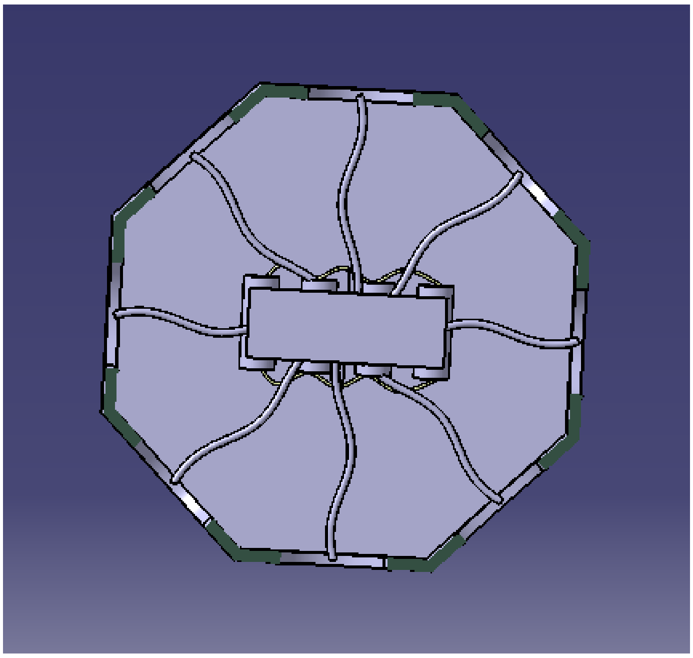

Figure 7.5: Sectioned top view of the inflation system housing

The booms will be connected to the deployment system at the housing, but the required elements are not planned in detail in this work. Figure 7.6 shows the end fittings on the inflatable boom of InflateSail, indicating that complex additions are not necessarily required. It is crucial to provide seals for the inflatable elements (also including a bladder for the DST baffle) and valves to control the flow of the gas, but these are left for future work as they go beyond the conceptual scope of this thesis.

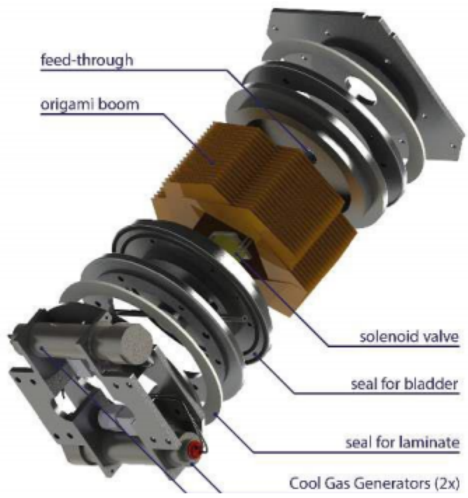

Figure 7.6: An example of the fittings at the end of an inflatable boom [96]

The effect of the baffle housing on the overall dimensions of the DST can be seen in Figure 7.7, which show it integrated onto the instrument housing. The volume increase is not notable compared to the stowing of the baffle itself, as described in the rest of this chapter, but the length of the stowed telescope is naturally increased from approximately 771 mm to 931 mm. Assuming the housing is made of CFRP (common density is 1600 kg/m^3) with e.g. 1 cm wall thickness, the approximate mass is 6.9 kg, which is half the mass of the actual baffle. Therefore, clearly optimisation of the overall design is required.

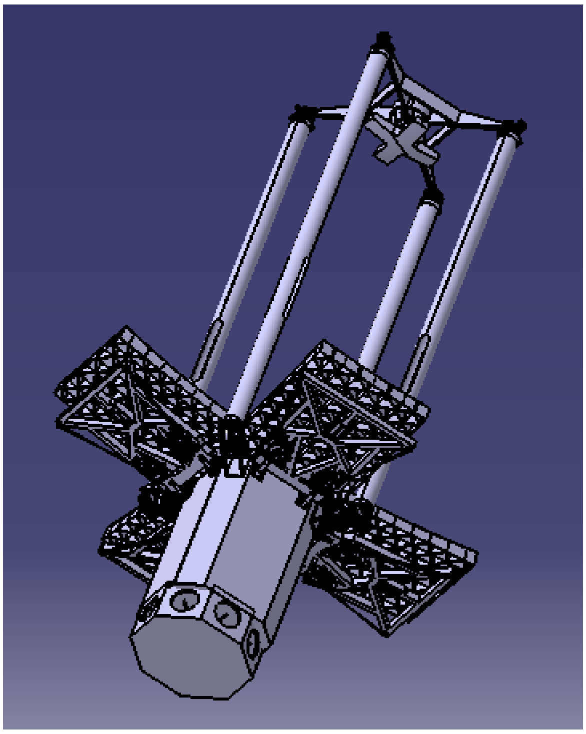

Figure 7.7: View of the inflation system housing on the DST

7.4. Stowed geometry

In this section the folding patterns of the booms and MLI and the resulting geometry in pre-deployed state are designed. The folding method of the baffle is a key consideration for successful deployment, storage and launch survival. For this reason, multiple types of folding are considered for the stowed state of the different elements. The boom folding is treated in Subsection 7.4.1, the bottom thermal shielding in Subsection 7.4.2 and the sides of the shielding in Subsection 7.4.3. The final stowed configuration of the whole baffle is shown in Subsection 7.4.4 and discussion of the results is given in Subsection 7.4.5.

While mathematically the folding of membranes is possible in various ways, in reality the geometry is severely limited by the non-zero thickness of the material. The bending radii of the folds will be greater than the theoretical folding patterns imply, and this will affect the achievable efficiency. This is especially true for the MLI, since it has a significant thickness which cannot be neglected. For avoiding punctures and tears at fold lines, it is preferable to both reduce their number and increase the bending radius, both of which lead to an increase in the stowed volume of the baffle. The design choice will therefore be a compromise between performance and reliability.

7.4.1. Folding of the booms

The booms, which form the backbone of the structure, will need to be folded in a manner than enables reliable deployment as well as secure stowing geometry. It is necessary that the inflation of the system is as straight-forward as possible, and that the MLI blankets get deployed as intended. The radial and longitudinal booms are straight cylinders, which enables the consideration of more advanced folding techniques which improve the deployment characteristics compared to e.g. z-folding. It has been concluded by numerous researchers both numerically and experimentally that deployment of z-folded booms is unstable by nature [86]. While it might be a usable technique for the shorter inflatable elements, the deployment of the longitudinal booms which pull the MLI with them is desired to be as stable as possible with the given means. The stowed volume naturally should be as low as possible, especially to enable the efficient storage of the MLI adjacent to the booms.

Multiple different types of origami-inspired folding patterns have been studied for engineering applications. In the following paragraphs, patterns that have been applied to axially shortening cylindrical structures will be discussed. The most suitable pattern will be chosen from these patterns. Some examples are shown in Figure 7.8, of which not all will be discussed here.

A traditional pattern for folding cylinders is the Yoshimura pattern, or diamond pattern. This is seen on the far left in Figure 7.8. The pattern can be found in axially loaded thin-walled cylinders after buckling and when folded, multiple polygonal cross-sections are possible. Cylinders folded using it are in a stable configuration, so further folding will cause strains in the material [19, 68]. This limits the thickness of the usable material [68]. However, by twisting the pattern the stresses can be reduced. This is seen on the far right of Figure 7.8. Triangulated helical cylinders have been subject to a fair amount of studies [86].

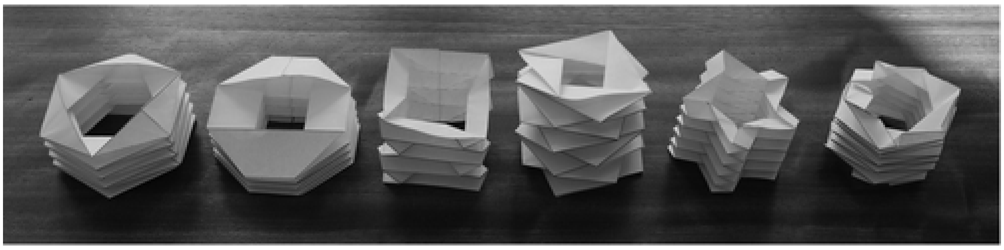

Figure 7.8: Various origami patterns for folding of cylinders [86]

Kresling pattern is reminiscent of the state of a cylinder under torsion, and is similar to the twisted Yoshimura [60]. Geometrical design of Kresling-folded cylinders has been reported [20]. A polyhedral sunshield folded with a Kresling pattern was conceptualised for the International X-ray Observatory, with the specific advantages of interfacing easiness and ability to self-deploy and stay in that state without an applied load [108]. A prototype was constructed out of Kapton and the deployment tests showed that the concept can reliably deploy without endangering the telescope.

The best-known pattern for origami folding in space might be the Miura-ori [67]. Each node of Miura-ori consists of three mountain and one valley fold; or vice versa. It has only one degree of freedom and is rigid-foldable, which makes it advantageous for deployable systems [34]. Numerous researchers have studied the geometry and mechanics of structures folded in this way, especially for flat membranes such as solar sails. Cylindrical Miura-ori is a bit less efficient, as most designed structures require deformation of the pattern [68]. The deployment of cylinders folded with Miura-ori has however been observed to be in a more straight line than for Yoshimura patterns due to the lower deformation [87]. An example of a pentagonal Miura cylinder is seen second from the right in Figure 7.8.

Without conducting a complex analysis, it is selected to use the five-sided Miura "pentalpha" pattern, as it has been experimentally been found to provide a stable deployment compared to multiple other origami-inspired folding methods [87]. The pattern has been successfully demonstrarted on the InflateSail inflatable boom as well [96]. The geometric definition of the pattern can be seen in Figure 7.9 along with the cross section with the InflateSail boom dimensions. The radius R is 50 mm for all the booms of the baffle. The other geometric relations are kept the same, so the relation H/R is 0.67, making the unit height (2H) 67 mm for the baffle booms. The angle ϕ_1 is 67°. These values completely define the folding pattern. For the radial booms, there are then 12 repeating units, and using the same pattern, 45 for the longitudinal booms. It is possible to vary the parameters for the different booms, but at this stage the design will be based on tested reliable patterns. In the deployment experiments by Senda et al., the ratio H/R was 0.377, suggesting that the geometry can be changed quite a lot and that the optimal should be found during the next design phases [87].

The length of the folded InflateSail cylinder is 63 mm with all the end fittings, indicating a compression ratio

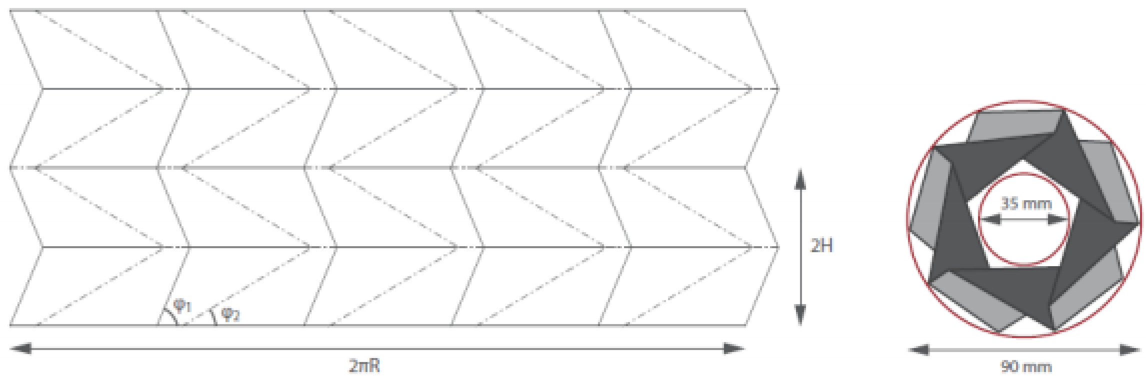

Figure 7.9: Geometric parameters of the pentalpha folded cylinder and its cross section [96]

of approximately 16. Assuming the same is achievable on the DST, the shorter booms will be approximately 50 mm long when stowed, and the longer ones approximately 188 mm. The total volume of all folded booms (assuming 100 mm diameter is maintained) is approximately 0.015 m^3. In the actual case, the boom interfacing blocks will add to the volume significantly, as they cannot be folded. This will be taken into account in subsequent calculations.

The longitudinal booms will have to be stowed outside the M1 segments with sufficient clearance for a hold-down and release mechanism (HDRM) if required between the mirror segments and the booms. For this reason, the lateral booms will actually be folded to a longer length than the approximate 50 mm indicated above. There is approximately 180 mm between the baffle housing and the furthermost point of M1 laterally, which means that the interface between the lateral and longitudinal booms will be placed this distance from the housing, leading to a folded boom length more than 3 times the minimum. This is not expected to prove problematic, and might in fact lead to a more stable deployment due to the significantly shortened deployment distance of the radial booms.

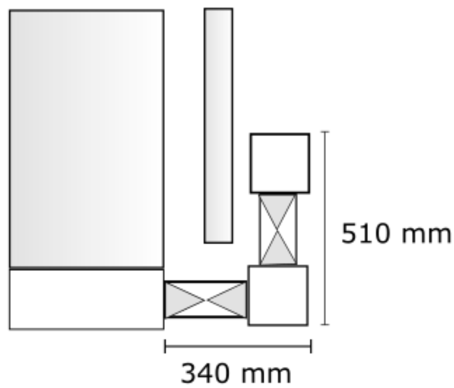

Figure 7.10: Dimensions of the envelope resulting from the boom folding (one vertex)

7.4.2. Bottom shield folding

The vertices of the bottom MLI shield should be connected to the boom interfacing element on the bottom, with the booms running above it. It is seen in Figure 7.10 that the stowed dimension is then 340 mm at each vertex. Based on this, a folded dimensions of the bottom blanket can be designed to fit the configuration of the stowed booms. The general requirements for the folding/unfolding are as follows:

- The MLI needs to fold in radial direction with a factor of at least 2.9 in diameter reduction
- The folded blanket needs to deploy smoothly when the torus and booms are inflated

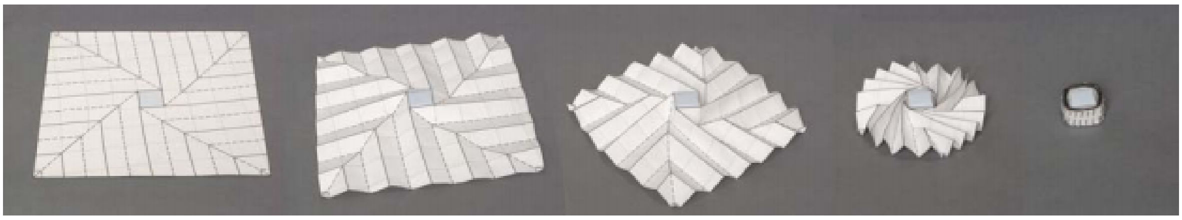

(a) Spiral folding of a square membrane

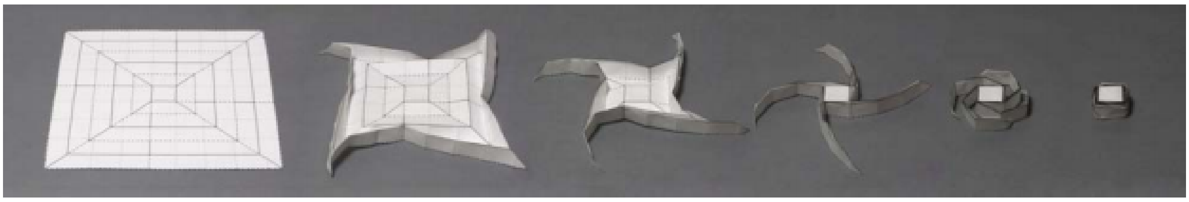

(b) Circumferential folding of a square membrane

Figure 7.11: Spiral and circumferential folding patterns and sequences of a square membrane [73]

- Rotation during deployment is disadvantageous due to the complex overall geometry

There have been multiple concepts of deployable membrane shield structures in recent literature. The packing efficiency that can be achieved is quite good (judging qualitatively from figures), which makes the techniques used interesting. Due to the shape of the bottom of the baffle, the blanket can be thought of as a shield which deploys only radially. This realisation enables the application of folding patterns for membrane shields for the folding of MLI. Especially of interest is research made into polygonal membranes, in which inflatable tubes are embedded [73]. This can be seen to resemble the construction of the baffle, since the inflatable structure at the bottom is an octagon with a torus circumscribing it. Natori et al. have discovered folding methods which include the inflatable tubes and allow for smooth deployment [73]. The possibility of inflatable elements in radial direction is also briefly discussed, which makes the methods seem feasible for the design where the booms are a part of the blanket construction as described in the previous chapter.

The two folding patterns initially considered are the spiral and circumferential folding for polygonal shields. They both consist of a combination of fan and roll-up folding, but the directions are opposite. The diagrams of both with fold lines indicated can be seen in Figure 7.11 where solid lines are hill folds and dashed lines are valley folds. Circumferential folding and deployment of a solar sail has been successfully performed in space by the IKAROS demonstration mission [95]. Another option is z-folding, which was used for the square membrane of InflateSail. This method as well as the Ikaros solar sail deployment rely on rotation [95, 96].

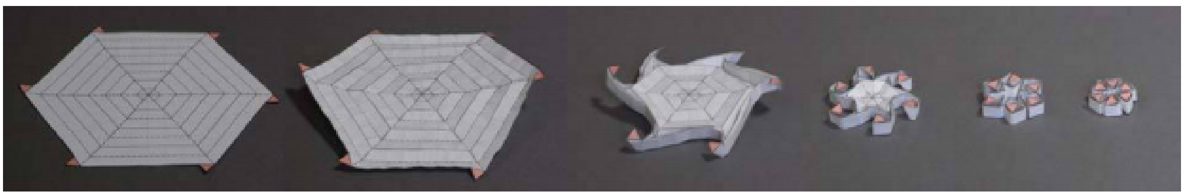

Figure 7.12: Method to fold vertices of a circumferentially folded polygon efficiently [73]

Due to the expected ability to unfold the bottom without rotation, it is chosen to use circumferential folding. Instead of the pattern shown in Figure 7.11b, a slightly modified version is used. The MLI as well as the torus circumscribing it were initially designed as 16-sided to better approximate a circle. However, due to using 8 booms for deployment, it is more simple to have a bottom made of 8 segments joined together and use an octagonal folding pattern. This can be seen in Figure 7.13. It is noted that it is not possible to embed the inflatable elements radially when this pattern is used, but this poses no issue [82]. However, it is possible to connect the torus to the MLI along the full length, as the inflatable tubes can be folded along with the blanket on the outer rim.

As can be seen in Figure 7.12, the vertices can be roll-up folded after the shield is folded with the pattern. It has been estimated from paper models that the folding ratio is about 2 for the vertices, while the rest of the bottom is package more efficiently. However, with the rolling, the required deployment ratio can be met with some rotation induced. It is most likely possible to adjust the folding pattern a bit to avoid rotation and keep the lateral booms in their final orientation at all times, but this is left for the future. The number of circumferential folds is the parameter that defines the height of the folded shield, as well as the diameter. It is more simple to estimate the height in this case, so the number of folds is based on that, as the effect on the diameter is not as straight-forward. The bottom MLI should be placed below the booms on the baffle housing for simplicity, but it is also possible to attach it to the bottom of the housing. A storage height of half the instrument bus, 80 mm, is taken here as a preliminary estimate. As the distance from the bus to the edge is approximately 800 mm, 9 folds are required to meet this. As the attachment point of the MLI to the boom skeleton is above the folded bottom, the final fold is a valley fold, so the outer edge points upwards. As a result of the odd number of folds, the first fold is then also a valley fold, meaning that the attachment of the inner edge to the baffle housing can be done at any location. The folding pattern can be seen in Figure 7.13, where it is shown that the octagonal pattern can be made to use with the 16-sided thermal shield.

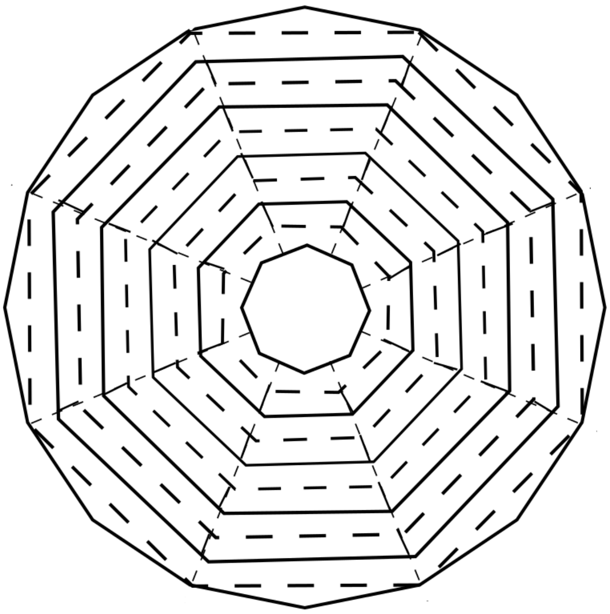

Figure 7.13: Folding pattern for the bottom of the baffle

7.4.3. Folding of the face blankets

To keep the envelope of the stowed telescope below 0.75 m^3 in volume, and taking into account the baffle housing, the allowable diameter of the stowed MLI is 901 mm. This is only 134 mm more than the size of the stowed M1 segments, and as can be seen in Figure 7.10, infeasible based on the boom folding alone. Therefore, if the 1.5 m^3 volume limit is used, the allotted space increases beyond the current volume enclosed by the telescope and the volume can be used to design the folding method. Taking the housing into account for the height of the stowed DST, the allowed footprint is a 1.09 m square, or for the same area, an octagon with 1.198 m medium diagonal, i.e. distance between two opposing edges. Assuming the stowed baffle remains octagonal with the added folded face blankets, the allowed thickness of each face stowed is 71 mm. Due to height of the longitudinal booms stowed and the interface parts, the available height is about 510 mm as seen in Figure 7.10. Furthermore, the width available is approximately 452 mm per sheet, based on the perimeter of an octagon formed by the folded booms. The allowed volume of each face is then 0.016 m^3, which for a sheet thickness of 2 mm means an efficiency of 30.35%, which is achievable for simple deployable structures based on literature on gossamer spacecraft [56].

Further complication is introduced by the planned deployment sequence of the baffle. The bottom part will first deploy radially outwards, followed by the longitudinal deployment. This means that the MLI blankets need to first deploy completely in one direction, followed by the full deployment in the other direction. The deployment in both directions should naturally also be smooth with the inflation of the booms. While there are folding patterns that enable deployment in two directions simultaneously such as Miura-ori folding, which usually would be ideal for applications such as the baffle, this is not applicable in this case. In fact, it was found that the simple option of double z-folding is highly suitable for the walls of the baffle. It allows the aforementioned two-part deployment process and is generally suitable for deploying large space structures due to the simplicity and good packing ratio. The principle is simple; the rectangular MLI is first z-folded longitudinally and the resulting stack is then folded in the same manner in the lateral direction. The end result is a cube of MLI, which can be stowed onto the instrument bus. The process is shown in Figure 7.14.

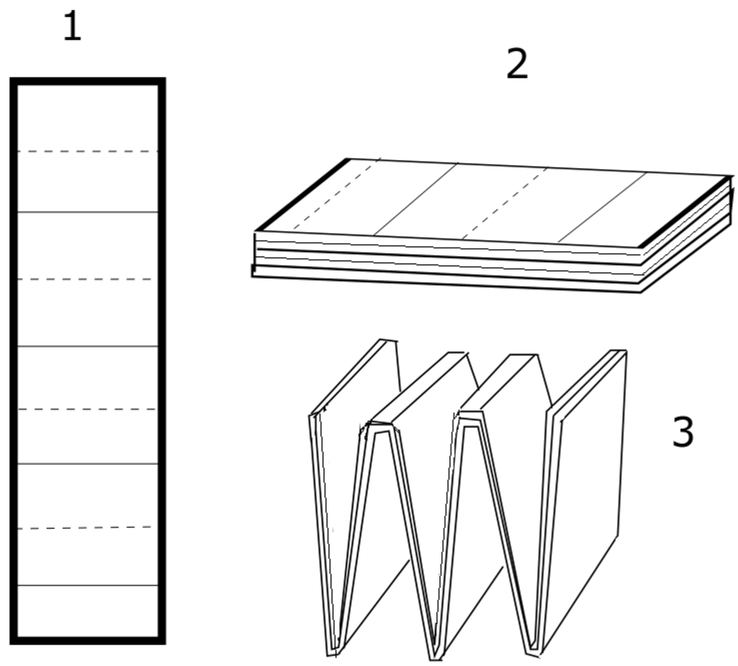

Figure 7.14: Folding sequence of the face blankets (not to scale)

It is noteworthy that this method requires careful planning of the inflatable boom folding, as the two elements are connected and required to deploy simultaneously. The adjacent blankets need to be in touch (via the inflatable elements) on both top and bottom corners. Simultaneous deployment of all sides is necessary for stability of the deployment, but it is assumed that this is achievable, provided that the inflation system works in a robust manner, which naturally necessitates a lot of testing.

For the longitudinal folding, the following guidelines hold:

- The edges of the blanket have to point in opposite direction when stowed, i.e. there has to be an even number of total folds
- The height of the folded MLI has to equal 510 mm due to the boom attachment

These two requirements are not mutually inclusive with regular z-folding without some adjustments. A minimum of 5 folds are needed to fold the blankets down to 510 mm, but this is an odd number and would lead to a height of 500 mm. This can be solved by creating folds with variable distances between them. With 6 folds (the blanket height divided into 7 strips), the average strip between folds becomes 429 mm in width. The required total shift is 81 mm. This can be achieved with e.g. five sections of 429 mm, one 469.5 mm one in the direction of the shift, and a 388.5 mm one in the opposite direction to shift the stack. The difference can be also divided over multiple sections. The nominal thickness of the stack is 14 mm, based on the thickness estimate of Chapter 5, but the folds are assumed to double the effective thickness here to be conservative, so the dimensions of the resulting stack are 28 mm by 429 mm (average) by 828 mm.

The stack of MLI will be oriented so that the width is determined by the packaging ratio in the lateral blanket direction. Guidelines for this folding direction are as follows:

- The width available is 452 mm, which is a folding ratio below 2
- The edges should be in opposite directions, requiring an even number of folds

It is clear from the requirements that the lateral folding is not complex to meet the requirements. For example, with two folds the average segment is 276 mm, and a shift of 176 mm is required to attach the edges. It is possible to have the edge segments be 320 mm wide, and the middle one be 188 mm for a symmetrical folding pattern. Each folded layer is 28 mm as assumed before, and the full stack becomes 112 mm in thickness with the same factor 2 taken for the effect of the folding on the thickness. It is seen that this does not agree with the dimensions given at the start of this section, as the total volume of each blanket is 0.0258 m^3 if the outermost dimensions are taken, with the total for 8 faces of 0.2065 m^3. Reducing the folding factor to 1.5, for example, would meet the requirement. However, at this stage it is not known how feasible this is. It is seen that this volume is quite significant with respect to the goal total DST stowed volume of 0.75 m^3, but it was expected due to the large enclosed volume and the use of MLI. However, the results of this section also further highlight the infeasibility of designing the baffle based on solid parts while still remaining within the volume budget.

7.4.4. Final stowed dimensions

The complete stowed configuration will be presented in this section. The results of the previous sections are put together and the final stowage volume of the baffle, as well as that of the full DST will be given.

The dimensions of all the elements folded can be seen in side view in Figure 7.15. The bottom shield is currently folded partially below the baffle housing, increasing the length of the telescope. It is expected that there will be a spacecraft bus attached at this location, at which point the design of the stowage might need to be revised.

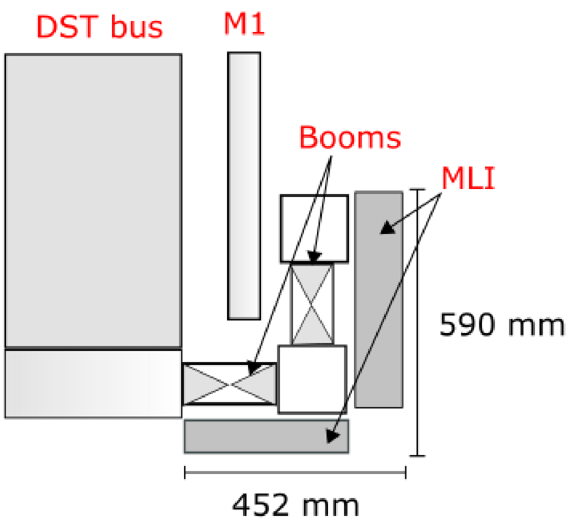

Figure 7.15: Dimensions of all elements folded (one vertex)

The top view can be seen in Figure 7.16 with the final width of the telescope with the stowed baffle. The diameter of the DST is increased by 547 mm from the original 767 mm, which is quite significant but necessary due to the large volume of elements to stow in a configuration that allows stable and reliable deployment. The obvious downside is that the towed diameter starts to get close to the deployed diameter of the primary mirror, which is one of the main drivers for the need to have a deployable telescope design instead of a traditional one. The baffle stowage should therefore be revised based on the results of this thesis, which shows the feasibility of stowing a baffling system within a small volume.

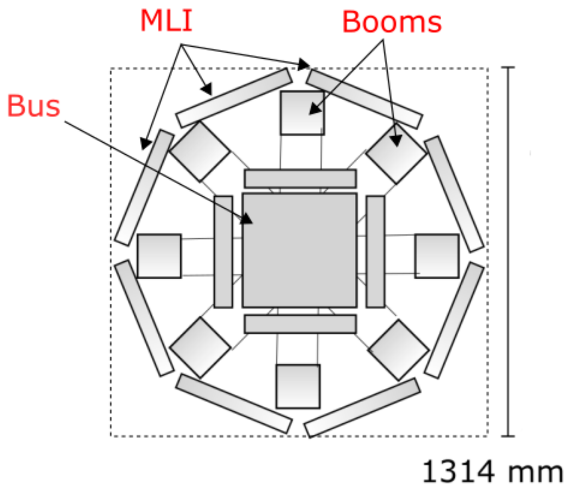

Figure 7.16: View of the stowed baffle from above (simplified, bottom shield not visible)

The total volume of the material used for the baffle is approximately 0.1129 m^3, while the stowed volume is approximately 0.7143 m^3, indicating a packaging efficiency of about 15.8%, or a packaging factor of 6.3. This is near the middle of the expected range (4 to 10) given in literature for the packaging efficiency of complex inflatable structures [56]. The designed stowed configuration is therefore well in line with previous research, and the results can be seen as realistic in that aspect.

7.4.5. Discussion

The total stowed volume of the telescope is 1.802 m^3 (calculated from the envelope formed by the outermost elements) compared to the enclosed volume of 10.2 m^3 when deployed, indicating a volume decrease by a factor 5.66. The comparison can be seen in Figure 7.17. Of course it should be noted that the non-inflatable telescope elements are included in this number, but the volume is largely defined by the baffle as it forms the outermost structure in both configurations. The actual volume taken by the DST is smaller than calculated here (1.38 m^3), but using that as a metric is not practical with respect to volume restrictions imposed by launch fairing dimensions. It is clear that the inclusion of the baffle increases the stowed volume beyond the threshold volume budget defined for the telescope, which is a significant issue for the original project aim as both the mass and volume budgets are now exceeded by a great margin. As the baffle is a critical component, its design should be revised so that the volume budget is met, if at all possible.

Further analytical and experimental work is required to determine the accurate dimensions of the stowed structure, as the behaviour of the MLI when folding is not currently known. It is assumed that the thickness of the blankets does not significantly change the required folding pattern, but this needs to be verified.

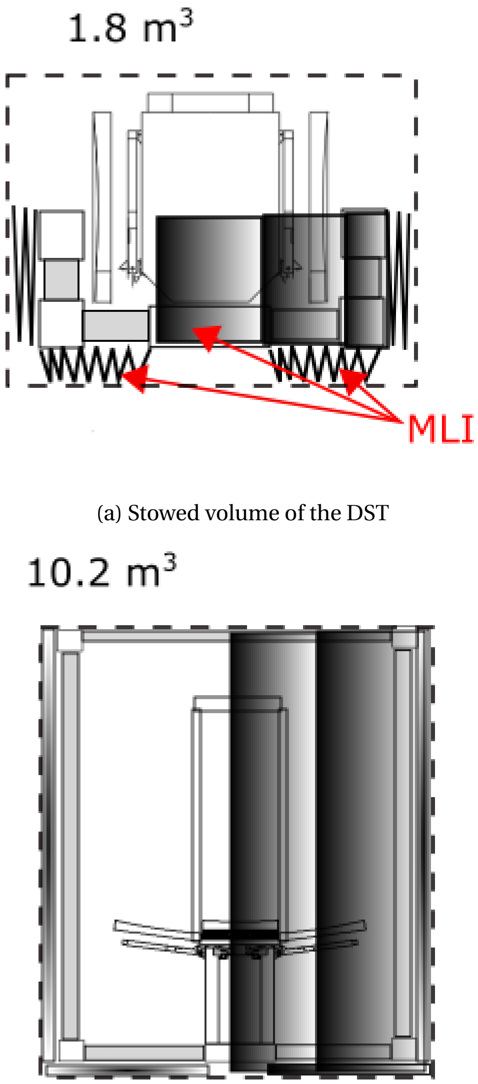

(a) Stowed volume of the DST

(b) Deployed volume of the DST

Figure 7.17: Stowed (a) and deployed (b) volume of the DST with the baffle (shown partially for clarity)

8
System analysis

In this chapter, the effects of the addition of the baffle to the DST are discussed. The thermal model results are shown and discussed in Section 8.1, as these were produced by T. van Wees as a part of modelling the whole telescope thermal environment. The effect of the baffle on the ADCS budgets is explored in Section 8.2. The findings of the chapter are summarised in Section 8.3 along with some systems engineering implications from the whole report.

8.1. Thermal performance

In this section, the effect of the baffle on the thermal environment of the telescope in operation will be presented. Furthermore, the temperature variation and its effects on the baffle elements will also be discussed. The results will be based on the available resources from the research of van Wees. First, the ESATAN model and the available results are discussed in Subsections 8.1.1 and 8.1.2. Design changes in the baffle based on the results will be discussed in Subsection 8.1.3, and the thermal deformation of the baffle is assessed in Subsection 8.1.4. Finally, the thermal performance of the baffle regarding the stabilisation of DST temperatures is explored in Subsection 8.1.5.

8.1.1. Thermal model

Thermal modelling of the whole DST in ESATAN-TMS has been performed by Tim van Wees for his MSc thesis work. Due to the scope of this thesis not being able to include independent thermal analysis, the performance of the baffle will be presented with the results obtained by van Wees. Due to the shifting of the baffle design work into the mechanical aspects more than thermal design, the interaction between the thermal control subsystem and the baffle design has been especially important. Since the thermal model is not part of this thesis, only a brief explanation of the model will be given here. The visualisation of the ESATAN model of the baffle can be seen in Figure 8.1.

The MLI could not be designed layer by layer in ESATAN-TMS, which required the input of a comparable, existing MLI blanket into the model. The properties are assumed to be comparable enough to draw conclusions on the adequacy of the design, but further verification will be required in the future. Furthermore, the expectation was that a requirement on the effective emissivity of the MLI would be obtained from the model, but due to the difficulty in modelling radiative fluxes, the heat transfer through the MLI in the model is purely conductive.

The case considered in the analysis of this section is the maximum hot condition as identified by van Wees [100]. The case is named RA70-FSC-SOLR-MAX and was found to produce the highest temperatures in the top part of the telescope. The signifier FSC stands for full Sun condition, and SOLR-MAX is a case defined as maximum Solar flux combined with average albedo and maximum Earth infrared radiation [100]. The parameters of the orbit and fluxes are summarised in Table 8.1.

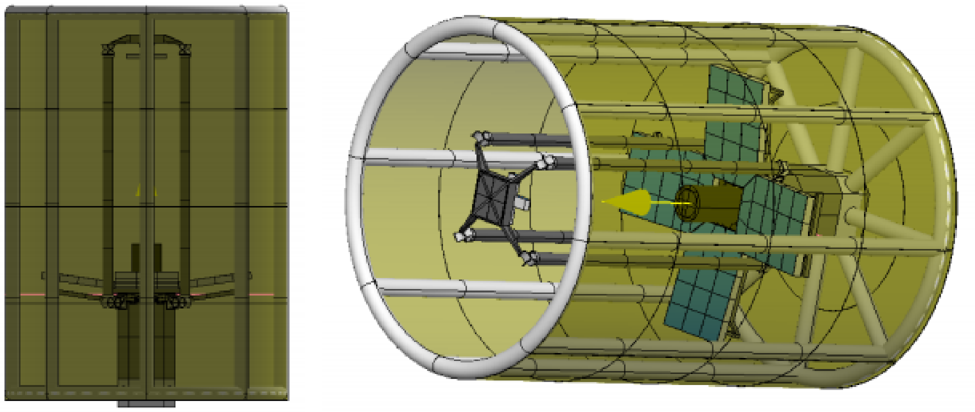

Figure 8.1: Model of the baffle in ESATAN-TMS, courtesy of T. van Wees [100]

Table 8.1: Parameters of the worst hot case used as the thermal environment [100]

Parameter	Value	Unit
Solar flux	1414	W/m^2
Earth albedo	0.22	-
Earth infrared flux	332	W/m^2
Altitude	500	km
Right ascension	70	deg
Inclination	97.4	deg

8.1.2. Available results

While it would be ideal to have data to compare the thermal environment of the DST without and with the baffle in the imaging stage, this is currently unavailable due to the complexity of retrieving that accurate information. The temperature stability requirement of ± 1 K cannot therefore be verified at this stage. It is likely that the albedo flux alone makes this impossible. The temperature variation of the various elements in the nominal case can be obtained over the orbit, but the temporal resolution is quite low. The results over an orbit with and without a baffle will be shown as an indication of the thermal performance, however.

For the baffle itself, the maximum and minimum temperatures over the orbit can be found, and gradients for the conditions at different nodes can be obtained per time step. This information can be used to estimate the static thermal loading effects at this stage of the design. It is possible in principle to perform a transient deformation analysis based on the data, but this was found infeasible with the available ANSYS functionalities. Therefore, the possibility of thermally induced vibrations cannot be assessed which reduces the trust in the performance the design at this point.

In the future, when the thermal model gets developed further, the stability of the thermal environment can be determined in the imaging time frame. At this point, the survival temperature requirements of the DST elements including the baffle can be compared to the performance and some analysis on the baffle is done based on its known temperatures.

8.1.3. Design changes based on thermal results

In this section, the conclusions of the thermal modelling work will already be discussed to apply the design changes suggested by van Wees, where possible. As the main function of the baffle is to adhere to thermal requirements, the response to any input from thermal work is considered a first priority.

It was found in the parametric analysis of the baffle by van Wees that decreasing the diameter or increasing the length, or both, increases the performance and leads to decreased temperatures of the M2 and its support structure [100]. Since increasing the length of the baffle is a simple change with respect to safety margins and structural requirements, it is selected to make the total length approximately 3000 mm at this stage. This is the only increased length considered, so an optimal dimension does not exist at this stage. A reduction in the diameter is also possible within the operational requirements, as there is still a margin of approximately 50 mm on each side with respect to the requirement on a 100 mm clearance to M1. However, the deployment of M2 prevents the reduction of diameter. It should be explored what the actual path of the SMSS is in relation to the baffle and whether the diameter can be reduced. For now, the diameter is kept the same to ensure the safe deployment of M2.

While the change cannot be included in the mechanical analysis which was already performed, it will be taken into account when the stowage of the baffle is designed in the following chapter. In future work, the changed design should be analysed numerically, which was not possible here due to the timing of the receiving of the results. Other effects of the change can be taken into account within the rest of the thesis. The mass of the booms and MLI will naturally be increased, and this will be quantified later. The mass increase is not significant enough to cause concern, especially compared to the benefits in the thermal environment. The temperatures of telescope elements with the baffle will be taken from the analyses with this longer design.

8.1.4. Thermal deformation

In this section, the survival of the baffle structure as a result of the temperatures it encounters during its operational life is evaluated. The thermal environment is based on the ESATAN-TMS analyses done by T. van Wees, and will be used as input for structural FEM analysis done in the ANSYS Mechanical Workbench. Multiple cases were considered by van Wees in his thermal modelling work, with different constants used for e.g. solar radiation and Earth temperature, which affect the heat flux received by the telescope. It was decided together that the hot case is the most suitable for analysing the worst case thermal environment, and therefore those results will be used in this section.

In Figure 8.2 the temperatures on the baffle elements over multiple orbits can be seen. The locations of the maximum or minimum temperatures cannot be seen from this data, and instead have to be analysed per each time step if spatial variation is wanted. The temperatures at different segments for one of the peaks in the graph can be seen in Figure 8.3. The reason for the top section of one boom being significantly hotter is sunlight impinging on it due to the orbital configuration.

The temperatures seen in Figure 8.3 were used as a thermal condition for a static structural analysis in ANSYS Mechanical Workbench. The thermal properties of the baffle were modelled to be those of aluminium 1100-0, for simplicity. This means that the thermal conduction and specific heat properties are slightly different from the real case, but the difference is assumed to be sufficiently small for now. With just the temperature used as loading, the results in terms of total deformation of the structure can be seen in Figure 8.4. It is clear that the deformation due to just the spatial temperature gradients is not expected to pose any issues for the survival or operation of the baffle.

Temporal gradients in temperature might prove to be more harmful for both structural integrity and the dynamic behaviour of the baffle. As can be seen from Figure 8.3, the temperature variation over the orbit is large and the rate of change of temperature is quite high. To estimate the effect of this continuous thermal cycling, a transient analysis of the structure is required, with varying temperature condition. However, this is not possible at this stage, as dynamic effects could not be analysed with ANSYS.

Due to these results, or lack thereof, the thermal loading is not considered when the effect of the baffle on the ADCS budgets is evaluated. The loads caused by harmonic excitation will be considered as the main drivers of disturbances from the baffle. This will be discussed further in Section 8.2.

8.1.5. Telescope thermal environment

In this section, the thermal variations in the other telescope elements will be explored. The main purpose of the baffle design is to minimise these gradients below the operational requirement of ± 1 K, for which the telescope is designed. However, survival temperature requirements have also been identified earlier. The adherence to these will be checked with the results of the worst hot case analysis done by van Wees, which are also presented in his thesis [100]. For this section, the results of the analysis with the 3 m baffle will be used, as the design is selected to be changed to reflect the better thermal environment achieved with it.

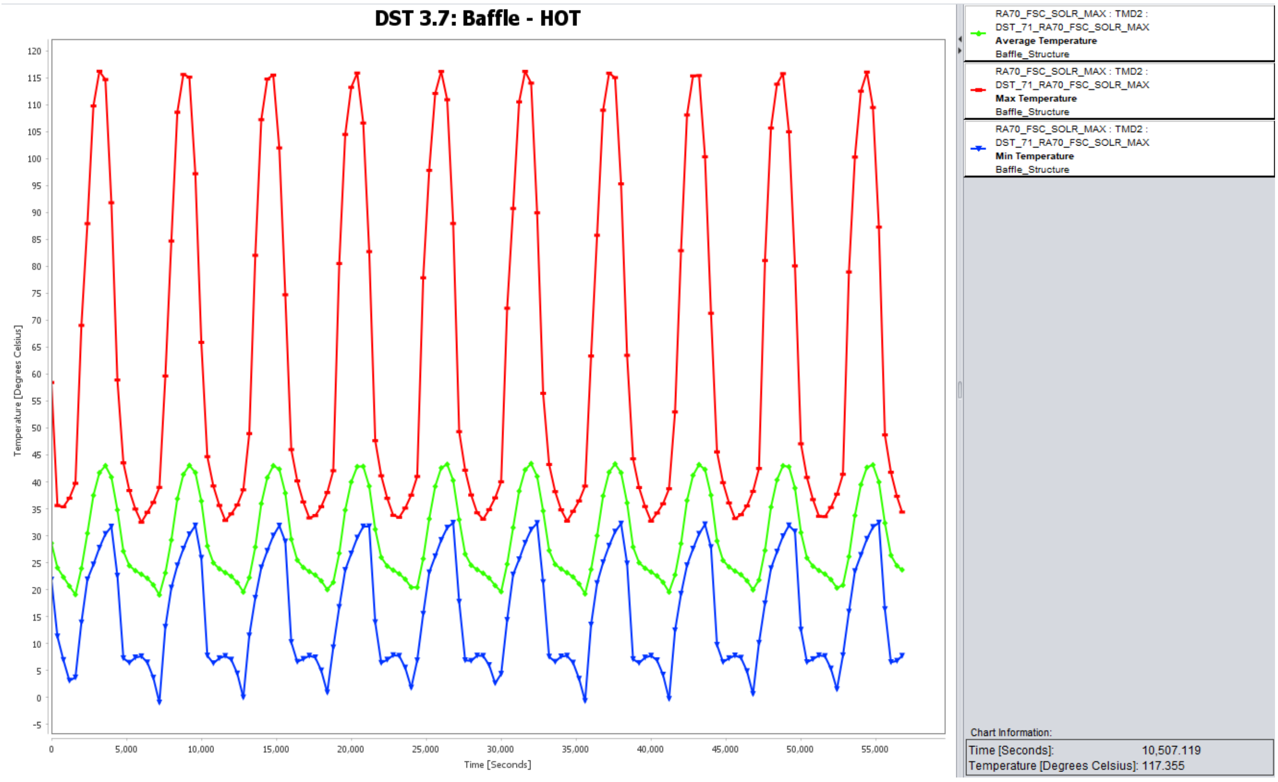

Figure 8.2: Temperatures of the baffle in the hot analysis case in Celsius, courtesy of T. van Wees

The maximum temperatures of elements are listed in Table 8.2. It has been identified by van Wees that some of the extreme temperatures without the baffle are unrealistic, and the average temperatures are more representative [100]. The values will however be used here to assess the general improvement in the temperatures.

Table 8.2: Maximum temperatures of DST elements in hot case analysis [100]

Element	Max temperature without baffle [K]	Max temperature with baffle [K]
M2 spider	358	358
SMSS top hinge	328	343
M2	405.5	318
SMSS booms	340.5	320.5
SMSS root hinge	985.5	303
M1	490.5	303
PMSS	7593	308
Instrument housing	400.5	308

The decrease in the maximum temperatures present in the telescope elements is clearly seen from the thermal results. All of the temperatures are within the maximum bulk temperatures as found in DST requirements, although the only modelled element for which a requirement currently exists are the secondary mirror support system booms. However, the temperatures are moderate enough that they can be assumed to be well within any margins for survival.

The mean temperatures of the elements are another parameter that can be seen to change with the inclusion of the baffle. In Table 8.3 these can be compared for the case with and without the baffle. It is clearly seen that the average temperatures of the different elements get closer to each other, which is good for the reduction of thermal gradients across parts. The mean temperatures are also within 5 K of the nominal operational temperature of 298 K, which is a clear improvement as there were >100 K variations from this design point without the baffle. It is noted, however, that the results do not say anything about the gradients within the

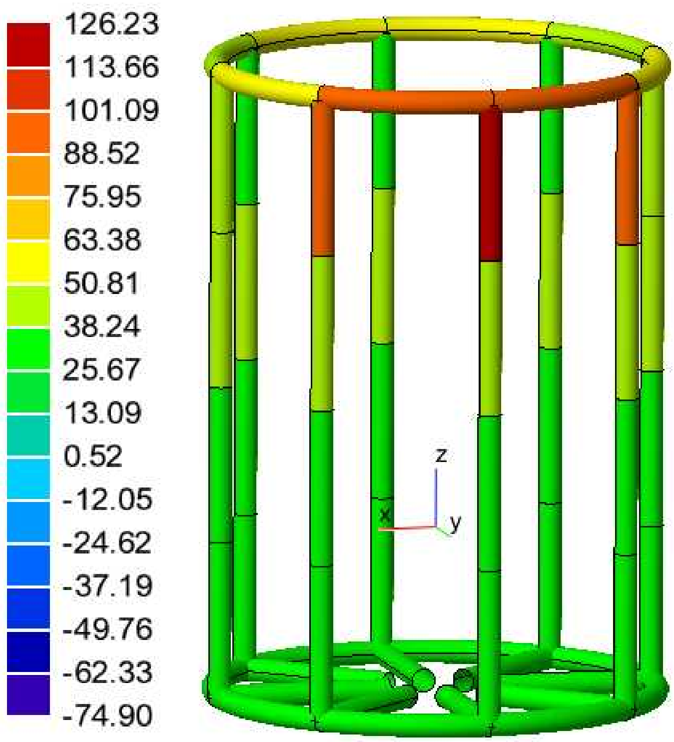

Figure 8.3: Temperatures of baffle elements at the hottest point in the orbit, courtesy of T. van Wees

parts, and therefore the possible reduction in thermal deflection of the optical elements cannot be established. An analysis with more temporal and spatial resolution is required to find if the telescope elements can be kept at a stable enough temperature for the alignment budgets.

Table 8.3: Mean temperatures of DST elements in hot case analysis [100]

Element	Mean temperature without baffle [K]	Mean temperature with baffle [K]
M2 spider	307	299
SMSS top hinge	316	302
M2	404.5	303
SMSS booms	314	302.5
SMSS root hinge	281.5	300.5
M1	334	299
PMSS	267.5	300
Instrument housing	282	301

As a conclusion to this section, it can be said that the baffle improves the temperatures in the DST based on preliminary results. The maximum temperatures are clearly decreased and the mean temperatures of the various parts get closer to both 298 K and each other. These results do not yet verify the design for the intended performance, but they provide evidence that the thermal properties are positively affected by the baffle.

8.2. Disturbance torques

Due to the large deflections at the tip of the baffle, it is expected that disturbances will be imposed on the instrument bus. The forces resulting from the harmonic response as presented above can affect the required attitude control budgets, and the effect should therefore be evaluated. Torques caused by slew manoeuvring of the telescope will be calculated in Subsection 8.2.1 followed by disturbance torques resulting from the response of the baffle to the harmonic accelerations from reaction wheels in Subsection 8.2.2.

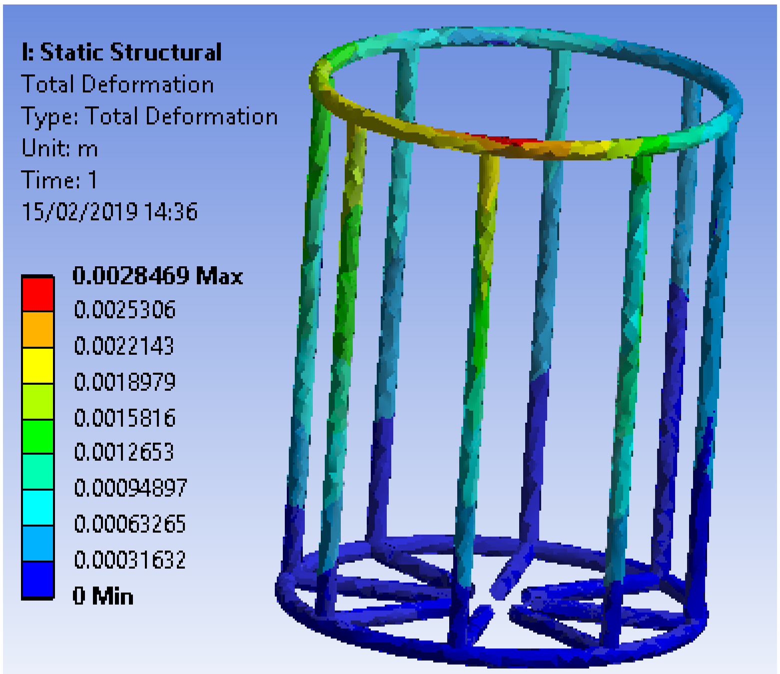

Figure 8.4: Total deflection of the baffle as a result of the hottest case thermal loading

8.2.1. Slew manoeuvre

The dynamics of the DST when performing routine slewing manoeuvres can be significantly changed due to the addition of a flexible baffle. The expected effect of the baffle on the ADCS budget will be analytically assessed in this section so that recommendations on the sizing of the ADCS subsystem can be made.

The situation of the DST orbiting the Earth can be seen in Figure 8.5. Here, h is the orbital height, R is Earth radius, ω is the angular speed of the satellite in its orbit, and α and θ are the angles depicting the motion of the DST with respect to a point on the surface of the Earth, and the centre of the Earth, respectively.

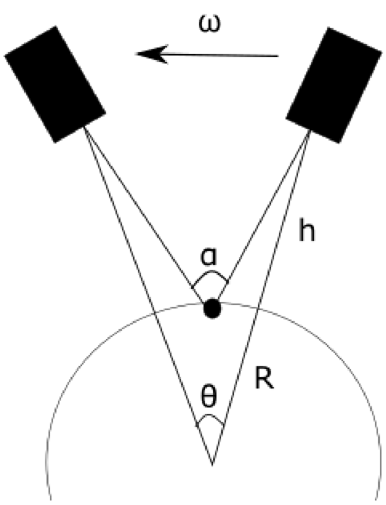

Figure 8.5: Slew rate to track an object on the ground

The nominal slew rate of the DST is not defined at this point, but an estimate can be made based on a requirement of tracking an object on the ground while orbiting overhead. A circular, 500 km altitude orbit will be assumed to simplify the calculations for this estimation. The relation for angular velocity in a circular orbit is expressed as Equation (8.1), and is calculated with the DST parameters.

$$\omega = \sqrt{\frac{\mu}{(R+h)^3}} = \sqrt{\frac{3.986 \cdot 10^{14}\ m^3 s^{-2}}{(6378000\ m + 500000\ m)^3}} = 1.107 \cdot 10^{-3}\ rad/s = 0.0634\ °/s \tag{8.1}$$

This means that in one second, the angle θ increases by 0.0634°. This translates to a change of 0.8723° per second in the angle α when small angles are assumed for the calculation. Therefore, this is the required constant slew rate to keep pointing at an object on Earth. The time taken to accelerate to this angular speed is not known, but a value can be assumed for the angular acceleration based on existing LEO platforms [75]. A value of $0.2°/s^2$ is assumed here, which means that reaching the slew velocity takes approximately 4 seconds. The torque required to produce this acceleration of the spacecraft bus is calculated by assuming a moment of inertia for it. The total mass has previously been estimated a 325.7 kg by S. Pepper and V. Villalba based on statistical methods. Assuming rectangular dimensions of 2-3 metres per side for the whole system, the MOI can be taken as 400 $kg \cdot m^2$ as a first estimate. The torque required to produce this angular acceleration is approximately 1.396 Nm, which is a reasonable value for a LEO satellite and therefore the slew acceleration of $0.2°/s^2$ is used for 4 seconds to simulate the slew manoeuvre.

The slewing motion acts perpendicular to the longitudinal axis of the baffle, so the angular acceleration is applied around the x-axis. This is used as a loading in ANSYS in a transient structural analysis. It was found that the computational time using the thin walled baffle model was infeasibly high again, so the simple model had to be used. The total analysis time is taken as 10 seconds so the behaviour of the system after the loading is removed is seen. A time step of 0.01 seconds was used. The maximum deformation at each time step can subsequently be seen in Figure 8.6. Damped sinusoidal variation can clearly be seen in the deformation time history, which is expected. The magnitude of the motion can also clearly be seen to decrease once the acceleration is removed. It is readily seen that since the maximum deformation is of the order of tens of microns (less than 40 microns maximum), the slew manoeuvre itself is not expected to prove problematic for the baffle. Of course only the acceleration to slew speed is considered here, but as a first estimate the results are expected to indicate the magnitude of the encountered deformations.

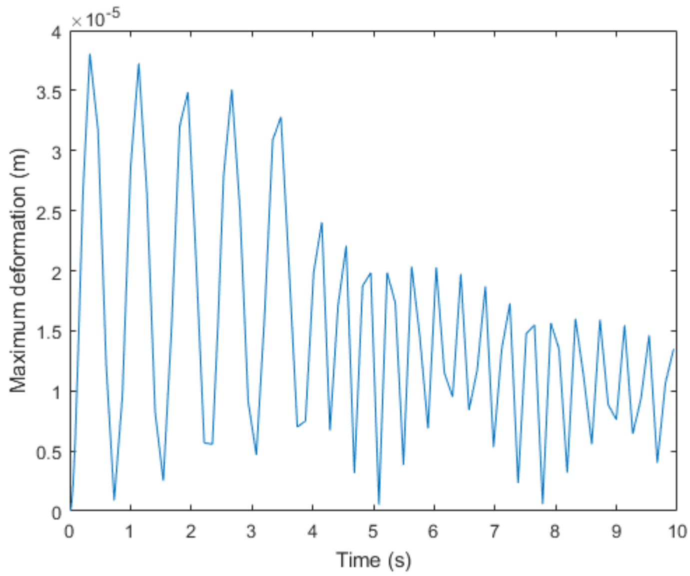

Figure 8.6: Maximum deformation of the baffle with an angular acceleration of 0.2 $°/s^2$ applied for 4 seconds around the x-axis

Since the magnitude of the vibrations is small compared to what was found in the harmonic response analysis, the torque caused by the slewing deformation is not calculated here. The maximum expected disturbance will be assessed in the next subsection based on the frequency response of the baffle to the reaction wheel vibration, as found in the previous chapter.

8.2.2. Moment reaction to spacecraft bus

The greatest force and moment responses were found to follow from the harmonic excitation of the baffle at high reaction wheel speeds, as was seen in Chapter 6. The reactionary forces of the deformation on the spacecraft will be estimated in this section so that the effect on the attitude control budgets can be evaluated.

The maximum x/y-response found in Section 6.4 will be used as the condition of the baffle. The consequent force and moment on the spacecraft bus will be estimated with ANSYS, where these reactions at the support points can be calculated. These are directly the forces on the bus due to the baffle, that will need mitigating to keep the pointing stability of the telescope within the specification. The total reaction force and moment from up to 3 Hz of harmonic response spectrum input can be seen in Figure 8.7. The greatest reactions are produced near the main bending eigenfrequency, as could be expected from the deformation response.

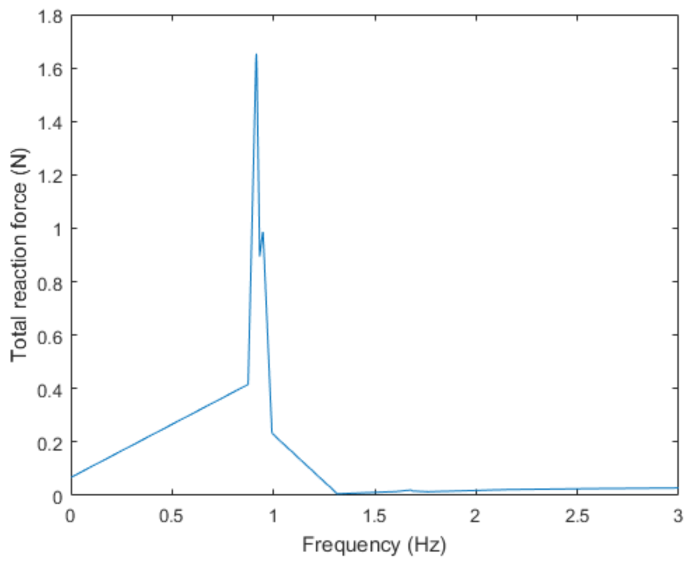

(a) Total reaction force on the instrument bus due to harmonic excitation of the baffle (up to 3 Hz)

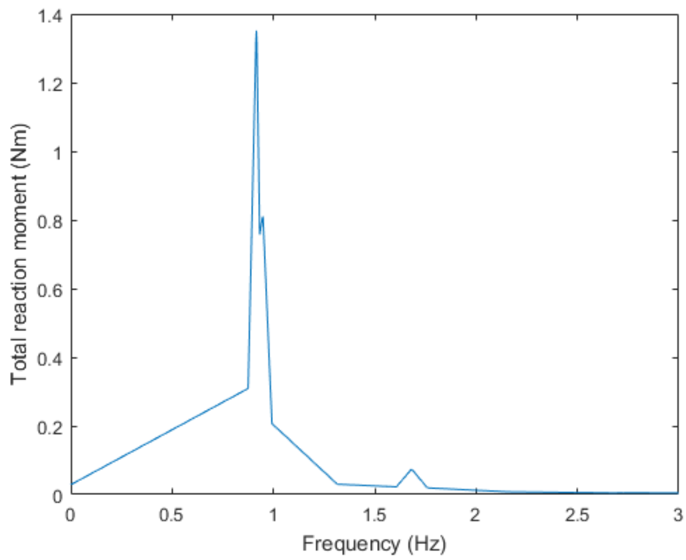

(b) Total reaction moment on the instrument bus due to harmonic excitation of the baffle (up to 3 Hz)

Figure 8.7: Total reaction force (a) and moment (b) on the instrument bus due to harmonic excitation of the baffle (up to 3 Hz)

The rest of the spectrum was verified with the simple ANSYS model, and the magnitude of the reaction moments is significantly lower at high frequencies. Regardless, the reaction forces clearly act as a harmonic disturbance to the spacecraft, which need to be attenuated for optimal performance. The magnitude of the accelerations resulting from the reactions can be estimated based on the inertia properties of the DST bus. With the estimated total mass of 325.7 kg, the maximum acceleration encountered is $5.08 \cdot 10^{-3}$ m/s^2 in the direction of the resultant force. This is seen to be close to the maximum magnitude of the acceleration produced by the reaction wheels, which was used as the input for the harmonic analysis. It is therefore required of the ADC subsystem to counteract twice the magnitude of vibrations as the reaction wheels alone would produce as a result of the inclusion of the baffle.

The angular acceleration resulting from the maximum reaction torque of approximately 1.4 Nm is approximately $3.38 \cdot 10^{-3}$ rad/s^2 (0.19 °/s), assuming a moment of inertia of 400 kg$\cdot$m^2. This is also coincidentally very close to the assumed slew acceleration for the DST which was used above. Therefore, it is also expected that the torque can be counteracted by the ADCS torquers that provide the acceleration required for pointing the telescope in the correct direction in the first place.

8.3. Systems engineering impact

This section summarises the findings of the chapter and combines them with the system level implications of the design choices and analysis results from earlier. First, the telescope thermal environment effects are discussed, followed by the structural interaction of the baffle with the DST. Lastly, the effect of the baffle on the engineering budgets of the project is assessed.

8.3.1. Thermal implications

As the thermal gradients on the optical support elements were the driver for the inclusion of a baffle, the effect of the design on the thermal environment is the main aspect to evaluate. As discussed earlier in this chapter, the full performance in the operational condition could not be assessed yet, but the results obtained so far and their implications are summarised here.

Thermal performance of the baffle was estimated using the results from the ESATAN-TMS model of Tim van Wees, which was worked on concurrently with this thesis. Maximum temperatures of the primary and secondary mirror elements were generally found to decrease, and therefore a more suitable thermal environment results from the addition of the baffle. Average temperatures of the different elements are all within 5 K of 298 K after the baffle is included, which is a great improvement from the original range of 267.5-404.5 K. Stability of the temperatures during imaging operations could not be verified yet. However, the results are promising for future work. When the operational thermal gradients are obtained in the future, the performance of the baffle can be optimised for in the design. This can include design variations such as changing the top opening into an oblique shape, but most importantly the MLI design can be easily changed to fit the thermal requirements.

There are no identified requirements imposed on the thermal control subsystem as of yet. The baffle structure was found to not experience temperatures that threaten the survivability of the selected materials. However, it is possible that the rest of DST will require active thermal control to reduce the thermal gradients sufficiently.

8.3.2. Bus and telescope interaction

The force and moment response to the spacecraft bus was assessed based on the expected slew manoeuvring of the DST as well as the maximum harmonic response of the baffle found earlier. The vibration magnitude as a result of the slew acceleration was found to be in the order of 10^{-5} metres and therefore not significant in the scale of the system. The acceleration caused by the frequency response of the baffle was found to be $5.08 \cdot 10^{-3}$ m/s^2. This is close to the magnitude of the acceleration caused by the reaction wheels, which was used as the driving force. The angular acceleration caused by the resulting disturbance torque is 0.19 °/s^2, which was assumed as the slew acceleration of the bus. Therefore, the resulting disturbances from baffle motions are close to the forces and moments present in the telescope already, and the attitude control subsystem will need to only be able to counter the same magnitude of torque as it creates.

One of the main requirements of the system was that the operational functions of the telescope are not disturbed due to any expected deformation. The maximum motion of the baffle has been found to be a vibration of approximately 9 mm magnitude at the top torus, which does not obstruct the field of view with the applied margin in the baffle diameter. This result along with the observed improved thermal performance imply that the margin could be reduced, which would have the added benefit of lowered mass. It is however noted that the stowed volume would not be affected, as the radial dimension is limited by the clearance of M1 in stowed state.

8.3.3. Engineering budgets

The innovative nature of the Deployable Space Telescope lies in the significantly reduced launch volume and mass compared to existing space systems with the same imaging capabilities. The baffle, almost by definition, envelopes the whole telescope and therefore is the largest single element in the instrument. Therefore its effect on the budgets is crucial for the feasibility of meeting the engineering budgets.

The volume of the whole stowed system was discussed in Chapter 7, and the implications can be discussed here. The volume of the stowed telescope without the baffle was approximately 0.65 m^3, which was well within the goal top level requirement of 0.75 m^3. It was found the the final stowed volume of the DST exceeds the threshold volume budget of 1.5 m^3 by 20%, which is naturally a result that warrants further development if the top level mission requirements are to be met.

The mass budget defined for the baffle (15 kg) does not follow from the systems engineering document of the DST project, but followed from literature review on deployable light shields. In the internal document, a total mass of approximately 127 kg has been assigned to the DST based on the design work so far. To obtain this, a preliminary baffle mass of 14.4 kg was defined, as a design did not exist yet. Therefore, the total mass with the known mass of ca. 23.5 kg of the baffle and its associated elements equals 136.6 kg. Compared to the threshold value of 100 kg, the increase is not insignificant but it is also not the sole reason for the exceeding of the budget. The total spacecraft mass (as opposed to merely the telescope) has statistically been estimated as 325.7 kg, which changes the whole scale of the mass discussion.

9

Conclusion and recommendations

This chapter concludes the thesis work and provides a starting point for future efforts. The final design will be presented in Section 9.1 and recommendations for future work will be given in Section 9.2. The aim of this chapter is to provide an overview of the work done and a starting point for future work based on the findings.

9.1. Final design and conclusions

In this section, the design and the analysed behaviour of the baffle are presented. In Subsection 9.1.1 the design with the mechanical and physical properties is shown. The compliance to requirements set in Chapter 2 and the subsequent answer to the research question is discussed in Subsection 9.1.2.

9.1.1. Design and properties

This section will present the design of the baffle as well as its properties and analysed performance. The baffle consists of a support structure of inflatable booms which is fully enclosed by a multilayer insulation blanket. The booms form an octagonal cylinder, which has an inflatable torus at both ends. The configuration can be seen in Figures 9.1, 9.2, 9.3 and 9.4. The dimensions are given in Table 9.1.

The inflatable booms are made of an aluminium-Kapton laminate, where two 25 μm sheets of 1100-0 alloy aluminium with a 13 μm layer of Kapton between them. The structure is inflated by nitrogen gas produced by four cool gas generators. After deployment, the internal pressure is increased to 35 kPa which causes plastic deformation of the aluminium layers and rigidises the structure, which allows for the venting of the gas to space while maintaining structural integrity throughout the mission. This enables the use of a lightweight inflatable structure while reducing the risk of collapse of the baffle over the mission lifetime due to leaking.

The multilayer insulation blanket consists of 10 reflective layers of double-aluminised Kapton, separated by Dacron netting to decrease conductivity. The outermost layer of the blanket is a layer of silvered Teflon and the inner layer has a black coating to reduce stray light in the telescope. The total thickness of the insulation blanket is approximately 2 mm.

Various origami inspired stowage methodologies were used to make the baffle meet the launch volume requirements of the Deployable Space Telescope. During launch, the baffle can be stowed into a volume of 0.71 m^3, leading to a total stowed envelope of 1.8 m^3 for the telescope. The baffle therefore does not meet the stowage volume top level threshold requirement of 1.5 m^3 and iteration of the design is required.

The total estimated mass of the baffle and its supporting systems is given in Table 9.2 with the masses estimated throughout the work. It is noted that the boom and MLI mass are increased from the first estimates in Chapter 5 due to the increase in the total length of the baffle. In general, requirement BAF-MEC-07 cannot be said to be met with to the inclusion of the housing and the inflation system to the baffle. The total mass is 53% greater than the 15 kg requirement. However, a large part of the mass increase is the baffle housing addition which was done at a late stage in the design. The shielding structure itself has a mass of approximately 14.7

Table 9.1: Final baffle dimensions and parameters

Property	Value	Unit
Total height	3060	mm
Outer diameter	2120	mm
Inner diameter	1860	mm
Boom diameter	100	mm
Laminate thickness	63	µm
Total MLI area	23.5	m^2
MLI thickness	1.99	mm

kg, which is within the specified limit.

The overall mass budget of the DST has a threshold value of 100 kg, which has been exceeded previously. The current mass was estimated as 126 kg without the exact baffle mass known [76]. However, as a result of the conceptual baffle design, this is increased to approximately 137 kg. Therefore, mass optimisation of various elements is necessary to meet the mass budget, and in the case of the baffle system, there are also optimisable parts. The housing is an obvious one, as it has not been designed in much detail at this stage. The number of layers in the MLI is also variable, since the optimum has not been yet identified through thermal modelling. With the current design, a reduction by one layer reduces the total mass by approximately 600 g. However, the readily commercially available 10-layer MLI blanket used in the thermal model has a lower density than what has been calculated in this work.

Table 9.2: Baffle mass constituents and total mass

Part	Mass [kg]
Booms	2.1
MLI	11
Boom connectors	1.6
Baffle total	14.7
Housing	6.9
CGG's	2
Total	23.5

The baffle design has been numerically analysed to assess the fulfilment of the functional requirements. The thermal environment of the telescope has been obtained from thermal modelling work of Tim van Wees, and the addition of the baffle is found to be highly beneficial for the lowering of maximum temperatures and bringing the mean temperatures of various elements closer to each other and the nominal operational temperature of 298 K. The required thermal stability of ±1 K during imaging could not be verified at this stage, and it is possible that this is not possible with only a passive shielding structure.

The baffle design can withstand the microgravity loading in orbit, and will not interfere with telescope operations due to vibrations from reaction wheels. Furthermore, the disturbance torques inflicted by the baffle on the spacecraft bus are of the same order of magnitude as control torques assumed to be needed for slew manoeuvring. Therefore the ADCS design of the DST will not need to be significantly altered to counter the effects of the flexible baffle.

9.1.2. Compliance to requirements

The research question set in Chapter 1 is as follows:

Can a baffle be designed to provide the required thermal stability for the Deployable Space Telescope while staying within the engineering budgets?

The previous section presented a design that answers the research question, and it is partially shown that it is feasible to design a baffle for the Deployable Space Telescope that adheres to the engineering budgets. However, the thermal stability could not be verified, which leaves the bulk of the question unanswered. It can be said based on the findings of the thesis that the thermal environment has been improved with respect to the case without the baffle. Therefore, while the research cannot be said to be a complete success, a foundation has been laid down to continue the improvement of the DST design and meet the image quality requirements.

The compliance of the baffle design to the requirements set in Chapter 2 is assessed in this section. For some requirements, the actual values to be met are still to be determined, and they will not be included in this section. Likewise, some requirements could not be verified yet and therefore will also not be considered here. In the future, the compliance with respect to e.g. the launch survival requirements needs to be assessed. The list of requirement IDs and whether the requirement is met with the current design is listed in Table 9.3.

Table 9.3: Compliance of the baffle design to requirements

ID	Compliance of design
BAF-MEC-01	Compliant
BAF-MEC-02	Compliant
BAF-MEC-03	Not compliant
BAF-MEC-06-01	Compliant
BAF-MEC-06-02	Compliant
BAF-MEC-06-03	Compliant
BAF-MEC-06-04	Compliant
BAF-MEC-06-05	Compliant
BAF-MEC-07	Baffle mass within limit
BAF-SYS-01	Compliant
BAF-SYS-02	Compliant
BAF-THE-01	Compliant

9.2. Recommendations and future work

In this section, the recommendations that have risen from the thesis work are compiled and listed. Some items are relevant for future work, and some may remain open. As there were a lot of subjects explored for the conceptual design, several issues could not be investigated to a sufficient extent and therefore there are a lot of recommendations to be made.

Thermal

A major uncertainty in the baffle design is the required amount of insulation to meet the thermal stability requirements. It was hoped that a requirement for the effective emissivity of the baffle would be available to base the MLI design on, but this was infeasible due to ESATAN limitations. In the future, it would be very useful to optimise the number of MLI layers and layer properties based on the thermal needs of the DST. It is possible that the mass can be decreased if a smaller number of layers is sufficient. As the thermal model included only properties of existing blankets, this part of the design is quite immature.

As a continuation of the previous point, the thermal model of the baffle should be made to include the actual properties of the MLI as produced by the materials chosen here. This will improve the accuracy of the thermal results and verify the baffle design as done in this thesis.

It has been identified by the author and T. van Wees that the inclusion of a reflective top ring on the baffle would improve the thermal performance of the baffle [100]. However, this was deemed very complex for the scope of thesis and is therefore left as a future investigation.

Coatings for the booms of the baffle have not been considered, other than the absorptive black coating required for stray light prevention. It might be necessary to add coatings or protective sleeves, but the temperatures found for the booms did not yet warrant looking into it.

Numerical analysis

As the mechanical results have been obtained before the thermal model results indicated a need for some design changes, the behaviour is not perfectly accurate for the final design. Due to time limitations, the analyses were not repeated for the updated design, but this should be done just to ensure unexpected behaviour does not follow from the increased length. Furthermore, the models used for especially harmonic responses need to be made more accurate, which will involve either changing to another FEM software that allows more nodes to be used, or a less restricted ANSYS licence. In the work done, e.g. the boom connections were not modelled, which might have a large effect on the overall behaviour.

Similar to the need to seek other modelling software, the computing power required to analyse the vibrational response of an extremely thin walled structure such as the baffle was found to be vastly greater than what is available without using for example the TU Delft computing clusters. If accurate structural modelling is required, the issue is far from trivial as the moderately sized thin walled ANSYS model could not be simulated in any reasonable time for this thesis.

Deployment loads and vibrations have not been analysed in this thesis, but they are important to assess the overall reliability and feasibility of the baffle. The effect of the deployment on the instrument bus should be simulated as soon as possible, as well as the deployment process itself. E.g. inflation analysis can be done in FEM software to obtain an initial idea of the behaviour. The folding and unfolding of the booms is another aspect that needs to be investigated in much more detail than has been done here.

Future work

No hold down and release mechanism has been conceptualised yet, so this will need to be done in the future. The mass and volume of the baffle will likely increase as a result. It might be possible to combine the release mechanisms of multiple subsystems, such as the secondary mirror support system one, to the baffle mechanism. This would also increase the reliability of the deployment of the telescope, assuming that the combined system is designed to be robust.

Attitude control

Care should be taken to design slew manoeuvres for the telescope, so that vibrations in the main eigenfequencies of the baffle are not excited by the control inputs.

Testing

The properties of both aluminium foils as well as the full laminate have a lot of uncertainty in them, so testing of the actual mechanical properties is necessary. The elastic modulus especially needs to be determined, as the performance is highly dependant on it and therefore the results obtained by analysis in this work are uncertain.

Feasibility of the folding patterns as well as the folding/unfolding processes need to be tested to find the actual volume that can be achieved for the stowed baffle as well as that the structure stays undamaged.

The inflation system can be developed further by determining the optimal way of delivering the nitrogen gas to all the eight elements simultaneously ensuring a stable, symmetrical deployment. The ignition of the gas generators should be designed in more detail, so that the inflation rate is controlled and the correct pressurisation level can be achieved. On the same note, different pressure levels should be tested to find the required level, along with the level where bursting occurs.

Design variations

It has been experimentally verified that the strength of inflatable cylinders can be increased by helically winding a filament around them [63]. The rigidisation method remains the same as used for the baffle design. This should be investigated since the possible outcome is that the inflation process is more reliable and the performance of the rigidised booms is increased. It is likely that experimental comparisons are required for this.

The rigidisation method for the booms should be re-evaluated, which was a recommendation by Airbus Defence & Space due to a greater abundance of research done into UV and chemically rigidised inflatable structures. It is possible that one of these methods is more suitable if the technology is more mature than the stretched laminate method.

The dimensions of the baffle are not set by any requirement at this point, and finding an optimal length and diameter might be possible based on e.g. the thermal performance. The current geometry serves as a starting point for the feasibility of the concept, but iterations on it will most likely occur.

Stray light control

Stray light properties and requirements should be assessed for the telescope overall and the baffle design. This was intended to be a major part of the thesis, but due to a lack of quantifying the stray light at this point, as well as the already large scope of the work, it had to be left for the future. More detailed recommendations cannot be give as the stray light issue needs to be handled practically from scratch.

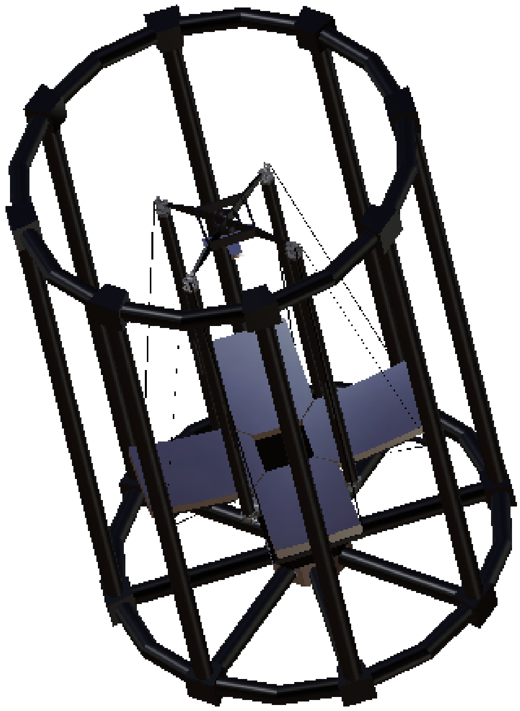

(a) Telescope with baffle (top view)

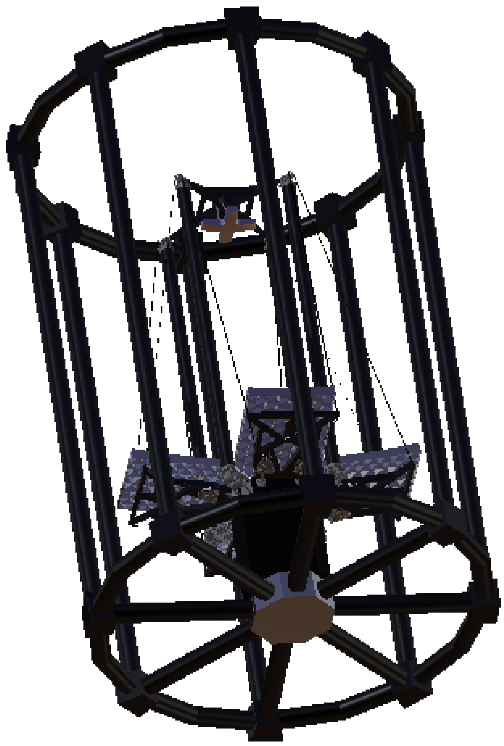

(b) Telescope with baffle (bottom view)

Figure 9.1: Final baffle design without MLI

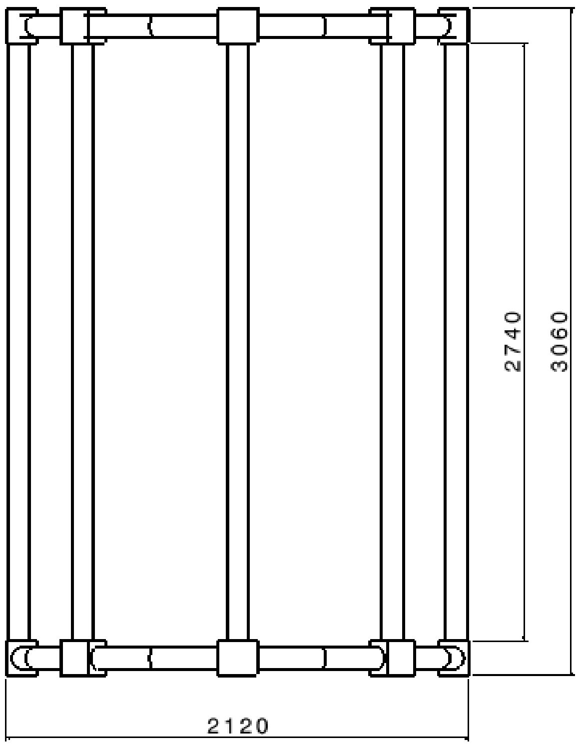

Figure 9.2: Side view and dimensions of the final baffle design

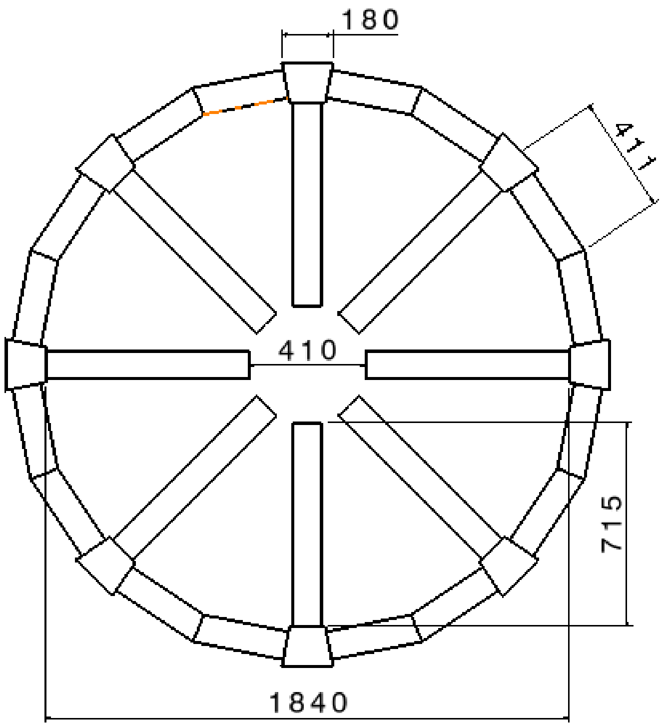

Figure 9.3: Bottom and dimensions of the final baffle design

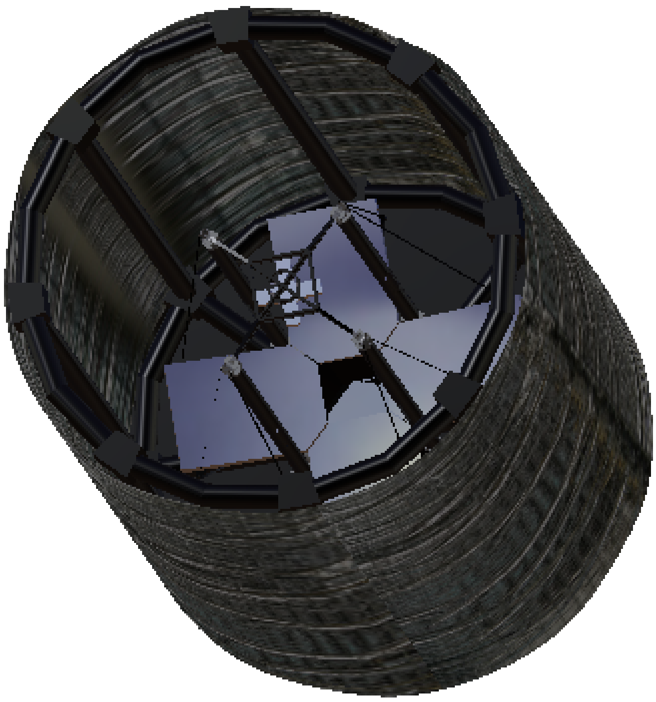

Figure 9.4: CAD model of the telescope with baffle (inside of MLI non-black for clarity)

Bibliography

[1] EnhancedView News Not So Rosy for GeoEye. https://spacepolicyonline.com/news/enhancedview-news-not-so-rosy-for-geoeye/, June 2012. Retrieved on March 14, 2019.

[2] 3M. 3M Adhesive Transfer Tape Y966. https://www.3m.com/3M/en_US/company-us/all-3m-products/~/3M-Adhesive-Transfer-Tape-966/?N=5002385+3293241971&rt=rud, . Retrieved on April 10, 2018.

[3] 3M. 3M Scotch-Weld Epoxy Adhesive EC-2216 B/A Gray. https://www.3m.com/3M/en_US/company-us/all-3m-products/~/3M-Scotch-Weld-Epoxy-Adhesive-EC-2216-B-A-Gray/?N=5002385+3292667630&rt=rud, . Retrieved on April 10, 2018.

[4] Acktar. Magic Black. https://www.acktar.com/product/magic-black/. Retrieved on September 17, 2018.

[5] E. Agasid, K. Ennico-Smith, and A. Rademacher. Collapsible space telescope (CST) for nanosatellite imaging and observation. *Proceedings of 27th Annual AIAA/USU Conference on Small Satellites*, 2013.

[6] *Soyuz User's Manual Issue 2 Revision 0.* Arianespace, March 2012.

[7] *Vega User's Manual Issue 4 Revision 0.* Arianespace, April 2014.

[8] *Ariane 5 User's Manual Issue 5 Revision 2.* Arianespace, October 2016.

[9] Avion Alloys. The Importance of Multi-layered Insulation. http://www.avionalloys.com/importance-of-multi-layered-insulation/. Retrieved on March 14, 2019.

[10] B.A. Banks, L. Gebauer, and C.M. Hill. Atomic oxygen interactions with FEP Teflon and silicones on LDEF. In *Proceedings of the First LDEF Post-Retrieval Symposium*, Kissimmee, FL, the United States, 1991.

[11] J.W. Lopes Barreto. Deployable Space Telescope: Optimal Boom Design for High Precision Deployment of the Secondary Mirror. Master's thesis, Delft University of Technology, May 2017.

[12] M. Bavdaz, Ph. Gondoin, K. Wallace, T. Oosterbroek, D. Lumb, D. Martin, P. Verhoeve, L. Puig, L. Torres Soto, and A.N. Parmar. IXO system studies and technology preparation. In *Proc. SPIE 7437, Optics for EUV, X-Ray, and Gamma-Ray Astronomy IV*, 2009.

[13] M.C. Bernasconi and S. Köse. The Space-Rigidised Thermal Shield for the ESA Far-Infrared Space Telecope (FIRST). In *Proc. of the 3rd European Symposium on Space Thermal Control & Life Support Systems*, Noordwijk, The Netherlands, October 1988.

[14] M.C. Bernasconi and G.G. Reibaldi. Inflatable, space-rigidized structures. Overview of applications and their technology impact. *Acta Astronautica*, 14:455–465, 1986.

[15] Bradford. Reaction Wheel Unit. Retrieved on March 15, 2019.

[16] Bradford. Third Cool Gas Generator aboard PROBA2 Successfully Fired. http://bradford-space.com/news2016-06-17.php, June 2016. Retrieved on August 7, 2018.

[17] D.P. Cadogan and J.K. Lin. Inflatable Solar Array Technology. In *37th AIAA Aerospace Sciences Meeting and Exhibit*, Reno, NV, the United States, January 1999. AIAA.

[18] D.P. Cadogan and S.E. Scarborough. Rigidizable materials for use in gossamer space inflatable structures. *42nd AIAA/ASME/ASCE/AHS/ASC Structures, Structural Dynamics, and Materials Conference and Exhibit*, 1417, 2001.

[19] J. Cai, X. Deng, J. Feng, and Y. Zhou. Geometric design and mechanical behavior of a deployable cylinder with Miura origami. *Smart Materials and Structures*, 24(12), 2015.

[20] J.G. Cai, X. Deng, Y. Zhou, J. Feng, and Y. Tu. Bistable Behavior of the Cylindrical Origami Structure With Kresling Pattern. *Journal of Mechanical Design*, 137(6), 2015.

[21] CGG Safety & Systems. Cool Gas Generators for space applications. `https://www.isispace.nl/brochures/CGG%20Safety%20&%20Systems%20-%20Presentation%20CGG's%20for%20space%20oct%202014.pdf`, November 2014. Retrieved on August 7, 2018.

[22] S.H. Cho, G. Kim, T.J. McCarthy, and R.J. Farris. Orthotropic elastic constants for polyimide film. *Polymer Engineering & Science*, 41(2):301–307, 2001.

[23] M. Corvers. Design of a Primary Mirror Deployment Mechanism for a Deployable Space Telescope. Master's thesis, Delft University of Technology, June 2018.

[24] G. Denis, A. Claverie, X. Pasco, J-P. Darnis, B. de Maupeou, M. Lafaye, and E. Morel. Towards disruptions in Earth observation? New Earth Observation systems and markets evolution: Possible scenarios and impacts. *Acta Astronautica*, 137:415–433, 2017.

[25] DigitalGlobe. Satellite information. `https://www.digitalglobe.com/resources/satellite-information`. Retrieved on February 21, 2018.

[26] D. Dolkens. A Deployable Telescope for Sub-Meter Resolutions from MicroSatellite Platforms. Master's thesis, Delft University of Technology, February 2015.

[27] D. Dolkens and H. Kuiper. Design and End-to-End Modelling of a Deployable Telescope. In *International Conference on Space Optics*, Biarritz, France, October 2016.

[28] D. Dooling and M.M. Finckenor. Material Selection Guidelines to Limit Atomic Oxygen Effects on Spacecraft Surfaces. Technical report, NASA Marshall Space Flight Center, 1999.

[29] K. Du, K.W. Yin, H. Li, S. Liao, and F.P. Long. Design and analysis of a novel self-deployable baffle. In *5th International Symposium on Photoelectronic Detection and Imaging (ISPDI) - Infrared Imaging and Applications*, volume 8907. SPIE, 2013.

[30] K. Du, S. Liao, H. Li, and Y. Zhang. A novel self-deployable baffle with vanes driven by rectangular section curving tape springs. In *7th International Symposium on Advanced Optical Manufacturing and Testing Technologies (AOMATT 2014)*. International Society for Optics and Photonics, 2014.

[31] DuPont. DuPont Kapton Summary of Properties. `http://www.dupont.com/content/dam/dupont/products-and-services/membranes-and-films/polyimde-films/documents/DEC-Kapton-summary-of-properties.pdf`, . Retrieved on April 30, 2018.

[32] DuPont. DuPont Kapton XC. `https://www.americandurafilm.com/data-sheets/kapton-xc.pdf`, . Retrieved on August 6, 2018.

[33] C. Dupuy and O. Le Couls. Gossamer technology to deorbit LEO non-propulsion fitted satellite. In *Proceedings of the 40th Aerospace Mechanisms Symposium*, pages 301–308, May 2010.

[34] D. Dureisseix. An overview of mechanisms and patterns with origami. *International Journal of Space Structures*, 27(1):1–14, 2012.

[35] H.W. Dursch, B.K. Keough, and H.G. Pippin. Evaluation of adhesive materials used on the Long Duration Exposure Facility. Technical report, Boeing Defense and Space Group, 1995.

[36] Earth Imaging Journal. Significant Supply Expansion for EO Industry: Data Demand Driven by Defense and Emerging Markets. `http://eijournal.com/print/articles/significant-supply-expansion-for-eo-industry-data-demand-driven-by-defense-and-emerging-markets`. Retrieved on April 3, 2019.

[37] ESA. Outgassing database. `http://esmat.esa.int/Services/outgassing_data/outgassing_data.html`. Retrieved on April 10, 2018.

[38] H. Fang, M. Lou, J. Huang, U. Quijano, and L. Hsia. Thermal distortion analyses of a three-meter inflatable reflectarray antenna. In *44th AIAA/ASME/ASCE/AHS/ASC Structures, Structural Dynamics & Materials Conference*, 2003.

[39] H. Fang, M. Lou, J. Huang, L. Hsia, and G. Kerdanyan. Inflatable structure for a three-meter reflectarray antenna. *Journal of spacecraft and rockets*, 41(4):543–550, 2004.

[40] H. Fang, M. Lou, J. Huang, L. Hsia, U. Quijano, G. Pelaez, and V. Svolopoulos. Development of a 7-meter inflatable reflectarray antenna. In *45th AIAA/ASME/ASCE/AHS/ASC Structures, Structural Dynamics & Materials Conference*, 2004.

[41] M.M. Finckenor and D. Dooling. Multilayer Insulation Material Guidelines. Technical report, National Aeronautics and Space Association, 1999.

[42] P. Fortescue, J. Stark, and G. Swinerd, editors. *Spacecraft Systems Engineering*. Wiley, 3 edition, 2003.

[43] C.L. Foster, M.L. Tinker, G.S. Nurre, and W.A. Till. The Solar Array-Induced Disturbance of the Hubble Space Telescope Pointing System. Technical report, National Aeronautics and Space Administration, Marshall Space Flight Center, 1995. NASA Technical Paper 3556.

[44] R. Freeland and G. Veal. Significance of the Inflatable Antenna Experiment technology. In *39th AIAA/ASME/ASCE/AHS/ASC Structures, Structural Dynamics, and Materials Conference and Exhibit* , page 2104, 1998.

[45] R.E. Freeland, G.D. Bilyeu, G.R. Veal, and M.M. Mikulas. Inflatable deployable space structures technology summary. In *Proc. 49th International Astronautical Congress,IAF-98-I.5.01*, Melbourne, Australia, September-October 1998.

[46] G.J. Friese, G.D. Bilyeu, and M. Thomas. Initial '80s Development of Inflated Antennas. Technical report, L'Garde, Inc, 1983.

[47] R. Gardi and G. Pica. Realization and preliminary tests on an innovative deployable structure for a high-resolution telescope for microsatellite. In *Sensors, Systems, and Next-Generation Satellites VIII*, volume 5570, pages 411–423. International Society for Optics and Photonics, 2004.

[48] D.G. Gilmore, editor. *Spacecraft Thermal Control Handbook, Volume I: Fundamental Technologies*. The Aerospace Press, 2002.

[49] G.M. Gladysz and K.K. Chawla. Coefficients of thermal expansion of some laminated ceramic composites. *Composites Part A: Applied Science and Manufacturing*, 32(2):173–178, 2001.

[50] Greater.Earth. Chemically Rigidized Expandable Structures. `http://greater.earth/chemically-rigidized-expandable-structures/`. Retrieved on December 11, 2018.

[51] A. Greenbaum, M. Knapp, G. Schaalman, T. Henderson, and S. Seager. Low-mass High-performance Deployable Optical Baffle for CubeSats. In *IEEE Aerospace Conference*. IEEE, 2013.

[52] D.T. Griffith and J.A. Main. Experimental Modal Analysis and Damping Estimation for an Inflated Thin-Film Torus. *Journal of Guidance, Control and Dynamics*, 25(4):609–617, July-August 2002.

[53] J. Guo, J. Bouwmeester, and E. Gill. In-orbit Results of Delfi-n3Xt: Lessons Learned and Move Forward. In *Proceedings of the 65th International Astronautical Congress (IAC 2014)*, Toronto, Canada, 2014.

[54] C.S. Hemminger, W.K. Stuckey, and J.C. Uht. Space Environmental Effects on Silvered Teflon Thermal Control Surfaces. Technical report, The Aerospace Corporation, September 1991.

[55] T. Inamori, K. Shimizu, Y. Mikawa, T. Tanaka, and S. Nakasuka. Attitude Stabilization for the Nano Remote Sensing Satellite PRISM. *Journal of Aerospace Engineering*, 26(3):594–602, July 2013.

[56] C.H.M. Jenkins, editor. *Gossamer Spacecraft : Membrane and Inflatable Structures Technology for Space Applications*. AIAA, 2001.

[57] J.D. Johnston and E.A. Thornton. An evaluation of thermally-induced structural disturbances of spacecraft solar arrays. In *Energy Conversion Engineering Conference, 1996. IECEC 96., Proceedings of the 31st Intersociety*. IEEE, 1996.

[58] P. Kansakar and F. Hossain. A review of applications of satellite Earth observation data for global societal benefit and stewardship of planet Earth. *Space Policy*, 36:46–54, 2016.

[59] M. Komatsu and S. Nakasuka. University of Tokyo Nano Satellite Project “PRISM”. *TRANSACTIONS OF THE JAPAN SOCIETY FOR AERONAUTICAL AND SPACE SCIENCES, SPACE TECHNOLOGY JAPAN*, 7 (ists26):Tf19–Tf24, 2009.

[60] B. Kresling and J.F. Abel. Natural twist buckling in shells: from the hawkmoth’s bellows to the deployable Kresling-pattern and cylindrical Miura-Ori. In *Proceedings of the 6th International Conference on Computation of Shell and Spatial Structures,*, Ithaca, New York, the United States, 2008.

[61] A. Krikken. Design of the Secondary Mirror Support Structure for the Deployable Space Telescope . Master’s thesis, Delft University of Technology, July 2018.

[62] M.P. Le. *Micro-disturbances in Reaction Wheels*. PhD thesis, Technische Universiteit Eindhoven, 2017.

[63] D. Lichodziejewski, G. Veal, and B. Derbes. Spiral wrapped aluminum laminate rigidization technology. In *43rd AIAA/ASME/ASCE/AHS/ASC Structures, Structural Dynamics, and Materials Conference*, 2002.

[64] D. Lichodziejewski, G. Veal, R. Helms, R. Freeland, and M. Kruer. Inflatable Rigidizable Solar Array for Small Satellites. In *44th AIAA/ASME/ASCE/AHS/ASC Structures, Structural Dynamics, and Materials Conference*, 2003.

[65] M. Lou, H. Fang, and L. Hsia. Development of space inflatable/rigidizable STR aluminum laminate booms. In *Space 2000 Conference and Exposition*, 2000.

[66] MatWeb. Aluminum 1100-O. `http://www.matweb.com/search/datasheettext.aspx?matguid=db0307742df14c8f817bd8d62207368e`. Retrieved on April 30, 2018.

[67] K. Miura. Method of Packaging and Deployment of Large Membranes in Space. Technical Report 618, The Institute of Space and Astronautical Science, 1980.

[68] K. Miura and T. Tachi. Synthesis of rigid-foldable cylindrical polyhedral. In *Symmetry: Art and Science, International Society for the Interdisciplinary Study of Symmetry*, Gmuend, Austria, 2010.

[69] Y. Miyazaki, M. Fukunaga, and D. Kousaka. Membrane Structure Supported by Self-Deployable Truss for Space Applications. In *2018 AIAA Spacecraft Structures Conference*, page 1201, 2018.

[70] C. Müller, L. Perez Lebbink, B. Zandbergen, G. Brouwer, R. Amini, D. Kajon, and B. Sanders. Implementation of the $T^3\mu PS$ in the Delfi-n3Xt Satellite. In *Small Satellite Missions for Earth Observation*, pages 411–424. Springer, November 2010.

[71] Y. Nakamura, R. Funase, M. Nagai, A. Enokuchi, Y. Nojiri, T. Funane, F. Sasaki, and S. Nakasuka. Extensible Boom-Based Optical System for Nano-Scale Remote Sensing Satellite "PRISM". In *Proceedings of 19th Annual AIAA/USU Conference on Small Satellites*, 2005.

[72] NASA. NASA Visible Earth: Finland. `https://visibleearth.nasa.gov/view.php?id=65699`, 2003. Retrieved on March 11, 2019.

[73] M.C. Natori, N. Katsumata, and H. Yamakawa. Membrane Modular Space Structure Systems and Deployment Characteristics of Their Inflatable Tube Elements. In *51st AIAA/ASME/ASCE/AHS/ASC Structures, Structural Dynamics, and Materials Conference*, April 2010.

[74] A.T. Nettles. Basic Mechanics of Laminated Composite Plates. Technical report, NASA Marshall Space Flight Center, October 1994.

[75] OHB System. Satellite Platforms. `https://www.ohb-system.de/files/images/mediathek/downloads/OHB-System_Satellite_Platforms_2018.pdf`. Retrieved on March 6, 2019.

[76] S. Pepper. Design of a Primary Mirror Fine Positioning Mechanism for a Deployable Space Telescope. Master's thesis, Delft University of Technology, November 2018.

[77] J.P. Peterson, P. Seide, and V.I. Weingarten. *Buckling of thin-walled circular cylinders.* NASA SP-8007, 1968.

[78] V. Peypoudat and O. Le Couls. Satellite air brake wing structure. US patent 8,123,172 B2, 2012.

[79] G. Pica, L. Ciofaniello, S. Mattei, M.R. Santovito, and R. Gardi. High resolution deployable telescope for satellite application. In *Conference on Sensors, Systems and Next-Generation Satellites VII*, volume 5234, pages 531–538. SPIE, 2003.

[80] L. Puig, A. Barton, and N. Rando. A review on large deployable structures for astrophysics missions. *Acta Astronautica*, 67(1):12–26, 2010.

[81] D. Risselada. Phase Diversity for the Deployable Space Telescope. Master's thesis, Delft University of Technology, February 2019.

[82] H. Sakamoto, M.C. Natori, S. Kadonishi, Y. Satou, Y. Shirasawa, N. Okuizumi, O. Mori, H. Furuya, and M. Okuma. Folding patterns of planar gossamer space structures consisting of membranes and booms. *Acta Astronautica*, 94(1):34–41, 2014.

[83] Y. Miron Salomon, N. Ariel Sternberg, I. Gouzman, G. Lempert, E. Grossman, D. Katsir, R. Cotostiano, and T. Minton. Qualification of Acktar Black Coatings for Space Application. In *Proceedings of the International Symposium on Materials in a Space Environment*, Aix-en-Provence, France, 2009.

[84] SatNews. European Space Agency... A Gaseous Rebirth (Satellite). `http://www.satnews.com/story.php?number=1846194626`, August 2011. Retrieved on August 7, 2018.

[85] M. Schenk, S. Kerr, A.M. Smyth, and S.D. Guest. Inflatable cylinders for deployable space structures. In *Proceedings of the First Conference Transformables*, pages 18–20, 2013.

[86] M. Schenk, A.D. Viquerat, K.A. Seffen, and S.D. Guest. Review of Inflatable Booms for Deployable Space Structures: Packing and Rigidization. *Journal of Spacecraft and Rockets*, 51(3):762–778, 2014.

[87] K. Senda, T. Oda, S. Ota, Y. Igarashi, A. Watanabe, T. Hori, H. Ito, H. Tsunoda, and K. Watanabe. Deploy experiment of inflatable tube using work hardening. In *Proceedings of AIAA Gossamer Spacecraft Forum*, pages 1–18, 2006.

[88] A.K. Sharma and N. Sridhara. Degradation of thermal control materials under a simulated radiative space environment. *Advances in Space Research*, 50(10):1411–1424, 2012.

[89] E.M. Silverman. Space Environmental Effects on Spacecraft: LEO Materials Selection Guide. Technical report, National Aeronautics and Space Administration Langley Research Center, August 1995.

[90] K.N. Slade, M.L. Tinker, J.O. Lassiter, and R. Engberg. Dynamics of an Inflatable Structure in Vacuum and Ambient Conditions. *AIAA Journal*, 39(5):894–901, May 2001.

[91] Surrey Nanosystems. Vantablack. `https://www.surreynanosystems.com/vantablack`. Retrieved on September 17, 2018.

[92] G.E. Sweet. An experimental and analytical investigation of balloon-type enclosures for thermal control of satellites. Technical report, NASA, 1969. TN D-5230.

[93] CGG Safety & Systems. Our projects. `http://www.cggss.com/our-projects/`. Retrieved on August 7, 2018.

[94] E.A. Thornton and Y.A. Kim. Thermally induced bending vibrations of a flexible rolled-up solar array. *Journal of Spacecraft and Rockets*, 30(4):438–448, 1993.

[95] Y. Tsuda, O. Mori, R. Funase, H. Sawada, T. Yamamoto, T. Saiki, T. Endo, and J.I. Kawaguchi. Flight status of IKAROS deep space solar sail demonstrator. *Acta Astronautica*, 69(9–10):833–840, 2011.

[96] C. Underwood, A. Viquerat, B. Taylor, C. Massimiani, R. Dukes, S. Fellowes, M. Schenk, et al. The InflateSail CubeSat Mission–The First European Demonstration of Drag-Sail De-Orbiting. *AAS Advances in the Astronautical Sciences Series*, 163, 2018.

[97] M. van der List, L.D. van Vliet, H.M. Sanders, P.A.G. Put, and J.W.E.C. Elst. Applications for Solid Propellant Cool Gas Generator Technology. In *Proceedings of the 4th International Spacecraft Propulsion Conference (ESA SP-555)*, Sardinia, Italy, June 2004.

[98] G. van Marrewijk. Design of an Aberration Correction System for a Deployable Space Telescope . Master's thesis, Delft University of Technology, May 2018.

[99] B.T. van Putten. Design of the Deployment Mechanism for the Primary Mirror Elements of a Deployable Space Telescope. Master's thesis, Delft University of Technology, April 2017.

[100] T. van Wees. Thermal Modelling of the Deployable Space Telescope. Master's thesis, Delft University of Technology, 2019.

[101] G. Veal and R. Freeland. IN-STEP Inflatable Antenna Description. In *AlAA 1995 Space Programs and Technologies Conference*, Huntsville, AL, the United States, September 1995. AIAA.

[102] A. Viquerat and M. Schenk. Viscoelastic Effects in Metal-Polymer Laminate Inflatable Structures. In *3rd AIAA Spacecraft Structures Conference*, 2016.

[103] A. Viquerat, M. Schenk, B. Sanders, and V. Lappas. Inflatable rigidisable mast for end-of-life deorbiting system. In *European Conference on Spacecraft Structures, Materials and Environmental Testing (SSMET)*, 2014.

[104] A. Viquerat, M. Schenk, V. Lappas, and B. Sanders. Functional and Qualification Testing of the InflateSail Technology Demonstrator. In *2nd AIAA Spacecraft Structures Conference*, 2015.

[105] M. Voorn. Initiating the Testing Phase of a Deployable Space Telescope: An Experimental Characterisation of Hysteresisin CORE Hinges. Master's thesis, Delft University of Technology, January 2019.

[106] P.A. Warren, M.J. Silver, and B.J. Dobson. Lightweight optical barrel assembly structures for large deployable space telescopes. In *Proc. SPIE 7436, UV/Optical/IR Space Telescopes: Innovative Technologies and Concepts IV*, volume 7436, pages 74360B–74360B–8. International Society for Optics and Photonics, 2009.

[107] P.A. Warren, M.J. Silver, B.J. Dobson, and H.A. MacEwen. Experimental characterization of deployable outer barrel assemblies for large space telescopes. In *Proc. SPIE 8860, UV/Optical/IR Space Telescopes and Instruments: Innovative Technologies and Concepts VI*, volume 8860, pages 886008–886008–13. International Society for Optics and Photonics, 2013.

[108] L. Wilson, S. Pellegrino, and R. Danner. Origami sunshield concepts for space telescopes. In *54th AIAA/ASME/ASCE/AHS/ASC Structures, Structural Dynamics, and Materials Conference*. AIAA, April 2013.

[109] C. Zhao, C. Li, N. Zhou, and H. Liao. Self-deployable structure designed for space telescope for microsatellite application. In *Eighth International Symposium on Advanced Optical Manufacturing and Testing Technology (AOMATT2016)*, Suzhou, China, October 2016. International Society for Optics and Photonics.